



U.S. DEPARTMENT OF  
**ENERGY**

PNNL-21802

Prepared for the U.S. Department of Energy  
under Contract DE-AC05-76RL01830

# FY 12 ARRA-NRAP Report – Studies to Support Risk Assessment of Geologic Carbon Sequestration

KJ Cantrell  
H Shao  
L Zhong

CJ Thompson  
HB Jung  
W Um

September 2012



**Pacific Northwest**  
NATIONAL LABORATORY

*Proudly Operated by **Battelle** Since 1965*

## DISCLAIMER

This report was prepared as an account of work sponsored by an agency of the United States Government. Neither the United States Government nor any agency thereof, nor Battelle Memorial Institute, nor any of their employees, makes **any warranty, express or implied, or assumes any legal liability or responsibility for the accuracy, completeness, or usefulness of any information, apparatus, product, or process disclosed, or represents that its use would not infringe privately owned rights.** Reference herein to any specific commercial product, process, or service by trade name, trademark, manufacturer, or otherwise does not necessarily constitute or imply its endorsement, recommendation, or favoring by the United States Government or any agency thereof, or Battelle Memorial Institute. The views and opinions of authors expressed herein do not necessarily state or reflect those of the United States Government or any agency thereof.

PACIFIC NORTHWEST NATIONAL LABORATORY  
*operated by*  
BATTELLE  
*for the*  
UNITED STATES DEPARTMENT OF ENERGY  
*under Contract DE-AC05-76RL01830*

Printed in the United States of America

Available to DOE and DOE contractors from the  
Office of Scientific and Technical Information,  
P.O. Box 62, Oak Ridge, TN 37831-0062;  
ph: (865) 576-8401  
fax: (865) 576-5728  
email: [reports@adonis.osti.gov](mailto:reports@adonis.osti.gov)

Available to the public from the National Technical Information Service  
5301 Shawnee Rd., Alexandria, VA 22312  
ph: (800) 553-NTIS (6847)  
email: [orders@ntis.gov](mailto:orders@ntis.gov) <<http://www.ntis.gov/about/form.aspx>>  
Online ordering: <http://www.ntis.gov>



This document was printed on recycled paper.

(8/2010)

# **FY 12 ARRA-NRAP Report – Studies to Support Risk Assessment of Geologic Carbon Sequestration**

KJ Cantrell  
H Shao  
L Zhong

CJ Thompson  
HB Jung  
W Um

September 2012

Prepared for  
the U.S. Department of Energy  
under Contract DE-AC05-76RL01830

Pacific Northwest National Laboratory  
Richland, Washington 99352



## Summary

This report summarizes results of research conducted during FY 2012 to support the assessment of environmental risks associated with geologic carbon dioxide (CO<sub>2</sub>) sequestration and storage. Several research focus areas are ongoing as part of this project. This includes the quantification of the leachability of metals and organic compounds from representative CO<sub>2</sub> storage reservoir and caprock materials, the fate of metals and organic compounds after release, and the development of a method to measure pH in situ under supercritical CO<sub>2</sub> (scCO<sub>2</sub>) conditions.

Metal leachability experiments were completed on six different rock samples in brine in equilibrium with scCO<sub>2</sub> at representative geologic reservoir conditions. In general, the leaching of *Resource Conservation and Recovery Act of 1976* metals and other metals of concern was found to be limited and not likely to be a significant issue (at least, for the rocks tested). Metals leaching experiments were also completed on one rock sample with scCO<sub>2</sub> containing oxygen at concentrations of 0%, 1%, 4%, and 8% to simulate injection of CO<sub>2</sub> originating from the oxy-fuel combustion process. Significant differences in the leaching behavior of certain metals were observed when oxygen is present in the CO<sub>2</sub>. These differences resulted from oxidation of sulfides, release of sulfate, ferric iron and other metals, and subsequent precipitation of iron oxides and some sulfates such as barite.

Experiments to evaluate the potential for mobilization of organic compounds from representative reservoir materials and cap rock and their fate in porous media (quartz sand) have been conducted. Results with Fruitland coal and Gothic shale indicate that lighter organic compounds were more susceptible to mobilization by scCO<sub>2</sub> compared to heavier compounds. Alkanes demonstrated very low extractability by scCO<sub>2</sub>. No significant differences were observed between the extractability of organic compounds by dry or water saturated scCO<sub>2</sub>. Reaction equilibrium appears to have been reached by 96 hours.

When the scCO<sub>2</sub> was released from the reactor, less than 60% of the injected lighter compounds (benzene, toluene) were transported through the dry sand column by the CO<sub>2</sub>, while more than 90% of the heavier organics were trapped in the sand column. For wet sand columns, most (80% to 100%) of the organic compounds injected into the sand column passed through, except for naphthalene which was substantially removed from the CO<sub>2</sub> within the column.

A spectrophotometric method was developed to measure pH in brines in contact with scCO<sub>2</sub>. This method provides an alternative to fragile glass pH electrodes and thermodynamic modeling approaches for estimating pH. The method was tested in simulated reservoir fluids (CO<sub>2</sub>-NaCl-H<sub>2</sub>O) at different temperatures, pressures, and ionic strengths, and the results were compared with other experimental studies and geochemical models. Measured pH values were generally in agreement with the models, but inconsistencies were present between some of the models.



## Acknowledgments

This work was completed as part of National Risk Assessment Partnership (NRAP) project. Support for this project came from the U.S. Department of Energy Office of Fossil Energy's Cross Cutting Research program. The authors wish to acknowledge Robert Romanosky (NETL Strategic Center for Coal) and Regis Conrad (DOE Office of Fossil Energy) for programmatic guidance, direction, and support.

NRAP is a multi-lab effort that leverages broad technical capabilities across the DOE complex. NRAP involves five DOE national laboratories: NETL, Lawrence Berkeley National Laboratory (LBNL), Lawrence Livermore National Laboratory (LLNL), Los Alamos National Laboratory (LANL), and Pacific Northwest National Laboratory (PNNL). This team is working together to develop a science-based method for quantifying the likelihood of risks (and associated potential liabilities) for carbon dioxide storage sites. The work in this report was reviewed by members of the NRAP Technical Leadership Team, including Chris Brown.

The authors acknowledge technical reviews by NP Qafoku and the editorial review by AJ Currie (Pacific Northwest National Laboratory) and word processing by KR Neiderhiser. Pacific Northwest National Laboratory is operated by Battelle Memorial Institute for the U.S. Department of Energy under Contract DE-AC05-76RL01830.



## Acronyms and Abbreviations

ARM	absorbance ratio method
BET	Brunauer-Emmett-Teller isotherm
BPB	bromophenol blue (dye)
BTEX	benzene, toluene, ethyl-benzene, xylene
CBD	citrate-bicarbonate-dithionite
CMR	chemical modeling regression
CO <sub>2</sub>	carbon dioxide
DOE	U.S. Department of Energy
EOR	enhanced oil recovery
EPA	U.S. Environmental Protection Agency
FY	fiscal year
GC-MS	gas chromatography–mass spectroscopy
GCS	geologic carbon dioxide sequestration
GWB	Geochemist’s Workbench
HDPE	high-density polyethylene
IC	ion chromatography
ICP-MS	inductively coupled plasma mass spectrometry
ICP-OES	inductively coupled plasma optical emission spectrometry
KPA	kinetic phosphorescence analyzer
LOI	loss-on-ignition
MCL	maximum contaminant level
NETL	National Energy Technology Laboratory
NRAP	National Risk Assessment Partnership
PAH	polycyclic aromatic hydrocarbon
PNNL	Pacific Northwest National Laboratory
PTFE	polytetrafluoroethylene
SARM	simplified absorbance ratio method
scCO <sub>2</sub>	supercritical carbon dioxide
SEM-EDS	scanning electron microscopy/energy dispersive spectroscopy
TOC	total organic carbon
UV-Vis	ultraviolet–visible spectrophotometry
VOC	volatile organic compound
WHO	World Health Organization
XRD	x-ray diffraction
XRF	x-ray fluorescence
ZERT	Zero Emission Research and Technology Center



## Units of Measure

Å	angstrom(s)
atm	atmosphere(s)
°C	temperature in degrees Celsius
g	gram(s)
h	hour(s)
in.	inch(es)
L	liter(s)
m	meter(s)
m <sup>2</sup>	square meter(s)
M	molar
m	molal
µm	micron(s)
min	minute(s)
mg	milligram(s)
mL	milliliter(s)
mm	millimeter(s)
mM	millimole
MPa	megapascal(s)
MΩ	megaohm(s)
nm	nanometer(s)
ppb	part(s) per billion
ppm	part(s) per million
ppmw	part(s) per million by weight
psi	pounds per square inch
s	second(s)
vol%	volume percent
wt%	weight percent



# Contents

Summary .....	iii
Acknowledgments.....	v
Acronyms and Abbreviations .....	vii
Units of Measure.....	ix
1.0 Introduction .....	1.1
2.0 Leaching of Toxic Metals from Geologic CO <sub>2</sub> Sequestration Reservoir Materials .....	2.1
2.1 Introduction.....	2.1
2.2 Materials and Methods.....	2.2
2.2.1 Chemicals and Rock Samples .....	2.2
2.2.2 High-Pressure–Temperature Reaction System and Rock–Brine–CO <sub>2</sub> Experiments.....	2.2
2.3 Results and Discussion.....	2.4
2.3.1 Major Element Release from Rocks.....	2.4
2.3.2 Comparison of Rock Dissolution under N <sub>2</sub> and CO <sub>2</sub> .....	2.6
2.3.3 Trace Metal Release from Rock.....	2.7
3.0 Impact of Oxygen on Leaching of Toxic Metals from Geologic CO <sub>2</sub> Sequestration Reservoir Materials.....	3.1
3.1 Introduction.....	3.1
3.2 Materials and Methods.....	3.1
3.2.1 Gothic Shale .....	3.1
3.2.2 Solids Characterization .....	3.2
3.2.3 Experimental Methods .....	3.3
3.3 Results.....	3.4
3.3.1 Mineralogical and Chemical Composition of Gothic Shale.....	3.4
3.3.2 Gothic Shale (4 g) CO <sub>2</sub> –Brine (180 mL) 4 Weeks Reaction with 0 and 1 vol% Oxygen.....	3.4
3.3.3 Gothic Shale (6 g) CO <sub>2</sub> –Brine (180 mL) 6 Weeks Reaction with 0, 1, 4, and 8 vol% Oxygen.....	3.6
3.3.4 Gothic Shale (17 g) CO <sub>2</sub> –Brine (100 mL) 4 Weeks Reaction with 0 and 4 vol% Oxygen.....	3.11
3.4 Discussion .....	3.12
3.4.1 Effect of Oxygen on Gothic Shale–CO <sub>2</sub> –Brine Interaction.....	3.12
3.4.2 Environmental Implications .....	3.16
3.5 Conclusions .....	3.17
4.0 Organic Mobilization and Transport in Geologic Carbon Sequestration .....	4.1
4.1 Introduction.....	4.1
4.2 Materials and Methods.....	4.1
4.3 Results and Discussion.....	4.4

4.3.1	Results of Organic Compound Extractions with Methylene Chloride .....	4.4
4.3.2	Organic Compound Mobilization from Gothic Shale (Rock-2).....	4.6
4.3.3	Organic Compound Mobilization from Fruitland Coal (Rock-3) .....	4.7
4.3.4	Fate and Transport of Organic Compounds Mobilized by scCO <sub>2</sub> .....	4.7
4.4	Summary and Conclusions.....	4.10
5.0	In Situ pH Determination Under Geologic CO <sub>2</sub> Sequestration Conditions .....	5.1
5.1	Introduction .....	5.1
5.2	Materials and Methods .....	5.2
5.2.1	Chemical and Rock Samples .....	5.2
5.2.2	Instrumentation.....	5.2
5.2.3	Data Analysis .....	5.3
5.3	Results and Discussion.....	5.6
5.3.1	Method Parameters and Dissociation Constants of BPB .....	5.6
5.3.2	Comparison of Calibration Methods .....	5.6
5.3.3	Comparison with Previous Studies and Geochemical Models.....	5.8
5.3.4	In Situ pH Measurement for Rock–CO <sub>2</sub> –Brine.....	5.10
6.0	References .....	6.1
Appendix A	– Additional Figures for In Site pH Measurement Method Development .....	A.1
Appendix B	– Geochemist’s Workbench Calculation to Determine Dominant Fe(III) Species in the CO <sub>2</sub> –Brine System.....	B.1
Appendix C	– Characterization of Rock Samples.....	C.1

## Figures

2.1	Experimental System for Rock Dissolution in Aqueous Solution under High Pressure and Temperature .....	2.4
2.2	Concentrations of Dissolved Major Elements Released from Wallula Reservoir Rock, Wallula Caprock, and Michigan Reservoir Rock in Rock–CO <sub>2</sub> –Brine Systems under 100 atm of CO <sub>2</sub> in 0.1 <i>m</i> NaCl at 75°C at Different Reaction Times after CO <sub>2</sub> Introduction.....	2.5
2.3	A Comparison of Element Concentrations in Rock–CO <sub>2</sub> –Brine and Rock–N <sub>2</sub> –Brine Systems for Wallula and Michigan Reservoir Rocks.....	2.6
2.4	Concentrations of Dissolved Trace Metals in Rock–CO <sub>2</sub> –Brine or Rock–N <sub>2</sub> –Brine Systems for Different Rock Samples as a Function of Time .....	2.8
2.5	Concentrations of Fe, Mn, and Zn in Rock–CO <sub>2</sub> –Brine or Rock–N <sub>2</sub> –Brine Systems for Different Rock Samples as a Function of Time .....	2.9
3.1	SEM-EDS Elemental Mapping of Gothic Shale Before the CO <sub>2</sub> Reaction .....	3.5
3.2	Observed and Calculated XRD Patterns for Unreacted Gothic Shale .....	3.5
3.3	Dissolved Ca, Mg, K, Si, S, Fe, Ba, and U as a Function of Reaction Time for Gothic Shale and CO <sub>2</sub> –Brine Without Oxygen and with 1% Oxygen Over a Period of 4 Weeks.....	3.7
3.4	SEM-EDS Elemental Maps and Spectra for Gothic Shale After 4-Weeks Reaction in CO <sub>2</sub> –Brine with and Without Oxygen .....	3.8
3.5	Dissolved Ca, Mg, K, Si, Ba, and Sr as a Function of Reaction Time for Reaction between Gothic Shale and CO <sub>2</sub> –Brine with 0%, 1%, 4%, and 8% Oxygen Over a Period of 6 Weeks .....	3.9
3.6	Dissolved S, Fe, Mn, Ni, Zn, Sn, U, and Re as a Function of Reaction Time for Gothic Shale and CO <sub>2</sub> –Brine with 0%, 1%, 4%, and 8% Oxygen Over a Period of 6 Weeks .....	3.10
3.7	Chemical Compositions of CO <sub>2</sub> –Brine After 24-h Reaction with Crushed Gothic Shale at Low and High Rock-to-Brine Ratios at ~1500 psi and ~75°C with and without Oxygen.....	3.11
3.8	Speciation of Dissolved Sulfur after the Reaction between Gothic Shale and CO <sub>2</sub> –Brine for 6 Weeks .....	3.13
3.9.	Fe(III) Concentration in Gothic Shale Determined by Citrate-Bicarbonate-Dithionite Extraction after the 6-Week Reaction with CO <sub>2</sub> –Brine at a Range of Oxygen Content.....	3.14
3.10	Correlation between Dissolved Fe and Dissolved Ni or Mn as a Function of Oxygen Content during Gothic Shale–CO <sub>2</sub> –Brine Interaction for 6 Weeks .....	3.15
3.11	Correlation between Solid Phase Fe(III) in Gothic Shale and Dissolved U Concentration.....	3.15
3.12	Speciation of Dissolved Uranium after the Reaction between Gothic Shale and CO <sub>2</sub> –Brine for 6 Weeks .....	3.16
4.1	Schematic of Organic Mobilization and Transport Experimental Setup and Photo of Testing System.....	4.3
4.2	Ratio of CH <sub>2</sub> Cl <sub>2</sub> Extractable Alkane Concentrations of Desert Creek Limestone Relative to its Caprock Gothic Shale.....	4.6
4.3	Extraction of VOCs, semi-VOCs, and Alkanes from Gothic Shale by scCO <sub>2</sub> and CH <sub>2</sub> Cl <sub>2</sub> .....	4.6
4.4	Comparison between Concentration of Organic Compounds Extracted by Dry scCO <sub>2</sub> and Water-Saturated scCO <sub>2</sub> .....	4.7

4.5	Extracted Organic Compound Concentration from Fruitland Coal versus Reaction Time for Water-Saturated scCO <sub>2</sub> .....	4.8
4.6	Comparison Organic Compounds Extractable by scCO <sub>2</sub> versus CH <sub>2</sub> Cl <sub>2</sub> .....	4.9
4.7	Percentage of Organic Compounds Transported Through Dry Sand Columns .....	4.10
4.8	Percentage of Organic Compounds Transported Through Wet Sand Columns.....	4.11
5.1	UV-Vis Spectra of BPB in Citrate Buffer Solutions at Different pH .....	5.4
5.2	Comparison of pH <sub>m</sub> Calculated with Different Calibration Methods .....	5.7
5.3	Comparison of Experimentally Measured pH <sub>m</sub> and Predicted Values with Models.....	5.9
5.4	Changes in pH <sub>m</sub> and Major Element Concentrations with Time in Rock-CO <sub>2</sub> -1 m NaCl System at 75°C and 100 atm.....	5.11

## Tables

2.1	Summary of Rock Sample Properties .....	2.3
3.1	Chemical Composition of Gothic Shale by SEM-EDS Analysis Before and After Reaction with CO <sub>2</sub> -Brine without Oxygen and with Oxygen After 4 Weeks of Reaction .....	3.4
3.2	Chemical Composition of Gothic Shale Determined by XRF and Acid Digestion Prior to Reaction with CO <sub>2</sub> .....	3.6
3.3	Change in Chemical Composition of Gothic Shale After Reaction with CO <sub>2</sub> -Brine After 6 Weeks as a Function of Oxygen Composition of the scCO <sub>2</sub> .....	3.12
4.1	Lithological Samples Used in Tests.....	4.2
4.2	Summary of Column Tests Completed.....	4.3
4.3	Organic Compounds Studied .....	4.4
4.4	Organic Compound Concentrations Extracted by CH <sub>2</sub> Cl <sub>2</sub> from Rock Samples .....	4.5
4.5	Organic Compound Concentrations Extracted from Fruitland Coal with scCO <sub>2</sub> .....	4.8
5.1	Molar Absorptivity Ratios and pK <sub>a</sub> of BPB at Ambient Pressure Calculated with ARM and CMR.....	5.5

# 1.0 Introduction

Injection of carbon dioxide (CO<sub>2</sub>) into deep subsurface reservoirs for permanent storage or sequestration has the potential to mobilize metal and organic contaminants from the storage reservoir materials and overlying caprock. Metal and organic contaminants can leach into the brine phase in these reservoirs, and organic contaminants can dissolve into the supercritical CO<sub>2</sub> (scCO<sub>2</sub>) phase. If either of these phases were to escape the storage reservoir through fractures or faults in the caprock or through faulty wells that penetrate the reservoir, then contamination of overlying aquifers could potentially result.

The National Risk Assessment Project (NRAP) is designed to address those issues. The NRAP has three primary objectives. The first is to determine the rates and mechanisms that govern contaminant migration from reservoir and caprock materials into the brine and scCO<sub>2</sub> phases within the CO<sub>2</sub> storage reservoirs. The second is to determine the fate of these contaminants during migration of contaminated brine and scCO<sub>2</sub> phases from the storage reservoir through overlying rock layers enroute to an overlying aquifer during a hypothetical leak from the reservoir. The third objective is to determine the impact of various leakage scenarios on overlying groundwater aquifers.

This report summarizes research conducted during FY 2012 to support the primary objectives of NRAP. The report is organized into sections that cover specific tasks completed as part of the project. Section 2 describes results of experiments to quantify the leaching behavior of toxic metals from CO<sub>2</sub> sequestration site reservoir materials in contact with brines in equilibrium with scCO<sub>2</sub>. In Section 3, results from experiments conducted to study the impact of small percentages of oxygen in the scCO<sub>2</sub> phase on metal leaching are presented. Small percentages of oxygen in the injected CO<sub>2</sub> could result from the oxy-fuel combustion process. Experimental results of organic mobilization and transport from representative reservoir materials and cap rock are included in Section 4. In Section 5, the development and application of an in situ method for conducting pH measurements under scCO<sub>2</sub> conditions is described.



## 2.0 Leaching of Toxic Metals from Geologic CO<sub>2</sub> Sequestration Reservoir Materials

### 2.1 Introduction

The injection of CO<sub>2</sub> into geologic formations will cause acidification of the brine in the formations due to CO<sub>2</sub> dissolution and thus may induce the release of toxic metal contaminants from preexisting rocks. Ideally, through proper site selection and engineering design, leakage of CO<sub>2</sub> or the brine can be avoided. However, analogue studies of geologic environments containing large, concentrated amounts of CO<sub>2</sub> have shown that the leakage processes are inherent in geologic carbon dioxide sequestration (GCS; Nelson et al. 2005). It has been estimated that allowing for no more than 1% leakage of stored CO<sub>2</sub> over 100 years is necessary for sequestration to be viable (DOE 2007). Thus, if these brines containing toxic metal contaminants were to escape the storage reservoir through a fracture, fault, or abandoned well, there is the potential to contaminate overlying aquifers containing valuable freshwater resources. Therefore, understanding the potential of the release of toxic metals to brines is important to assess the environmental risks associated with GCS.

To evaluate the impact of CO<sub>2</sub> or brine leakage on groundwater aquifers, it is necessary to know the maximum contaminant levels (MCL) of toxic metals as defined by the U.S. Environmental Protection Agency (EPA) (Wang and Jaffe 2004; Zheng et al. 2009). According to the National Drinking Water Regulations (EPA 2009), MCLs are divided into two categories: primary and secondary. The primary MCLs include concentration standards for trace metals As, Pb, Cr, Ni, Cd, Cu, U, Hg, Se, Tl, Be, Ba, and Sb (EPA 2003), which are legally enforced for the protection of public health by limiting the levels of contaminants in drinking water, whereas the secondary, including standards for Fe, Mn, and Zn are non-enforceable guidelines regulating contaminants that may cause cosmetic or aesthetic effects in drinking water.

Geochemical modeling and reactive transport simulations have been conducted to evaluate the impact of CO<sub>2</sub> intrusion into groundwater aquifers (Apps et al. 2010; Birkholzer et al. 2008; Lewicki et al. 2007; Lemieux 2011; Zheng et al. 2009), but only limited laboratory or field study data are available to validate the likelihood and environmental impact of CO<sub>2</sub> leakage. The measurement at the Zero Emission Research and Technology Center (ZERT) field site in Bozeman, Montana, suggested that injecting CO<sub>2</sub> into a shallow aquifer increased Pb and As concentrations but not to a level that exceeded their respective MCLs at the end of the experiments (Kharaka et al. 2010; Spangler et al. 2009). In Chimayo, New Mexico, high concentrations of As, Pb, and U that exceeded their MCLs in shallow groundwater were found to associate with the upwelling of brine enriched with CO<sub>2</sub> (Keating et al. 2010). In the Frio formation, Texas, CO<sub>2</sub> injection was conducted in a sandstone formation, and chemical analysis exhibited a rapid mineral dissolution, especially that of calcite and iron oxyhydroxide, which significantly increased Fe and Mn concentrations in the brine (Kharaka et al. 2009). However, 15 months later, the metal concentrations decreased significantly, suggesting that the reservoir had buffered any environmental impacts from the short (10-day) CO<sub>2</sub> injection test.

The objective of this study was to measure trace metal concentrations from the reaction of CO<sub>2</sub>, simulated brine, reservoir rock, and caprocks if the brines leaked into overlying groundwater aquifers. The results of this work will provide a likely range of concentrations that can be used as the trace element source term in risk simulations.

## 2.2 Materials and Methods

### 2.2.1 Chemicals and Rock Samples

Rock samples used in this research were obtained from existing or planned large-scale industrial GCS projects. Information on sites and experimental parameters is summarized in Table 2.1. Preparation of the rock samples included crushing and sieving to collect certain size fractions (see Table 2.1), washing and sonicating in water to remove small particles, and drying. Elemental analysis results for wash water suggested the loss of major elements were all well below 0.1 mg/g dried sample, thus the composition changes in rock due to the washing procedures can be neglected. The prepared samples were characterized with x-ray diffraction (XRD) to determine the mineralogical properties, bulk x-ray fluorescence (XRF) spectroscopy to determine total elemental composition, the Brunauer-Emmett-Teller isotherm (BET) method to determine the reactive surface area, and total organic carbon (TOC) (see Table 2.1 and the tables and figures in Appendix C).

### 2.2.2 High-Pressure–Temperature Reaction System and Rock–Brine–CO<sub>2</sub> Experiments

In this study, rock dissolution experiments were conducted in 300-mL Parr pressure vessels (Parr Instrument Company, Moline, Illinois) (Figure 2.1). Each vessel was equipped with a gauge block containing a valve, thermocouple, rupture disc, a sampling valve, and a jacket heater. Liquid CO<sub>2</sub> siphoned from a cylinder was pressurized by a syringe pump (Teledyne Isco, Inc., Lincoln, Nebraska) to a designated pressure and injected into the reactor. The temperature of the reactor was regulated by a temperature controller that is interfaced with the jacket heater and the thermocouple that was mounted on the outside wall of the pressure vessel. A second thermocouple mounted inside the reactor monitored the temperature of fluids inside the vessel.

Our preliminary experiments showed that at high temperature and high CO<sub>2</sub> pressure, metal elements such as Ni, Fe, Mn, Cr, and Mo in the construction material (HC alloy C-276) of the Parr vessel dissolved in CO<sub>2</sub>-saturated water. To avoid contamination, we made the following modification to the reactor: 1) a polytetrafluoroethylene (PTFE) liner was placed inside each reactor, and the rock sample was placed inside the PTFE liner; and 2) all wetted parts were made from either titanium or zirconium, including the reactor head, the thermocouple well, the diptube, the filter installed at the end of the diptube, and the sampling valve. The modification succeeded in preventing sample contamination. In our control experiments (experimental conditions of 100 atm of CO<sub>2</sub>, 75°C, in pure water without rock addition, 4-day reaction time), all concentrations of Ni, Cr, Fe, Mn, and Mo released from the HC alloy were below their detection limits (23, 5.8, 10, 9.4, and 19 ppb, respectively), and no Ti or Zr was detected above their quantification limits (20 and 30 ppb for Ti and Zr, respectively). Without the second modification (i.e., with the application of PTFE liner), the Ni concentration was up to 20,000 ppb.

**Table 2.1.** Summary of Rock Sample Properties

Name	Location	Rock Type	Depth	Formation	Particle Size (mm)	BET Surface area (m <sup>2</sup> /g)	TOC (mg/g)	TIC (mg/g)
Wallula reservoir rock	Wallula, WA	Basalt	2730	Grand Ronde Basalt	0.5–1.0	9.7	0.07	0.45
Wallula caprock	Wallula, WA	Basalt	2700	Grand Ronde Basalt	0.5–1.0	12.8	0.23	--
Michigan reservoir rock	Otsego County, Gaylord, MI	Dolomite	3472	Bass islands	0.5–1.0	0.40	0	140.0
Utah reservoir rock	Aneth Oil Field (depleted), San Juan County, near Bluff, UT	Limestone	5398–5405	Desert Creek and Ismay members of Paradox Fm	0.5–1.0	0.14	NA	NA
FutureGen reservoir rock	Illinois Basin, IL/IN/KY	Sandstone	3865.5–3866.0	Eau Claire	0.25–0.5	0.12	NA	NA
FutureGen caprock	Illinois Basin, IL/IN/KY	Carbonate and shale	3809.2–3809.7	Eau Claire	0.5–1.0	4.70	NA	NA

-- = Below detection limit.  
NA = Data not available.

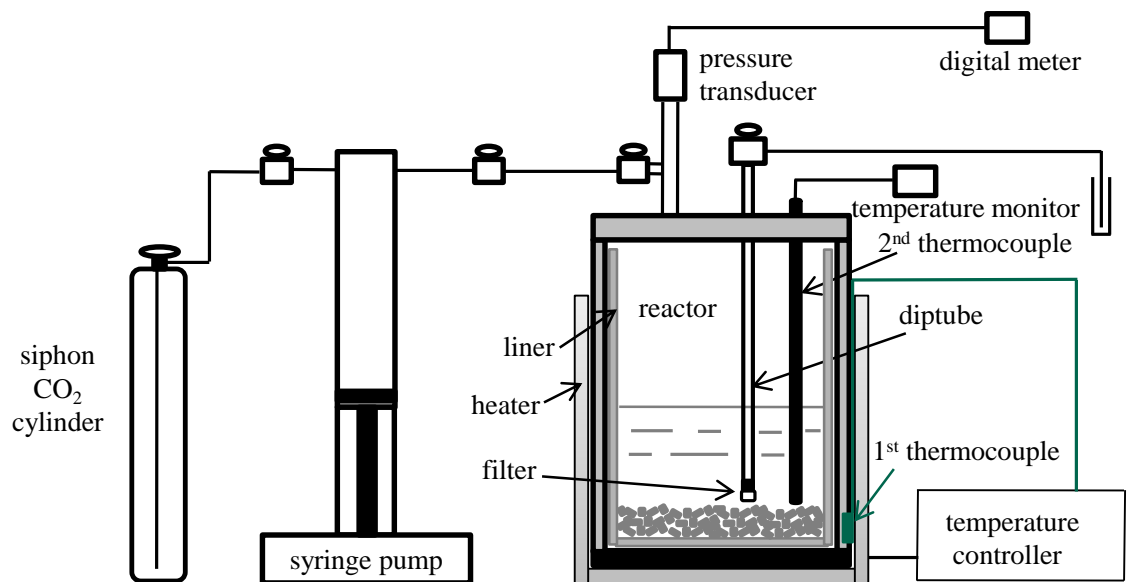


**Figure 2.1.** Experimental System for Rock Dissolution in Aqueous Solution under High Pressure and Temperature

All the rock dissolution experiments were conducted under 100 atm of CO<sub>2</sub> in 0.1 *m* NaCl solution at 75°C. The ratio of solid to liquid was 1:45. After both the rock samples and 0.1 *m* NaCl solution were added into the reactor, the suspension was sparged with nitrogen for 30 min to remove oxygen. Then the reactor was sealed, and the temperature of the vessel was raised through the jacket heater to near 75°C before CO<sub>2</sub> was introduced. The vessel was connected with the syringe pump during the first 6 h to allow the reaction system to reach thermoequilibrium and the pressure of CO<sub>2</sub> to stabilize at 100 atm. The valve between the vessel and the syringe pump then was closed except during sampling. After the reaction started, aqueous samples were taken out periodically through the filter, diptube, and the sampling valve.

The filter was used to prevent the unintentional transfer of solids during sampling. The samples were filtered with 0.45- $\mu\text{m}$  syringe filters and acidified with nitric acid to a final nitric acid concentration of 2% (wt%) to avoid precipitation and to match the matrix for inductively coupled plasma optical emission spectrometry (ICP-OES) calibration standards. These samples were analyzed with ICP-OES for metal ion concentrations and inductively coupled plasma mass spectroscopy (ICP-MS) for trace metals. For some rock samples, we also conducted rock dissolution experiments under nitrogen in order to test if toxic metals could be released in the geologic formation without CO<sub>2</sub> injection. The experimental conditions were the same as CO<sub>2</sub> experiments except that N<sub>2</sub> was used instead of CO<sub>2</sub>.

## 2.3 Results and Discussion

### 2.3.1 Major Element Release from Rocks

Figure 2.2 shows the concentrations of major elements as a function of reaction time in CO<sub>2</sub>-rock-brine systems. For our control experiment, which was conducted under the same experimental conditions without the presence of rock (data not shown), the concentrations of all major elements were below their detection limits. For the experiments conducted with rock samples, fast initial rock dissolution was

observed after CO<sub>2</sub> was introduced to the reaction systems. A steady state was reached for the aqueous species for Michigan reservoir rock (Figure 2.2E and F), whereas for Wallula reservoir rock and caprock, the concentrations of most metal species kept increasing throughout the reaction, suggesting their dissolution was still far from equilibrium. The dissolution of Michigan reservoir rock was faster than that of two other basalt rocks: within 2 days, Ca concentration reached 260 ppm for Michigan reservoir rock, whereas it was only about 50 and 30 ppb, respectively, for Wallula reservoir rock and cap rock (Figure 2.2A and C). If rock surface areas in the reaction systems are considered (1.6, 38.8, and 51.2 m<sup>2</sup> for Michigan reservoir rock (dolomite), Wallula reservoir rock (basalt), and Wallula caprock (basalt) respectively), then the difference in dissolution rates between dolomite and basalt is even more significant. This observation is consistent with previous study for the high dissolution rate of carbonate minerals (Marini 2007; White et al. 2003).

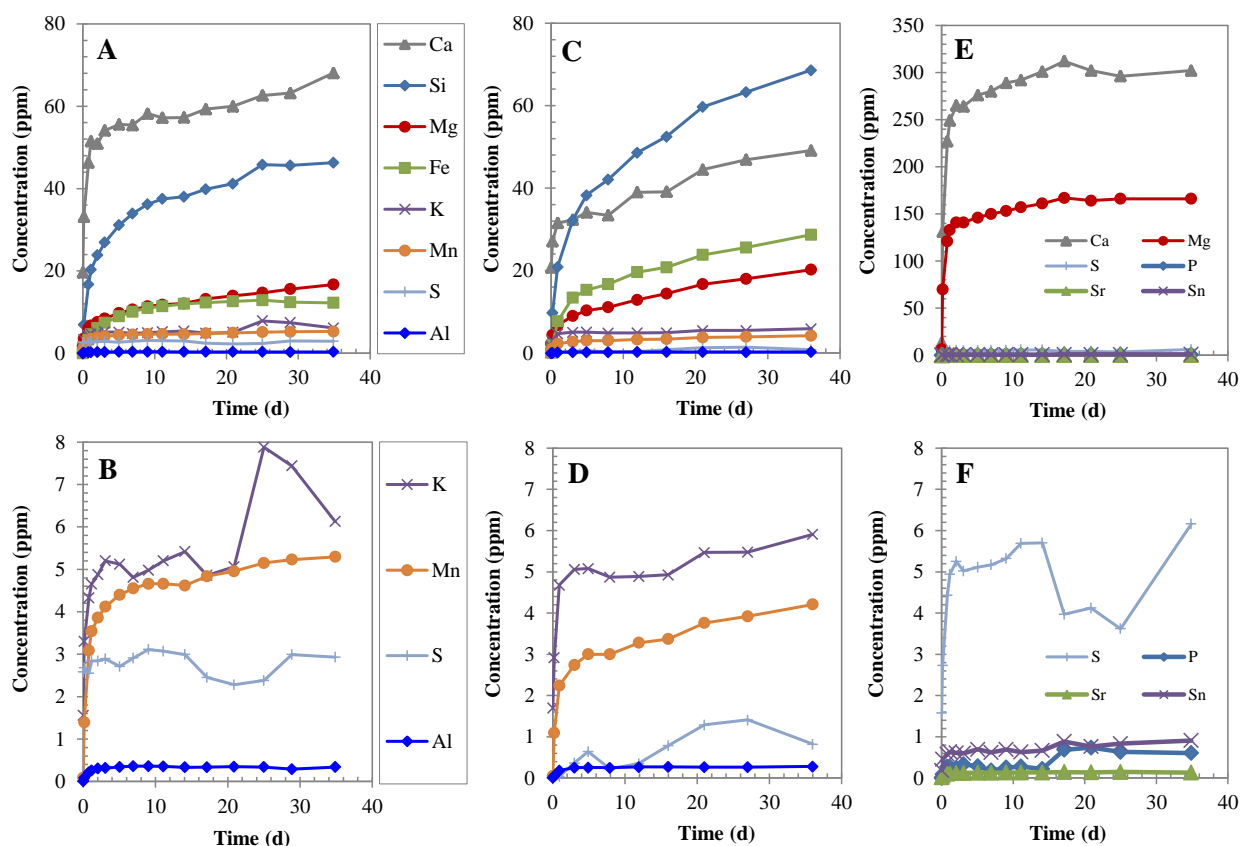


**Figure 2.2.** Concentrations of Dissolved Major Elements Released from Wallula Reservoir Rock (A and B, notice B in enlarged from A by using small scale to show the low concentration elements. The same is for other D and F), Wallula Caprock (C and D), and Michigan Reservoir Rock (E and F) in Rock–CO<sub>2</sub>–Brine Systems under 100 atm of CO<sub>2</sub> in 0.1 *m* NaCl at 75°C at Different Reaction Times after CO<sub>2</sub> Introduction. A and C, B and D share the same legends.

Sulfur and/or phosphorus were also observed in the aqueous solution during rock dissolution. The sulfur species are likely to be sulfate or sulfite, and phosphorus is likely to be phosphate. We analyzed our samples at the last time points of our experiments with ion chromatography (IC) and identified the presence of sulfate in the aqueous phase for all three rocks and phosphate for Michigan rock only. Those

anions may influence the fate of toxic trace metals because they may complex with those metals or adsorb on rock surface and change the surface charge properties (Stumm 1992).

Except for high concentration Ca, Mg, and Si, significant amounts of Fe and Mn, which are non-enforceably regulated contaminants, were detected for Wallula reservoir rock and caprock (Figure 2.2A, B, C, and D). The concentrations of Fe and Mn in the brine exceeded their secondary MCL (0.3 and 0.05 ppm for Fe and Mn, respectively) only 3 h after the reaction started (see more discussion below).

### 2.3.2 Comparison of Rock Dissolution under N<sub>2</sub> and CO<sub>2</sub>

To differentiate the effect of CO<sub>2</sub> on rock dissolution from the effect of temperature, pressure, or the presence of electrolyte (NaCl), we also conducted a rock dissolution experiment with Michigan and Wallula reservoir rocks under the same temperature and ionic strength but used N<sub>2</sub> to keep the pressure. The nitrogen experiments were conducted to more closely represent conditions prior to CO<sub>2</sub> injection. Figure 2.3 shows a comparison of the concentrations of different elements in the rock–CO<sub>2</sub>–brine and rock–N<sub>2</sub>–brine systems for Wallula and Michigan reservoir rocks.

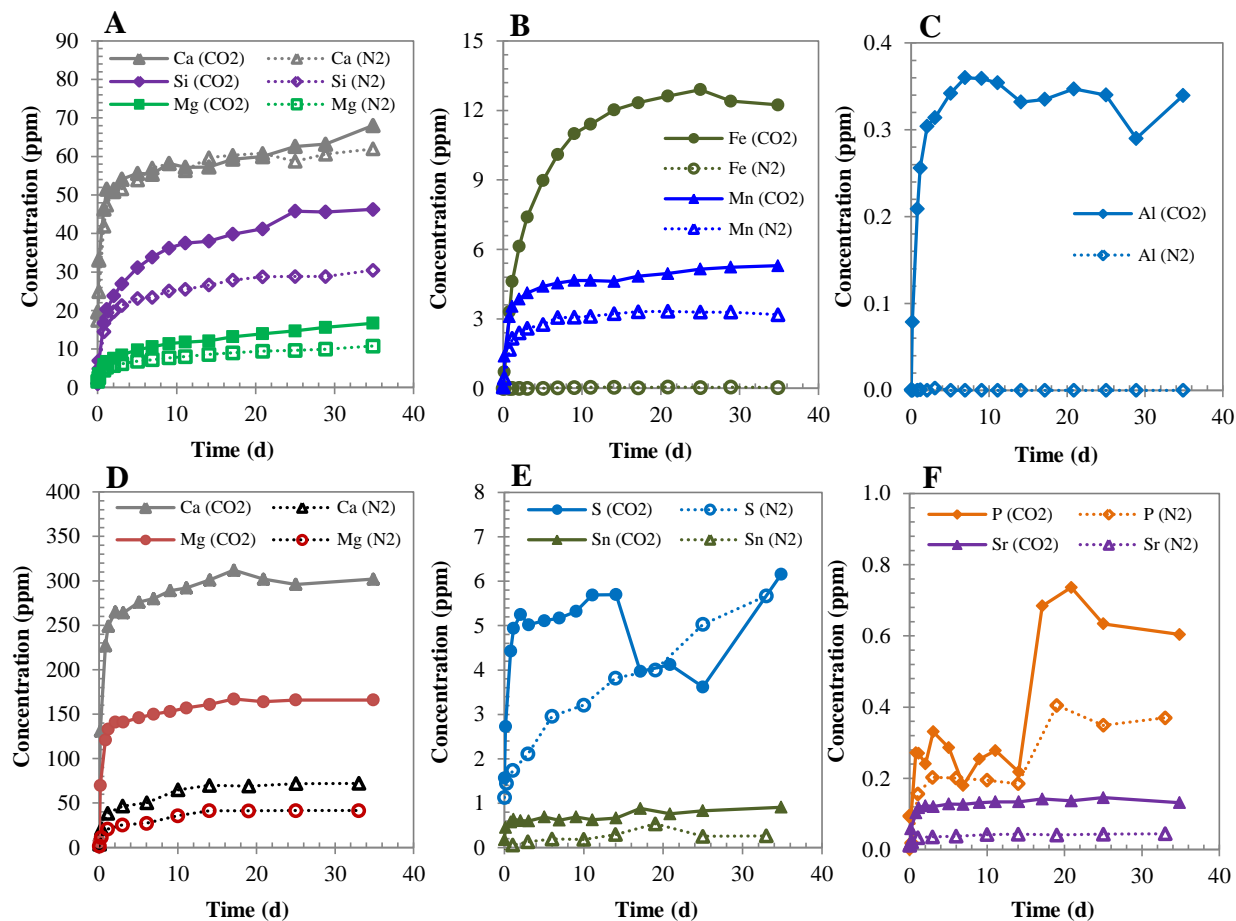


**Figure 2.3.** A Comparison of Element Concentrations in Rock–CO<sub>2</sub>–Brine and Rock–N<sub>2</sub>–Brine Systems for Wallula (A, B, and C) and Michigan (D, E, and F) Reservoir Rocks

In general, introduction of CO<sub>2</sub> facilitated the dissolution of rock and increased the concentrations of dissolved species, but the extent was different among rocks and dissolved species. For Wallula reservoir rock (Figure 2.2A, B, and C), which is basalt (Table 2.1), the dissolution of Fe and Al was significantly enhanced by CO<sub>2</sub> introduction. Mn, Mg, and Si were enhanced, but to a lesser extent compared to Fe and Al, whereas Ca concentrations were essentially the same for rock–CO<sub>2</sub>–brine and rock–N<sub>2</sub>–brine experiments. A similar observation has been reported for sandstone–CO<sub>2</sub>–brine system under GCS conditions (Carroll et al. 2011). In this work, for Michigan reservoir rock, which is predominantly dolomite (Table 2.1), however, Ca dissolution was significantly enhanced by the introduction of CO<sub>2</sub>, and Mg, Sn, Sr, and P showed the same trend as Ca. The different enhancement of rock dissolution by CO<sub>2</sub> might be associated with the different dissolution mechanisms under the experimental conditions.

### 2.3.3 Trace Metal Release from Rock

The measured trace metal concentrations in rock dissolution experiments show that reaction of simulated CO<sub>2</sub>-rich brine with reservoir rocks and a caprock enhanced the solubility of some trace metals. The trace metal generally achieved steady-state concentrations within about 2 or 3 days. Figure 2.4 shows the concentration of toxic trace metals (Cd, Cr, Pb, Cu, Ba, U, and Tl) in rock–CO<sub>2</sub>–brine or rock–N<sub>2</sub>–brine systems as a function of time. Concentrations of these metals are legally regulated by the EPA to protect public health. Other metals, including As, Ni, Hg, Se, and Sb, which also are regulated by the EPA, were not detected in all our experiments and thus are not shown in Figure 2.4.

To confirm whether the trace metals were released from rock samples or from the reactor or simulated brine (NaCl solution), we conducted a reactor control experiment in which only 0.1 *m* NaCl was added into the reactor while no rock sample was present. The result (Figure 2.4) shows that Cd, Cu, Ba, U, and Tl concentrations were significantly higher when rocks were present than levels released in the reactor control experiment, suggesting these metals were released from rocks. However, for Cr and Pb, their concentrations in the rock experiments were near or even lower than that in the reactor control experiment, suggesting they were not from rock dissolution but rather from brine solution or from reactor contamination. Based on our preliminary experiments and the relatively stable concentrations of these two elements throughout the dissolution experiments, it is likely that the detected Cr or Pb were from the NaCl solution. In the presence of rocks, the relatively lower concentrations of these two metals might be due to their adsorption to the rock or precipitation during the reaction.

As discussed above, comparison of rock dissolution in rock–brine systems under CO<sub>2</sub> and N<sub>2</sub> can help to differentiate the effect of CO<sub>2</sub> from effects of other parameters such as pressure, temperature, and the presence of electrolytes. Similar to the dissolution of major elements, the effect of CO<sub>2</sub> on trace metal release also depended on rock type and metal species. For Wallula reservoir rock, Cd and Tl concentrations in the rock–CO<sub>2</sub>–brine and rock–N<sub>2</sub>–brine systems are similar, suggesting CO<sub>2</sub> injection into the deep Wallula basalt formation will not enhance the dissolution of these two metals (Figure 2.4A and G). For the same rock, however, the release of Cu, Ba, and U was significantly higher when CO<sub>2</sub> was present (Figure 2.4D, E, and F). For Michigan reservoir rock, releases of Cu and U were more significant in the rock–CO<sub>2</sub>–brine system than in the rock–N<sub>2</sub>–brine system (Figure 2.4D and F).

Although CO<sub>2</sub> can enhance the dissolution of toxic metals that are regulated by EPA, the concentrations of the metals detected in this work were well below their MCL (primary MCL). This

finding suggests that if brine from a CO<sub>2</sub> storage reservoir did leak into an overlying groundwater aquifer, the impact due to toxic metals is likely to be minimal or insignificant.

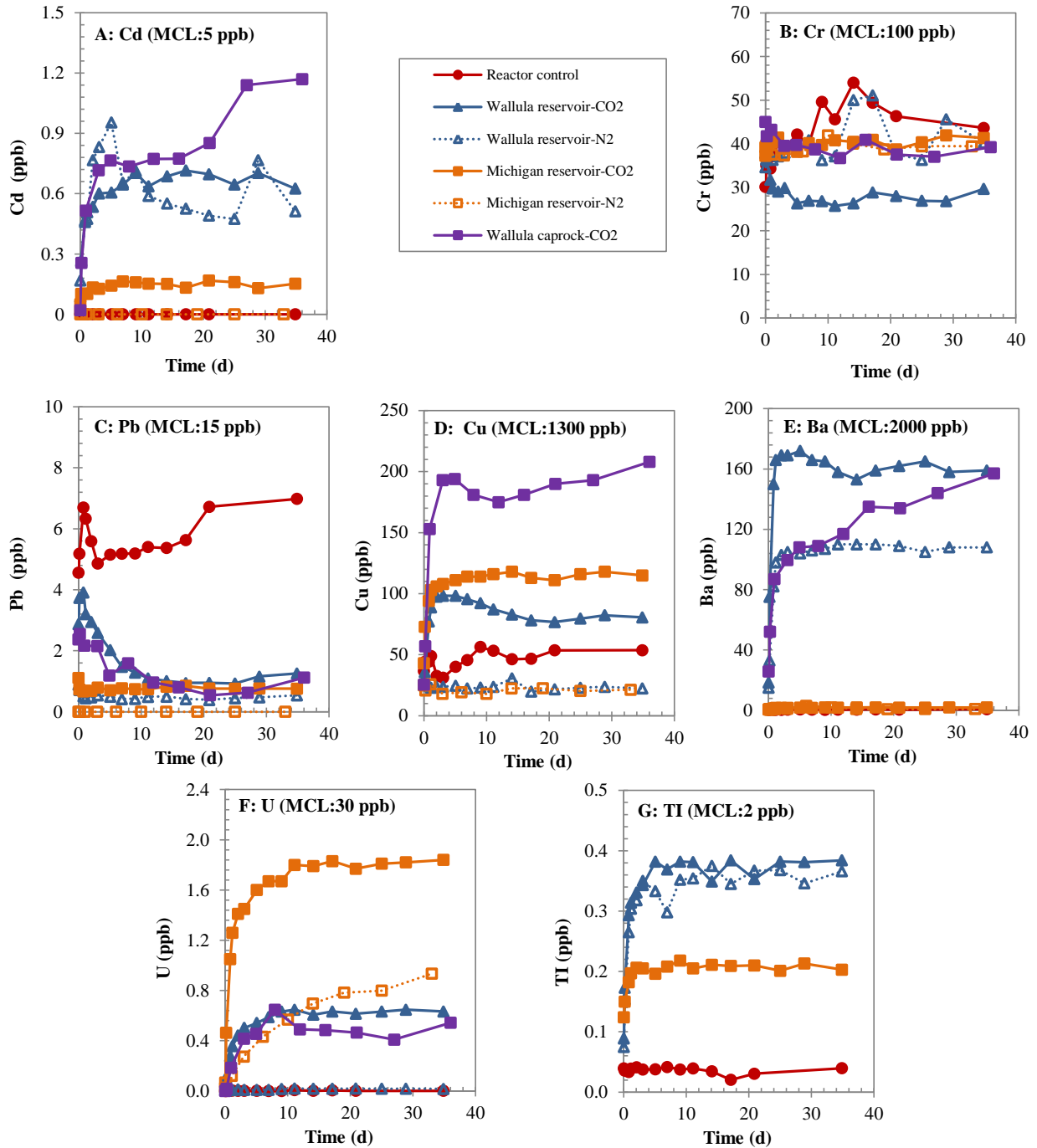


**Figure 2.4.** Concentrations of Dissolved Trace Metals in Rock–CO<sub>2</sub>–Brine or Rock–N<sub>2</sub>–Brine Systems for Different Rock Samples as a Function of Time

Although all toxic trace metals (Cd, Cr, Pb, Cu, Ba, U, and Tl) were below their primary MCLs in this study, we observed that the second MCLs were exceeded for Fe and Mn for both Wallula reservoir rock and caprock (Figure 2.5). In the Wallula reservoir rock–CO<sub>2</sub>–brine system, Fe concentrations reached steady state after about 10 days, and the steady-state concentrations were approximately 40 times higher than the second MCL for Fe (Figure 2.5A and B). For Wallula caprock, Fe concentrations continued to increase throughout the reaction and exceeded its secondary MCL only 5 h after CO<sub>2</sub> was introduced into the reactor system. For both rocks, Fe concentrations in rock–N<sub>2</sub>–brine systems were negligible compared to the CO<sub>2</sub> system, suggesting that injection of CO<sub>2</sub> will significantly enhance Fe release from basalt rocks at the Wallula sequestration site. For Michigan reservoir rock, Fe was not observed in the N<sub>2</sub> experiment; however, in the presence of CO<sub>2</sub>, Fe concentration increased to about 400 ppb within a day and then gradually decreased to well below its MCL (Figure 2.5B). The decreased Fe concentration in the aqueous phase might be due to the precipitation of Fe as the pH of the aqueous solution increased, induced by rock dissolution and proton consumption.

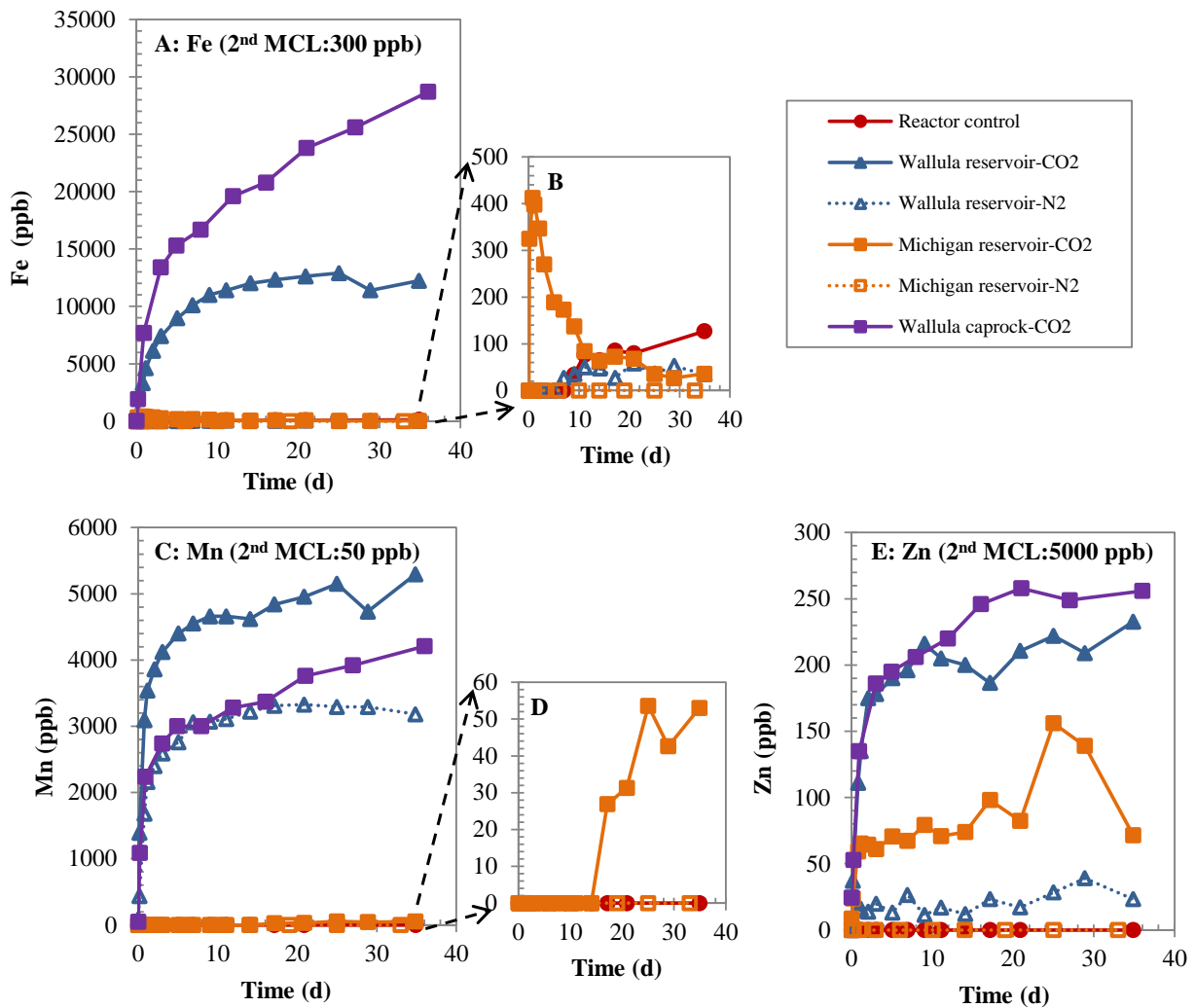


**Figure 2.5.** Concentrations of Fe, Mn, and Zn in Rock–CO<sub>2</sub>–Brine or Rock–N<sub>2</sub>–Brine Systems for Different Rock Samples as a Function of Time. B and D are enlarged figures from A and C, respectively, to show the low concentration data.

Similar to Fe, the concentrations of Mn released from the Wallula reservoir and cap rocks were significantly higher than the contaminant's secondary MCL (Figure 2.5C and D). According to the result from the N<sub>2</sub> experiment, about 3000 ppb of Mn were present in the brine of the Wallula storage formation before the CO<sub>2</sub> injection (Figure 2.5C); however, the introduction of CO<sub>2</sub> enhanced Mn dissolution and rendered an even higher Mn concentration (about 5000 ppb) in the aqueous phase. For Michigan reservoir rock, a trace amount (less than 60 ppb) of Mn was observed after about 17 days under CO<sub>2</sub>, whereas no Mn was detected in the N<sub>2</sub> experiment. In this study, all concentrations detected for Zn, another metal regulated under secondary MCL, were well below the MCL (Figure 2.5E).

Although the concentrations of some metals (Fe and Mn) exceeded their MCLs and others did not, their impact on groundwater quality may not be considered large. This is because the final concentrations of metals in an affected aquifer will depend on the chemical evolution that takes place from the storage reservoir to groundwater aquifers. This will involve degassing of CO<sub>2</sub>, an increase in pH, precipitation of carbonate and iron hydroxide minerals, and adsorption of metals onto rocks, as temperature and pressure decrease along the leakage pathways. All of these processes are likely to lower the aqueous trace metal concentration. Leakage into many groundwaters will be accompanied also by a change from reducing to oxidizing conditions that should result in much lower Fe and Mn concentrations from hydroxide precipitation (Flaathen et al. 2009). The results from this study can be coupled with aquifer models to assess risk during the site selection and permitting processes.

## 3.0 Impact of Oxygen on Leaching of Toxic Metals from Geologic CO<sub>2</sub> Sequestration Reservoir Materials

### 3.1 Introduction

In the oxyfuel combustion process, substantial amounts of oxygen can be present in the effluent CO<sub>2</sub> stream. For example, the effluent CO<sub>2</sub> stream from oxyfuel combustion from a fluidized bed pilot plant combustor (CanmetENERGY, Ottawa, Ontario, Canada) contained gas impurities that included 5.2 vol% O<sub>2</sub>, 221 ppm CO, 1431 ppm SO<sub>2</sub>, and 243 ppm NO (Jia et al. 2007). The expected CO<sub>2</sub> stream from an oxyfuel combustion plant includes 5.8 vol% N<sub>2</sub>, 4.7 vol% O<sub>2</sub>, 4.47 vol% Ar, 100 ppm NO<sub>x</sub>, 50 ppm SO<sub>2</sub>, 20 ppm SO<sub>3</sub>, and 50 ppm CO (IEAGHG 2004).

Although oxygen is a common impurity gas in CO<sub>2</sub> stream and co-injection of oxygen can significantly alter the redox state of deep geologic formations, few studies have focused on the effect of co-injected oxygen on the CO<sub>2</sub>-brine-rock interaction. During geologic carbon sequestration, oxidative dissolution of sulfide minerals in the reservoir rock or caprock can occur in the presence of dissolved oxygen (Evangelou and Zhang 1995; Lawson 1982; Moses et al. 1987) and subsequently release toxic metals and radionuclides such as uranium into the brine (Keating et al. 2010; Little and Jackson 2010). Although a number of previous experimental studies have focused on changes in the major ion composition and mineralogical alteration during the interaction between caprock and CO<sub>2</sub>-brine or supercritical CO<sub>2</sub> (Alemu et al. 2011; Credo et al. 2009; Liu et al. 2012; Wilke et al. 2012), few studies have addressed the effects of redox processes on toxic contaminant mobilization due to other gases co-injected with CO<sub>2</sub> during geologic carbon sequestration.

This study focuses on the effect of oxygen in the CO<sub>2</sub> stream on the mobilization of toxic contaminants (e.g., metals and radionuclides) from a caprock (Gothic shale from the Aneth Oil Field, Utah) during the interaction with CO<sub>2</sub>-brine under geological carbon sequestration conditions.

### 3.2 Materials and Methods

#### 3.2.1 Gothic Shale

A core sample of Gothic shale (caprock) overlying the Desert Creek Limestone (reservoir rock) at approximately 1640 m depth was collected from a Texaco well (H-117) located within a carbon sequestration site at the Aneth Oil Field in southeastern Utah. A core from the Aneth Unit H-117 well that contains a nearly complete unslabbed section of Gothic shale was selected for detailed representative analysis of the Desert Creek reservoir caprock. Located in the Paradox Basin of southeastern Utah within the Colorado Plateau, the Greater Aneth is a stratigraphic trap with fractures and small faults (Griffith et al. 2011). The Greater Aneth was selected to demonstrate combined enhanced oil recovery (EOR) and CO<sub>2</sub> sequestration under the auspices of the Southwest Regional Partnership on Carbon Sequestration, sponsored by DOE. In the Aneth Unit, the Gothic shale is remarkably uniform, consisting of black to gray, laminated to thin-bedded, dolomitic marine shale. It ranges in thickness from 5 to 27 ft (1.5–8.2 m), averaging 15 ft (3.6 m), and generally thins over the carbonate buildup complex in the Desert Creek zone. The Gothic shale strata consists of a fairly monotonous interval of dark brown to gray, faintly wavy laminated, calcareous mudstone, and diagenetic products include abundant pyrite and varying amounts of

rare to common dolomite/ankerite (Rutledge 2010). Modest amounts of clay microporosity likely occur, but the permeability is in the nanodarcy range (Rutledge 2010). Naturally occurring fractures in the shale caprock are documented mostly in the northern Paradox Basin, with some in the southern regions of the basin ranging from “hairline” to “massive,” and the fractures are filled with secondary precipitates of carbonates, halides, anhydrite, and pyrite (Hite and Lohman 1973; Tromp 1995; Tuttle and Klett 1996).

### 3.2.2 Solids Characterization

Before and after the reaction, the chemical composition and mineralogy of Gothic shale were characterized using XRD, scanning electron microscopy/energy dispersive spectroscopy (SEM-EDS), XRF, and chemical extraction.

**XRD** – X-ray diffractograms were collected using a Phillips X’Pert x-ray diffractometer with a Cu-K $\alpha$  radiation x-ray tube ( $\lambda = 1.5418 \text{ \AA}$ ) and a graphite monochromator. The x-ray source is a long-fine-focus ceramic x-ray tube with a Cu anode. Normal operating power is 40 kV and 50 mA (2.0 kW). Data were collected from 10 to 80 degree  $2\theta$  with a scanning step size of  $0.04^\circ$  and dwell time of 4 s. The electronic analysis was processed using JADE software (Materials Data Inc., Livermore, California). A database published by the Joint Committee on Powder Diffraction Standards International Center for Diffraction Data (Newtown Square, Pennsylvania) was used to identify crystalline phases by comparing standard single-phase patterns to the bulk XRD patterns measured for the sample.

**SEM-EDS Analysis** – The shale samples were analyzed using the Quanta 3D FEG instrument (FEI, North America Nanoport, Hillsboro, Oregon) after the samples were mounted with double-sided carbon tape to an aluminum stud. The EDS analysis was done using Genesis software from EDAX (Silicon Drift Detector, Mahwah, New Jersey). The electron-beam energy during the analysis was 20 keV at 4 nA. EDS area scans were conducted for 100 s. The EDS mapping was carried out at  $512 \times 400$ -pixel resolution with a total number of frames of 512. The dwell time during the analysis was 200 ms. For most of the analysis, the K $\alpha$  position was considered for the calculations. If the K $\alpha$  position was beyond the current energy range, L lines were considered in the calculations. Estimates of the atomic ratios were done using the ZAF correction procedure.<sup>1</sup> The background noise was subtracted from the data using Genesis software before calculations.

**XRF** – XRF analysis of Gothic shale was conducted using an ARL Advant’X XRF spectrometer (Thermo Scientific, Waltham, Massachusetts) in the Geoanalytical Laboratory at Washington State University–Pullman.

**Inorganic and Organic Carbon Analyses** – The total organic and inorganic carbon concentrations were measured using a TOC-V CSN instrument (Shimadzu with a SSM-5000A Total Organic Carbon Analyzer by combustion at approximately 900°C for total carbon and 200°C for inorganic carbon based on ASTM E1915-01, *Standard Test Methods for Analysis of Metal Bearing Ores and Related Materials by Combustion Infrared Absorption Spectrometry*. The amount of CO<sub>2</sub> measured after sample combustion is proportional to the total carbon and inorganic carbon content of the sample. Adequate system performance was confirmed by analyzing known quantities of a calcium carbonate standard. Organic carbon content was determined by the difference between the inorganic carbon and total carbon concentration.

---

<sup>1</sup> Z: atomic number correction, A: absorption correction, F: characteristic fluorescence correction.

**Acid Digestion** – Acid digestion was performed to determine the total elemental composition of Gothic shale (Liang et al. 2000). A 0.1-g sample, 5 mL of concentrated HNO<sub>3</sub>, 5 mL of concentrated HCl, and 5 mL of concentrated HF were combined in a PTFE cup. The acid digestion vessel (Model 4744, Parr Instrument Company, Moline, Illinois) was sealed and heated for 3 h at 150°C in a furnace. The vessel was cooled, and the content was transferred to a 60-mL high-density polyethylene (HDPE) bottle containing 2.5 g boric acid in 15 mL of deionized water. The final volume was adjusted to 50 mL before ICP-OES and ICP-MS analyses were performed.

**Citrate-Bicarbonate-Dithionite (CBD) Extraction** – 0.5 g of soil was added into a 50-mL plastic centrifuge tube with a mixture of 22.5 mL of 0.3 M sodium citrate (C<sub>6</sub>H<sub>5</sub>Na<sub>3</sub>O<sub>4</sub>·2H<sub>2</sub>O) and 2.5 mL of 1 M sodium bicarbonate (NaHCO<sub>3</sub>). The tubes were heated in a water bath at 80°C; then 1 g of sodium dithionite (Na<sub>2</sub>S<sub>2</sub>O<sub>4</sub>) powder was added to the tubes. The tubes were mixed constantly for 1 min and then intermittently every 5 min for 15 min. A second 1-g portion of sodium dithionite was added, and occasional mixing continued for another 10 min. Samples were filtered through a syringe filter with a 0.45-μm pore size and diluted by a factor of 10 for solution analysis using ICP-OES analysis.

### 3.2.3 Experimental Methods

Gothic shale was crushed to a sand-size fraction (0.063–2 mm) to increase the reactivity and then thoroughly homogenized. Gothic shale subsamples (4 or 6 g) were added to reaction vessels consisting of PTFE liners inserted into pressure vessels (Model 4760 with 300 mL capacity, Parr Instrument Company) containing a synthetic brine (0.1 M NaCl) of 180 mL. To minimize corrosion of the pressure vessels (HC alloy, Parr Instrument Company) during the experiments, the vessels, heads, and fittings were treated with a silicon coating (SilcoTek Corporation, Bellefonte, Pennsylvania). In addition, titanium thermowells were used. After each vessel was sealed, the system was purged with pure N<sub>2</sub> gas for 10 min to remove atmospheric oxygen. Then O<sub>2</sub> and CO<sub>2</sub> were injected using a high-pressure syringe pump (Teledyne Isco, Inc., Lincoln, Nebraska) through a gas inlet valve to produce a range of O<sub>2</sub>-to-CO<sub>2</sub> volume percentages (0%, 1%, 4%, and 8%). Pressure and temperature were maintained at approximately 1500 psi and 75°C throughout the experiments. The O<sub>2</sub>-to-CO<sub>2</sub> volume percentages of 1%, 4%, and 8% correspond to dissolved oxygen levels of 12, 61, and 126 mg/L based on PHREEQC modeling. The reaction period ranged from 4 to 6 weeks. During the reaction, liquid samples were collected periodically by opening the liquid sampling valve that was connected to a PTFE tube and a 20-μm pore size No-Met PTFE filter (VICI AG International, Schenkon, Switzerland) located inside the vessel. Each sampling episode resulted in a pressure drop of about 50 psi. Consequently, pressure decreased initially from 1600 to 1400 psi by the end of the experiment. After a liquid sample of about 4 mL was collected from each vessel, the sample was immediately filtered through a syringe filter with 0.45-μm pore size (Whatman International), and acidified to 1% HNO<sub>3</sub>. Prior to sampling, about 2 mL of liquid were purged from each vessel to remove liquid remaining within the dead space of the sample collection fittings. Dissolved constituents (Na, K, Ca, Mg, Si, S, Fe, Mn, Ba, Sr, Sn, Ni, Zn, Re, and U) were determined by ICP-OES and ICP-MS. After 6 weeks of reaction time, dissolved sulfate and dissolved U(VI) were determined spectrophotometrically (Hach DR-2000) with SulfaVer 4 AccuVac Ampuls and a Kinetic Phosphorescence Analyzer (KPA; Chemchek Instruments, Inc., Richland, Washington) immediately after sample collection. At the end of the experiment, the vessel was depressurized and the reacted Gothic shale was collected for solid phase characterization. The wet solid sample was washed with acetone (Fisher; certified ACS grade) immediately after depressurization to remove water.

### 3.3 Results

#### 3.3.1 Mineralogical and Chemical Composition of Gothic Shale

SEM-EDS analysis results indicated that Ca, Mg, Al, Si, and C (2.5–16.7 atom %) are the major components of the Gothic shale, while Fe and S (~1 atom %) are minor components (Table 3.1). EDS mapping revealed a strong correlation between Fe and S (Figure 3.1), suggesting the presence of Fe-sulfide minerals. Semi-quantification of XRD analysis identified quartz (25%), calcite (37%), dolomite (9%), and montmorillonite (22%) as major mineral phases and confirmed the presence of pyrite (7%) (Figure 3.2), which was consistent with the SEM-EDS results. The total carbon of the Gothic shale was determined to be 6.3 wt%. Inorganic carbon and organic carbon were 3.9 wt% and 2.4 wt%, respectively. Consistent with the SEM-EDS and XRD results, XRF data indicated that Si, Al, and Ca are the most abundant elements ( $\text{SiO}_2$ ,  $\text{Al}_2\text{O}_3$ ,  $\text{CaO} > 10$  wt%; unnormalized) in the Gothic shale, while Fe and Mg are approximately 4 wt% oxides (Table 3.2). XRF analysis also showed that Mn, Ni, Ba, Sr, and Zn concentrations in the shale are relatively high (>100 mg/kg), whereas the concentrations of Cu and Pb are lower than 50 mg/kg. XRF and acid digestion results indicated that U is present in Gothic shale at 10–16 mg/kg (Table 3.2). Loss-on-ignition (LOI) of 18% indicated that Gothic shale includes a high content of organic matter (Table 3.2).

**Table 3.1.** Chemical Composition of Gothic Shale by SEM-EDS Analysis Before and After Reaction with  $\text{CO}_2$ -Brine without Oxygen and with Oxygen (1% by volume) After 4 Weeks of Reaction

Element	Before Reaction	0% Oxygen	1% Oxygen
C K	9.2	12.2	12.1
O K	54.5	54.9	55.0
MgK	2.5	3.0	2.9
AlK	5.8	6.8	6.9
SiK	16.7	18.6	18.5
S K	1.1	0.6	<0.1
K K	1.6	1.7	1.7
CaK	7.6	1.6	1.3
FeK	0.9	0.7	1.6

#### 3.3.2 Gothic Shale (4 g) $\text{CO}_2$ -Brine (180 mL) 4 Weeks Reaction with 0 and 1 vol% Oxygen

During the gothic shale- $\text{CO}_2$ -brine interaction, dissolved Ca, Mg, K, and Si concentrations increased to 800~1000, 28~33, 16, and 11 mg/L, respectively (Figure 3.3). Based on the XRD results, Ca and Mg were released while calcite and dolomite were dissolved by carbonic acid; Si is considered to result from the dissolution of quartz and montmorillonite. It appears that K was released from montmorillonite by cation exchange between K and Ca (Inoue and Minato 1979). The presence of oxygen (1 vol%) during the interaction between Gothic shale and  $\text{CO}_2$ -brine resulted in a significant increase in S concentration to approximately 250 mg/L, whereas dissolved S remained below 50 mg/L in the vessel without oxygen

(Figure 3.3). Dissolved Fe concentration remained below 10 mg/L in all vessels throughout the experiment. Dissolved Ba increased to 378  $\mu\text{g/L}$  in the absence of oxygen, while it increased to 138  $\mu\text{g/L}$  in the presence of oxygen (Figure 3.3). Dissolved U increased to 12 and 9  $\mu\text{g/L}$  in the absence and presence of oxygen, respectively (Figure 3.3). SEM-EDS mapping indicates that Ca atom % in Gothic shale decreased from 7.6% to 1.3–1.6% after 1-month reaction (Figure 3.4, Table 3.1), suggesting significant dissolution of calcite from the surfaces of Gothic shale. After 1-month reaction with 1 vol% oxygen, Fe atom % increased from 0.9% to 1.6%, and S atom % decreased from 1.1% to  $<0.1\%$ . These results suggest that significant oxidation/dissolution of pyrite and subsequent precipitation of Fe(III) oxides occurred on the surfaces of Gothic shale in the presence of oxygen. In contrast, Fe and S atom % decreased from 0.9% to 0.7% and from 1.1% to 0.6%, respectively, after the reaction without oxygen, while the EDS mapping still shows a good correlation between Fe and S (Figure 3.4).

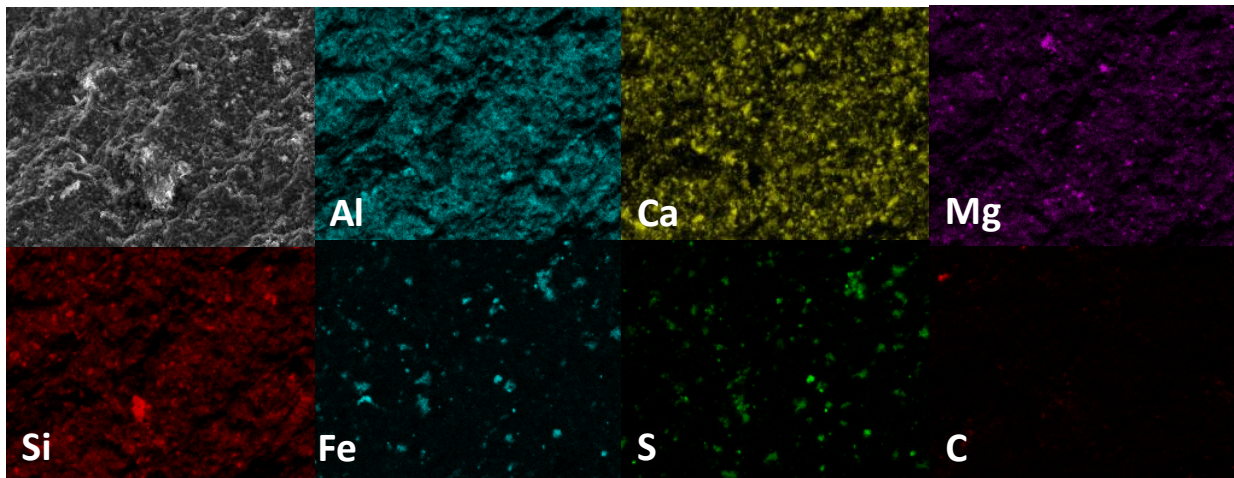


**Figure 3.1.** SEM-EDS Elemental Mapping of Gothic Shale Before the  $\text{CO}_2$  Reaction

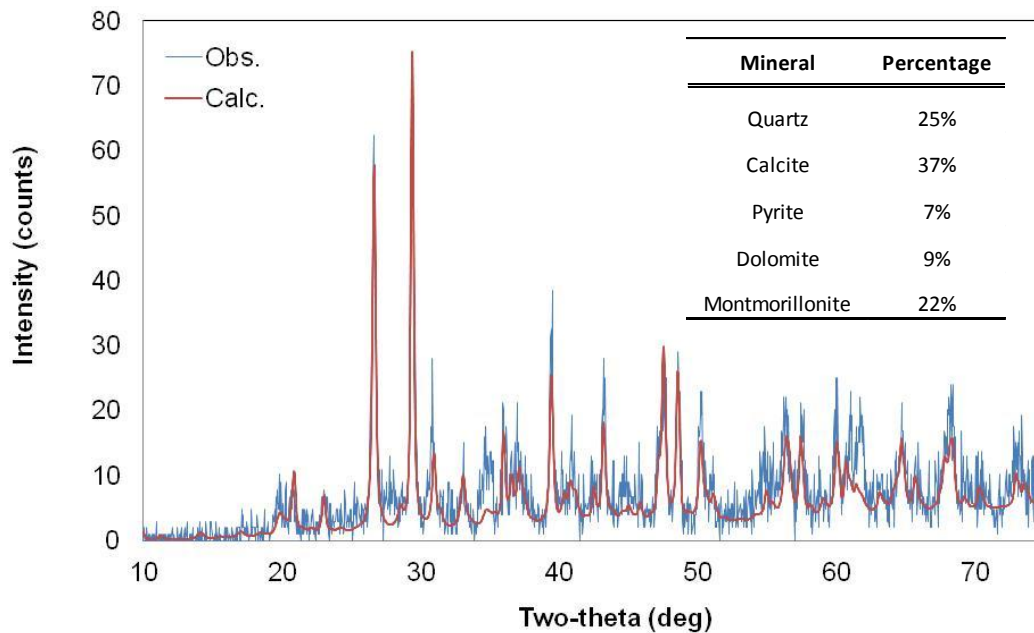


**Figure 3.2.** Observed and Calculated XRD Patterns for Unreacted Gothic Shale. Table shows semi-quantitative percentages of mineral phases.

**Table 3.2.** Chemical Composition (unnormalized) of Gothic Shale Determined by XRF and Acid Digestion (HCl-HNO<sub>3</sub>-HF) Prior to Reaction with CO<sub>2</sub>

Major Elements (wt%)	XRF	Acid Digestion
SiO <sub>2</sub>	38.29	
TiO <sub>2</sub>	0.45	
Al <sub>2</sub> O <sub>3</sub>	10.11	
FeO <sup>(a)</sup>	3.70	
MnO	0.02	
MgO	4.48	
CaO	16.03	
Na <sub>2</sub> O	0.62	
K <sub>2</sub> O	2.64	
P <sub>2</sub> O <sub>5</sub>	0.54	
Sum	76.88	
LOI%	17.74	
Trace Elements(ppm)	XRF	Acid Digestion
Ni	145	66
Ba	124	765
Sr	264	75
Cu	47	ND
Zn	202	509
Pb	5	ND
U	16	10

(a) Total Fe is expressed by FeO.  
ND = Not detected.

### 3.3.3 Gothic Shale (6 g) CO<sub>2</sub>-Brine (180 mL) 6 Weeks Reaction with 0, 1, 4, and 8 vol% Oxygen

As 6 g of Gothic shale were reacted with 180 mL of CO<sub>2</sub>-brine, the mobilization patterns for major and trace elements were generally similar to the reaction with 4 g of Gothic shale (Section 3.2). Dissolved Ca and K quickly reached steady state after a rapid increase to 800–1200 mg/L and about 22 mg/L, respectively, during the first week (Figure 3.5). In contrast, dissolved Mg and Si rapidly increased to 27–34 mg/L and approximately 10 mg/L, respectively, during the first week, and then continued to increase to 37–55 mg/L and approximately 15 mg/L, respectively, until the end of the 6-week reaction (Figure 3.5). The slower increase in dissolved Mg and Si than dissolved Ca is attributed to slower dissolution kinetics of dolomite and quartz than that of calcite (Knauss and Wolery 1988; Pokrovsky et al. 2005). Dissolved Sr increased rapidly to approximately 2,000–2,500 µg/L during the first week, and then remained relatively constant until the end of the reaction (Figure 3.5). The similar behavior of Ca and Sr as a function of reaction time suggests that Sr was incorporated in calcite and released during calcite dissolution (Pingitore et al. 1992).

In the vessels containing 4 and 8 vol% oxygen, dissolved S concentration increased rapidly to approximately 450 mg/L during the first week, and then reached steady state at about 500 mg/L (Figure 3.6). The rate of S mobilization during the first week was much slower in the vessel with 1 vol%

oxygen than the vessels with 4 and 8 vol% oxygen, but dissolved S continued to increase to 375 mg/L until the end of the 6-week reaction (Figure 3.6). Dissolved S concentration remained below 50 mg/L in the absence of oxygen (Figure 3.6).

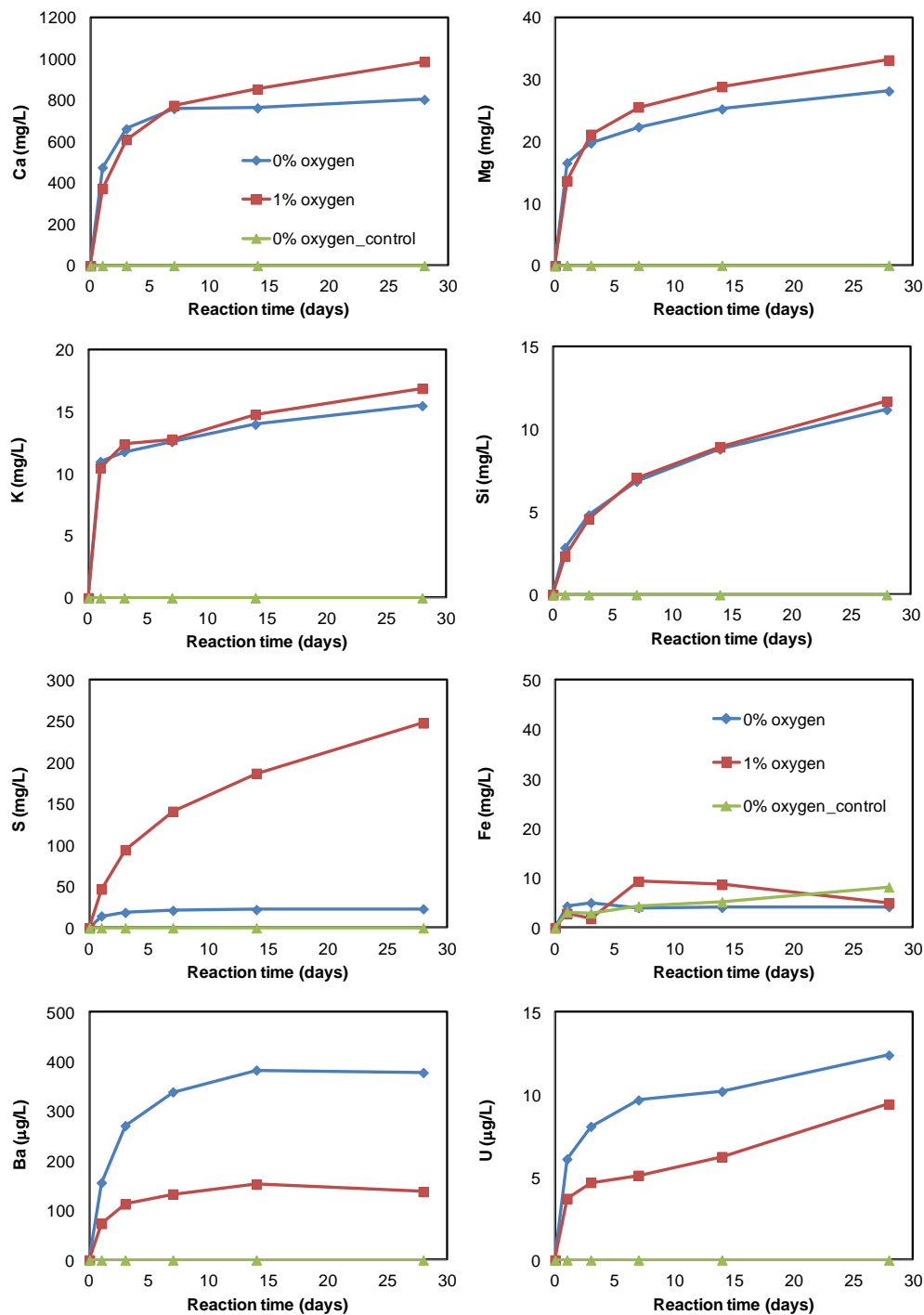


**Figure 3.3.** Dissolved Ca, Mg, K, Si, S, Fe, Ba, and U as a Function of Reaction Time for Gothic Shale (4 g) and CO<sub>2</sub>-Brine (0.1 M NaCl, 180 mL) Without Oxygen and with 1% Oxygen (by volume) Over a Period of 4 Weeks

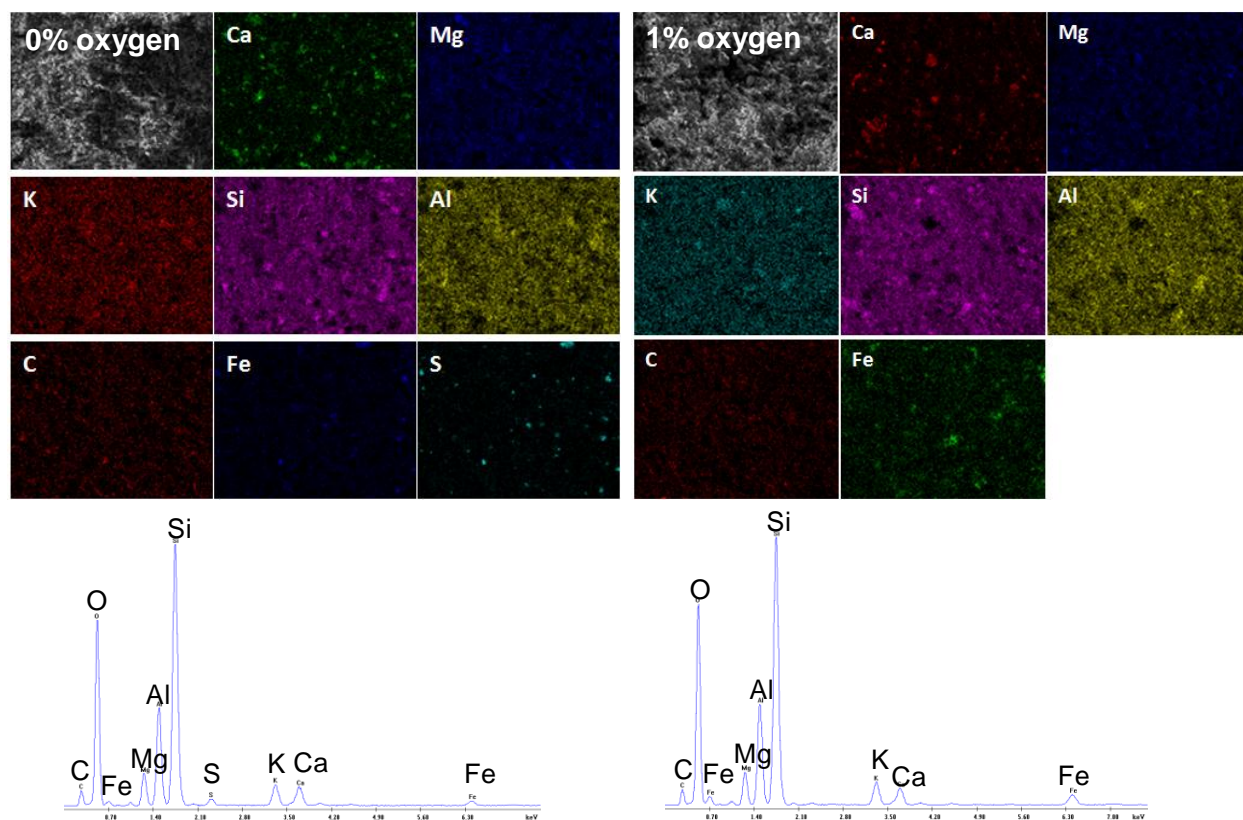


**Figure 3.4.** SEM-EDS Elemental Maps and Spectra for Gothic Shale After 4-Weeks Reaction in CO<sub>2</sub>-Brine with and Without Oxygen (1% by volume). Sulfur peak was below the detection limit for the 1% oxygen experiment.

In all vessels, dissolved Fe concentrations were lower by 1–2 orders of magnitude than dissolved S. Dissolved Fe was highest at 8 days reaction. The Fe concentrations measured at 8 days were 6.8 mg/L, 1.5 mg/L, 18.1 mg/L, and 27.4 mg/L in vessels with 0, 1, 4, and 8 vol% oxygen, respectively (Figure 3.6). After 8 days reaction, dissolved Fe concentration decreased gradually to below approximately 2 mg/L. Dissolved Mn and Ni were also correlated with oxygen content. With 4 and 8 vol% oxygen, dissolved Mn increased rapidly to 2,920 and 3,660 µg/L after 8 days and then varied between 2000 and 3000 µg/L until the end of the experiment (Figure 3.6). With 1 vol% oxygen, dissolved Mn continued to increase throughout the experiment to a final value of 1,090 µg/L. Dissolved Ni concentrations were also highest in the presence of 4 and 8 vol% oxygen; the highest concentrations of approximately 10 mg/L occurred at 8 days, whereas dissolved Ni concentration for 1 vol% oxygen was no higher than the Ni concentration (~1 mg/L) in control vessels (Figure 3.6).

Dissolved Zn concentrations increased to about 1000 µg/L with 4 and 8 vol% oxygen, whereas it was below the detection limit (299 µg/L) without oxygen or with 1 vol% oxygen (Figure 3.6). Dissolved Sn was not affected by the oxygen content and increased to 1600–1800 mg/L in all vessels. Dissolved Re increased to approximately 9 µg/L at 4 and 8 vol% oxygen, 6 µg/L at 1 vol% oxygen, and µg/L at 0% oxygen. Without oxygen, dissolved Ba concentrations rapidly increased to approximately 370 µg/L during the first week, and then continually increased to 427 µg/L at slower rate until the end of the

6-week reaction. In the presence of oxygen at 1–8 vol%, dissolved Ba increased to 100–150  $\mu\text{g/L}$  in 8 days and then decreased to below 100  $\mu\text{g/L}$  until the end of the reaction (Figure 3.5).

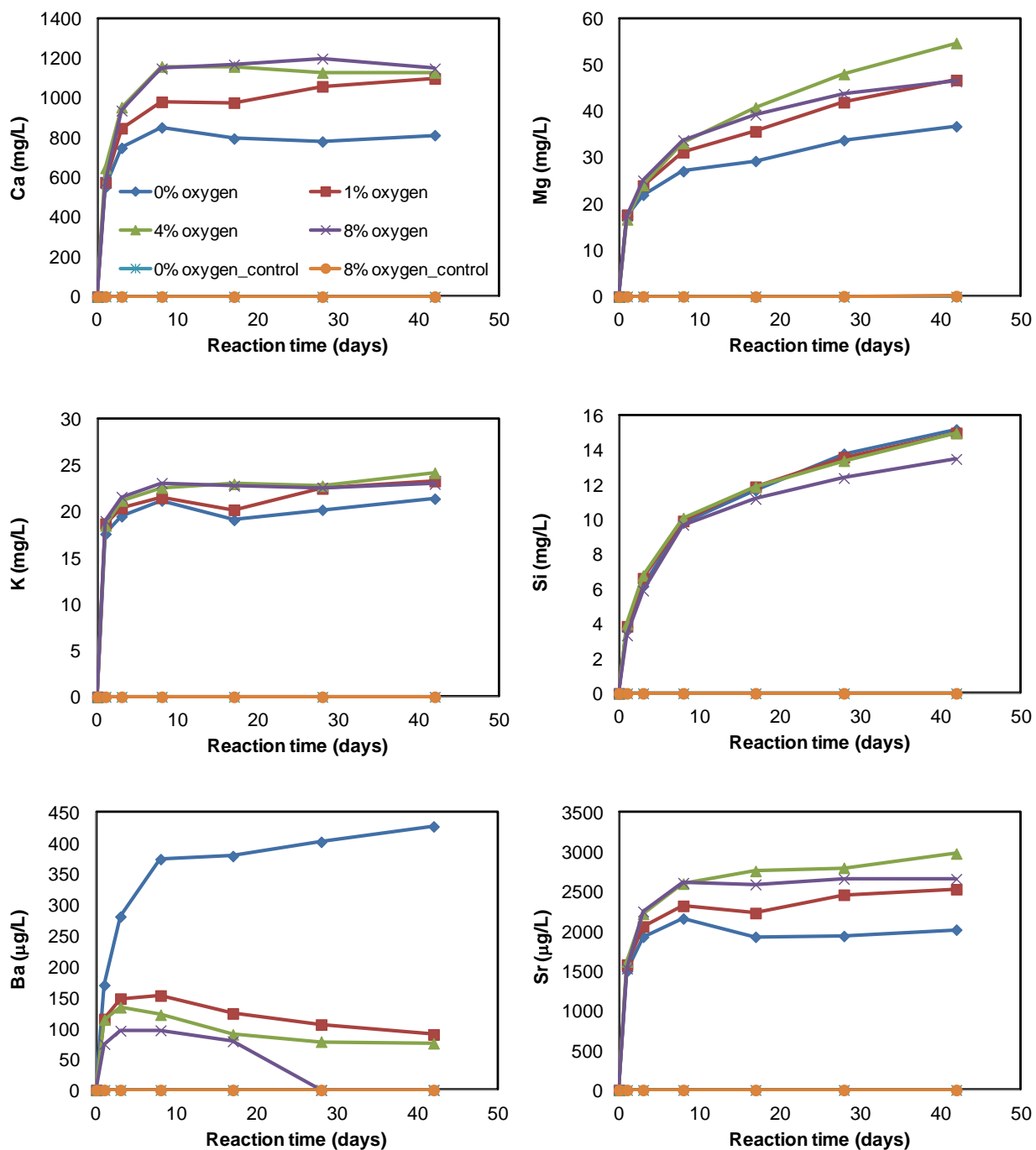


**Figure 3.5.** Dissolved Ca, Mg, K, Si, Ba, and Sr as a Function of Reaction Time for Reaction between Gothic Shale (6 g) and  $\text{CO}_2$ -Brine (0.1 M NaCl; 180 mL) with 0%, 1%, 4%, and 8% Oxygen (volume percentage) Over a Period of 6 Weeks

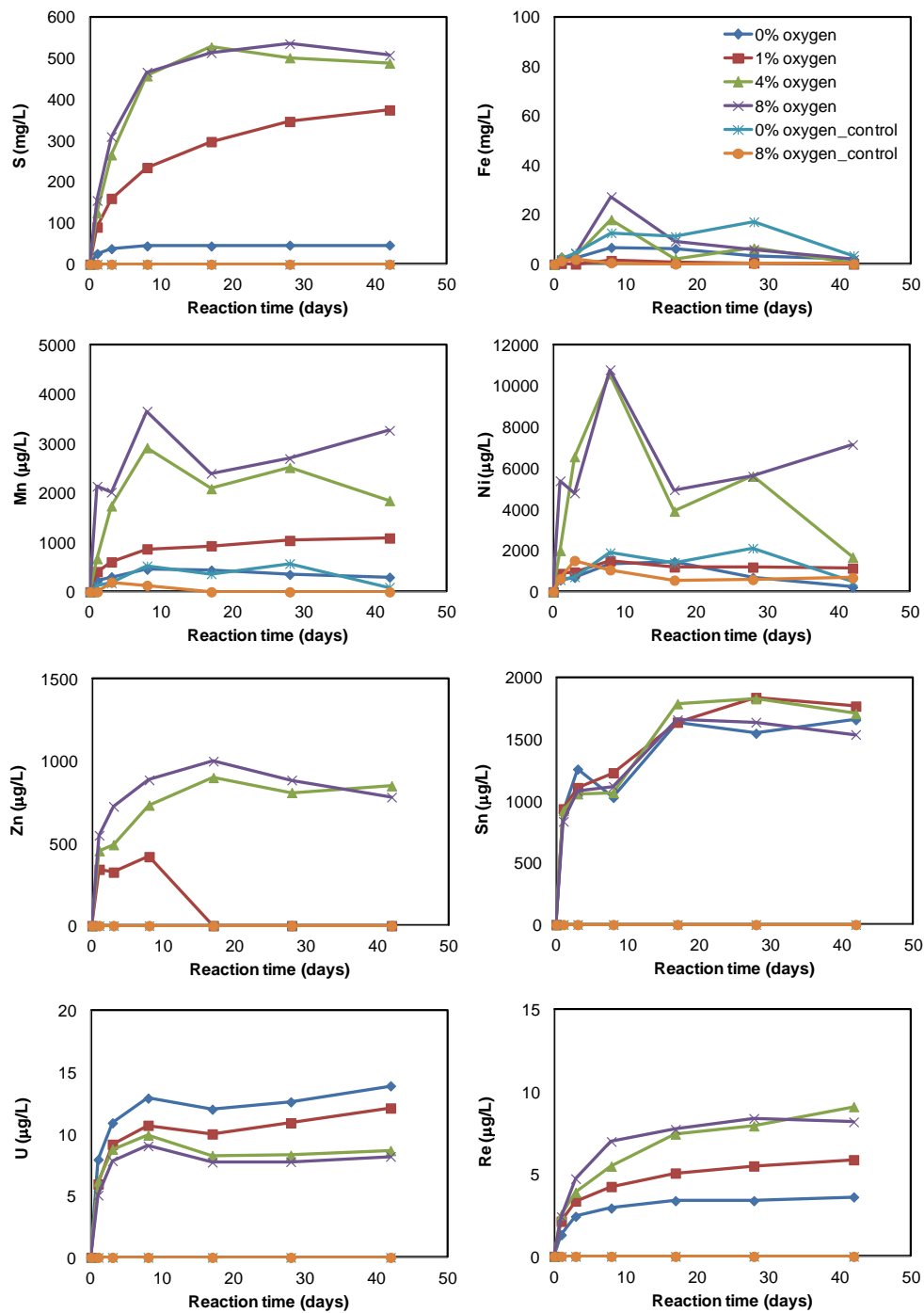


**Figure 3.6.** Dissolved S, Fe, Mn, Ni, Zn, Sn, U, and Re as a Function of Reaction Time for Gothic Shale (6 g) and CO<sub>2</sub>-Brine (0.1 M NaCl; 180 mL) with 0%, 1%, 4%, and 8% Oxygen (volume percentage) Over a Period of 6 Weeks

The dissolved U concentrations were negatively correlated with oxygen content (Figure 3.6). Dissolved U increased to 14 µg/L at 0 vol% oxygen, 12 µg/L at 1 vol% oxygen, and 8 µg/L at 4 vol% and 8 vol% oxygen over the period of 6 weeks.

### 3.3.4 Gothic Shale (17 g) CO<sub>2</sub>-Brine (100 mL) 4 Weeks Reaction with 0 and 4 vol% Oxygen

Rock-to-brine ratios for actual field or reservoir conditions are generally much higher than typical laboratory experimental conditions. To partially address this issue, another set of experiments was conducted at solid-to-solution ratio of 0.17 g/mL (17 g shale + 100 mL brine). These experiments were conducted at about 1500 psi and approximately 75°C with 4 vol% oxygen and without oxygen for a contact period of 24 h. The increase in solid-to-solution ratio from 0.033 g/mL to 0.170 g/mL (a factor of ~5) resulted in an increase in Ca, Mg, K, and Si by a factor of approximately 1.5, 2, 3, and 3, respectively, regardless of oxygen content (Figure 3.7). As solid-to-solution ratio increased, dissolved S increased from 26 mg/L to 106 mg/L for 0 vol% oxygen, and from 125 mg/L to 431 mg/L for 4 vol% oxygen (Figure 3.7). Increasing the solid-to-solution ratio also resulted in an increase in U concentration from 8 to 17 mg/L for 0 vol% oxygen and 6 to 11 mg/L for 4 vol% oxygen (Figure 3.7). Although the solid-to-solution ratio was increased by a factor of 5, dissolved element concentrations increased only by a factor of 1.5 to approximately 4. It appears that increased dissolution of calcite at higher solid-to-solution ratios results in a greater increase in pH, which limits further mineral dissolution and metal mobilization.

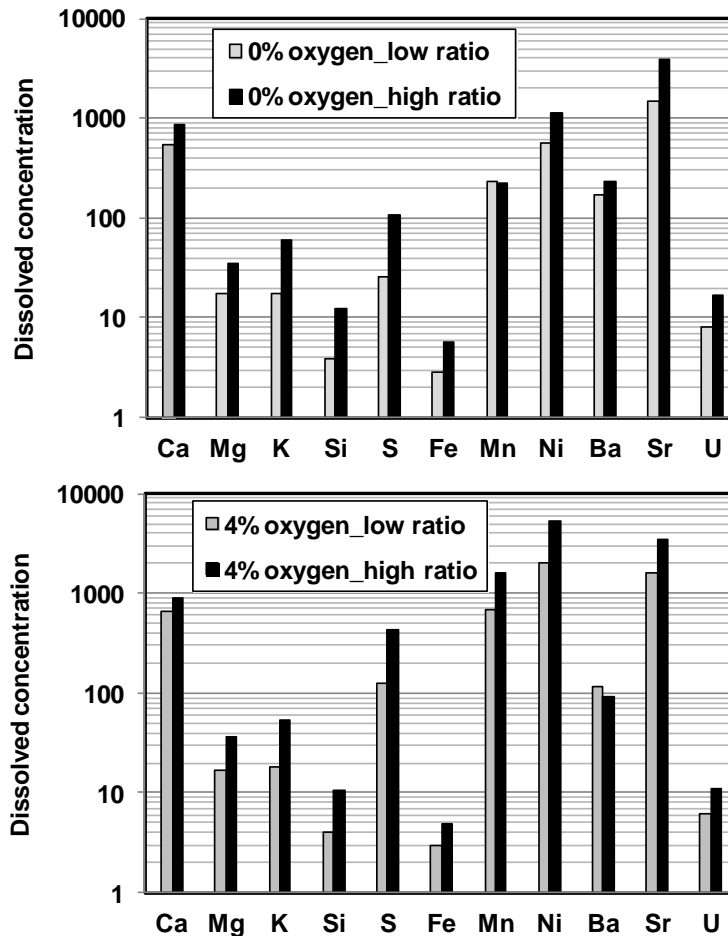
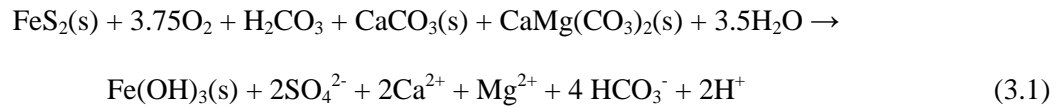


**Figure 3.7.** Chemical Compositions of CO<sub>2</sub>-Brine After 24-h Reaction with Crushed Gothic Shale at Low (6 g + 180 mL) and High (17 g + 100 mL) Rock-to-Brine Ratios at ~1500 psi and ~75°C with and without Oxygen (4% by volume) (units: mg/L for Ca, Mg, K, Si, S, and Fe; µg/L for Mn, Ni, Ba, and U).

## 3.4 Discussion

### 3.4.1 Effect of Oxygen on Gothic Shale–CO<sub>2</sub>–Brine Interaction

In general, oxygen exerted a minor effect on the dissolution of the major elements (Ca, Mg, K, and Si) because these elements are not redox-sensitive. Dissolved K and Si concentrations after the reaction for 4–6 weeks (Figure 3.3 and Figure 3.5) were similar in vessels prepared with or without oxygen. However, there was a remarkable difference in the concentrations of dissolved Ca and Mg depending on the presence of oxygen (Figure 3.3 and Figure 3.5). The higher concentrations of dissolved Ca and Mg in the experiments with oxygen (1–8 vol%) than the experiment without oxygen is attributed to increased dissolution of calcite and dolomite at lower pH caused by added acidification resulting from oxidative dissolution of pyrite in the presence of oxygen as below:



SEM-EDS results also confirm a significantly enhanced dissolution of calcite on the surface of Gothic shale with higher content of oxygen during the 6-week reaction period because of lower pH caused by pyrite oxidation. The Ca atom % decreased from 7.6% to 4.4%, 2.8%, 1.9%, and 1.6% in vessels with 0, 1, 4, and 8 vol% oxygen (Table 3.3). Based on XRF results for Gothic shale prior to the CO<sub>2</sub> reaction (Table 3.2), the concentrations of calcite, dolomite, and pyrite in Gothic shale are estimated to be 20.6 wt%, 20.6 wt%, and 6.2 wt%, respectively. Based on ICP-OES results for the reaction between 6 g of Gothic shale and 180 mL of CO<sub>2</sub>–brine, it is estimated that 27%–39% of calcite and 5% of dolomite were dissolved from the surface of Gothic shale during the period of 6 weeks. This is consistent with previous experimental results showing higher dissolution kinetics for calcite than dolomite (Chou et al. 1989; Pokrovsky et al. 2005). In the same manner, it is estimated that approximately 34%, 45%, and 46% of pyrite were subjected to oxidative dissolution in the vessels with 1, 4, and 8 vol% oxygen during the 6-week period, indicating that oxidation of pyrite on the surfaces of Gothic shale occurred rapidly and extensively in the presence of oxygen.

**Table 3.3.** Change in Chemical Composition of Gothic Shale After Reaction with CO<sub>2</sub>–Brine After 6 Weeks as a Function of Oxygen Composition of the scCO<sub>2</sub> (0, 1, 4, and 8% by volume)

Element	Before Reaction	0% Oxygen	1% Oxygen	4% Oxygen	8% Oxygen
C K	9.2	18.3	14.0	11.7	14.7
O K	54.5	52.8	54.0	55.1	52.4
MgK	2.5	2.5	2.7	3.0	2.9
AlK	5.8	5.4	6.0	7.0	6.7
SiK	16.7	14.4	18.8	18.9	18.3
S K	1.1	0.7	<0.1	0.2	0.3
K K	1.6	1.0	1.3	1.5	1.5
CaK	7.6	4.4	2.8	1.9	1.6
FeK	0.9	0.5	0.6	0.7	1.6

The above reaction (1) shows that a combination of pyrite oxidation and dissolution of calcite and dolomite results in the increase of dissolved sulfate in addition to the increase of dissolved Ca and Mg. ICP-OES results exhibited higher concentration of dissolved S at higher oxygen vol%, which was similar to dissolved sulfate–S concentration measured using a spectrophotometer for the same sample (Figure 3.8). This confirms that the rapid increase of dissolved S concentration in the presence of oxygen resulted from oxidative dissolution of pyrite. A significant increase of sulfate in the presence of oxygen affected the mobility of Ba. The significantly lower concentration of dissolved Ba in the presence of oxygen (<~100 µg/L Ba) than in the absence of oxygen (~400 µg/L Ba) is attributed to precipitation of barite (BaSO<sub>4</sub>) as a consequence of the significant increase in sulfate due to pyrite oxidation. PHREEQC modeling predicted that the CO<sub>2</sub>–brine reacted with Gothic shale in the presence of oxygen was oversaturated with respect to barite (SI > 1).

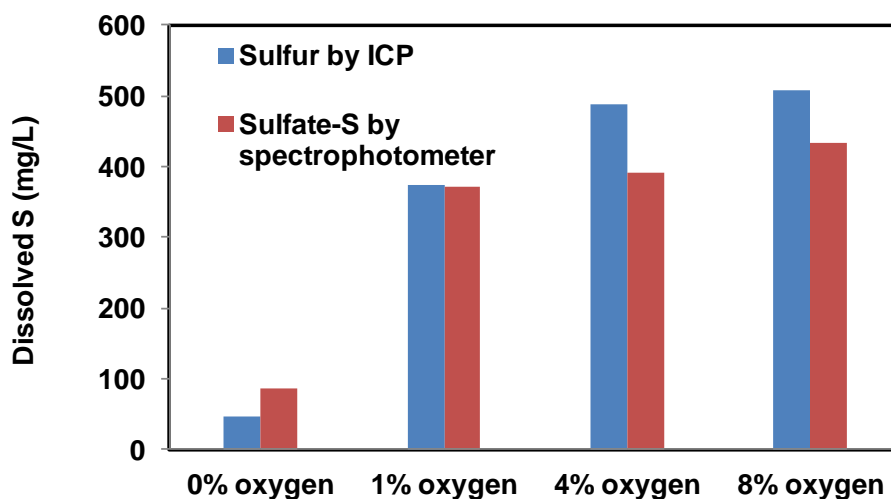


**Figure 3.8.** Speciation of Dissolved Sulfur after the Reaction between Gothic Shale and CO<sub>2</sub>–Brine for 6 Weeks. Dissolved S and sulfate were determined by ICP-OES and spectrophotometry, respectively.

Reaction (1) also indicates that the precipitation of Fe(III) oxides can occur at the pH (~4.8) buffered by the dissolution of calcite and dolomite subsequently after the oxidative dissolution of pyrite. Dissolved Fe concentrations mostly remained below about 10 mg/L in all vessels throughout the experiment, while dissolved S concentration increased to 250–500 mg/L in the vessels with oxygen during the reaction for 4–6 weeks (Figure 3.2 and Figure 3.6). CBD extractions confirm that the amount of Fe(III) oxide at the surfaces of Gothic shale was higher when the shale was reacted with CO<sub>2</sub>–brine at higher oxygen content. The average CBD extractable Fe(III) concentration from the Gothic shale was 648, 4,570, 9,075, and 8,450 mg/kg after 6 weeks of reaction with 0, 1, 4, and 8 vol% oxygen, respectively (Figure 3.9). Based on Reaction (1) and ICP-OES results for dissolved S, the concentration of Fe(III) in Gothic shale is predicted to be 9,844, 12,836, and 13,335 mg/kg for the reaction with 1, 4, and 8 vol% oxygen, respectively. The predicted Fe(III) concentrations are higher than the Fe(III) concentrations determined by the CBD extraction by 30%–50%, possibly because CBD extraction did not completely extract the precipitated Fe(III) oxide. The oxidative dissolution of pyrite and precipitation of Fe(III) oxides in the presence of oxygen are also suggested by semi-quantitative SEM-EDS results of the reacted shale (Table 3.3). The atom percentages of S (1.1 atom% prior to the reaction) measured on shale

samples were reduced after reaction with CO<sub>2</sub>-brines containing oxygen (<0.1–0.3 atom%) relative to those without oxygen (0.7 atom%), while the Fe atom percentage in the shale samples increased after reaction with CO<sub>2</sub>-brines in increasing oxygen content relative to no oxygen (Table 3.3).

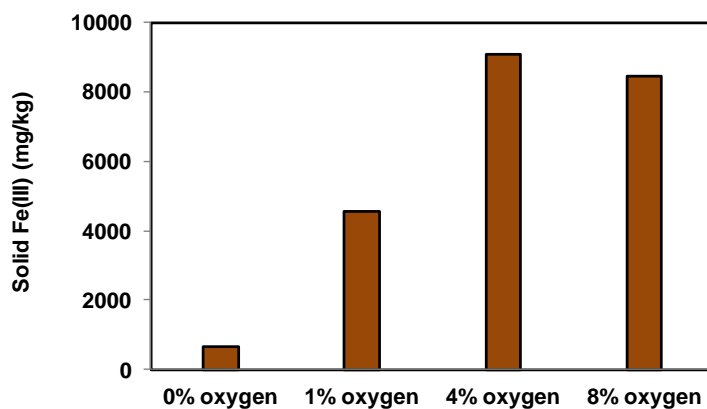


**Figure 3.9.** Fe(III) Concentration in Gothic Shale Determined by Citrate-Bicarbonate-Dithionite (CBD) Extraction after the 6-Week Reaction with CO<sub>2</sub>-Brine at a Range of Oxygen Content (0, 1, 4, and 8% by volume)

It appears that the pyrite oxidation–Fe(III) oxide precipitation also exerts a significant control on the mobility of toxic metals such as Mn and Ni. The behavior of dissolved Ni and Mn is correlated to that of dissolved Fe (Figure 3.10;  $R^2 = 0.43\text{--}0.80$  for Ni,  $R^2 = 0.43\text{--}0.45$  for Mn except for 1 vol% oxygen). The highest concentrations of Ni and Mn are found after the 8-day reaction in the vessel with 4 and 8 vol% oxygen, which is consistent with the mobilization pattern for dissolved Fe (Figure 3.6). This suggests that Mn and Ni were mobilized during the oxidation of pyrite on the surface of Gothic shale (Huertadiaz and Morse 1990; Larsen and Postma 1997; Sohlenius and Oborn 2004).

The source of Re in Gothic shale is uncertain, but organic-rich marine shale is often enriched with Re because anoxic marine sediments with high organic carbon content can efficiently scavenge oxyanion trace elements such as Re, Os, U, and Mo (Peucker-Ehrenbrink and Hannigan 2000). Oxidative black shale weathering is considered an important source of Re to river and seawater (Dalai et al. 2002; Jaffe et al. 2002). A positive correlation between oxygen content and dissolved Re observed from our experiments indicates that Re was mobilized possibly by the oxidative dissolution of pyrite or other sulfide minerals containing Re (Miller et al. 2011).

Substantially high concentrations of U (8–16  $\mu\text{g/L}$ ) were mobilized from Gothic shale during the reaction with CO<sub>2</sub>-brine for 1 day through 6 weeks. The source of U in Gothic shale is not certain, but black shale is frequently enriched with uranium of 10–100 ppm, and organic matter is considered directly or indirectly responsible for concentrating uranium in shale (Fisher and Wignall 2001; Swanson 1961). A negative correlation is found between the total dissolved U concentration and the CBD extractable Fe(III) oxide content (Figure 3.11). This suggests that the dissolved U concentration was partially controlled by Fe(III) oxides precipitated on the surfaces of the shale. Comparison between the ICP and KPA measurements for the same samples indicate that dissolved U was dominated by U(VI) in the presence of oxygen, whereas dissolved U was present as both U(VI) (9  $\mu\text{g/L}$ ) and U(IV) (5  $\mu\text{g/L}$ ) after the reaction

without oxygen (Figure 3.12). We speculate that U(IV) can be mobilized by CO<sub>2</sub>-brine only under anoxic condition, while U(VI) can be mobilized under either oxic or anoxic conditions.

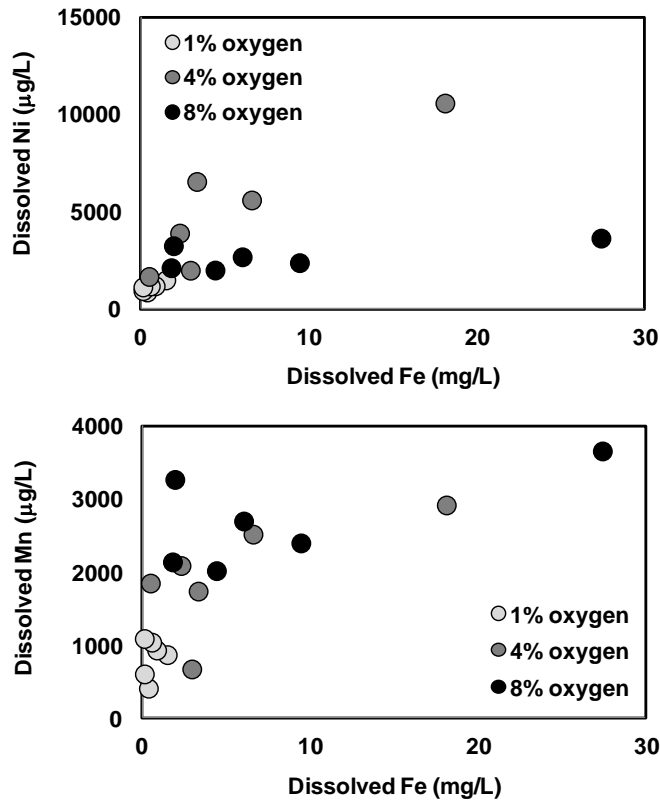


**Figure 3.10.** Correlation between Dissolved Fe and Dissolved Ni or Mn as a Function of Oxygen Content during Gothic Shale (6 g)-CO<sub>2</sub>-Brine (180 mL) Interaction for 6 Weeks

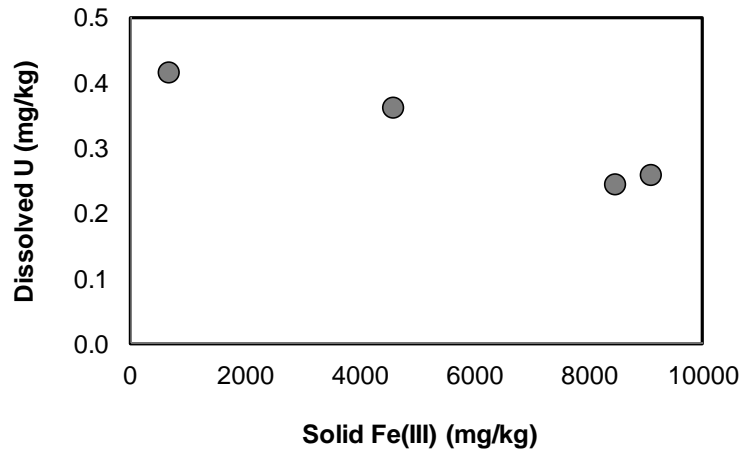


**Figure 3.11.** Correlation between Solid Phase Fe(III) in Gothic Shale (determined by CBD extraction) and Dissolved U Concentration

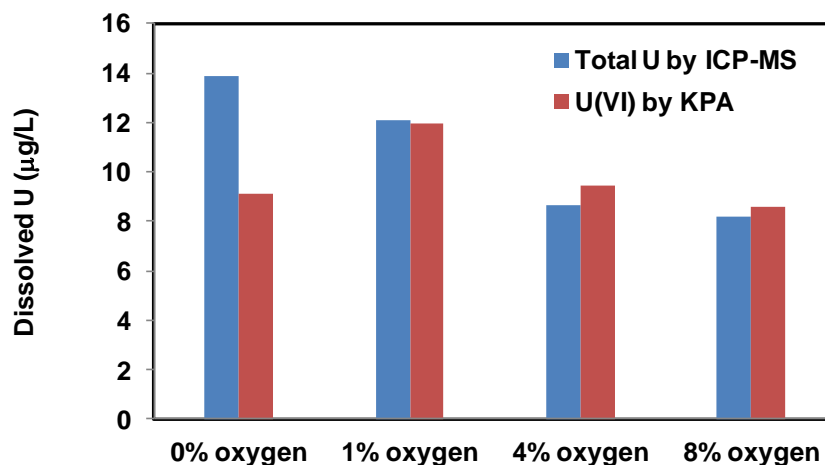


**Figure 3.12.** Speciation of Dissolved Uranium after the Reaction between Gothic Shale and CO<sub>2</sub>-Brine for 6 Weeks. Dissolved total U and U(VI) were determined by ICP-MS and KPA, respectively.

### 3.4.2 Environmental Implications

Our experimental results for the Gothic shale–CO<sub>2</sub>–brine interaction over a period of 4–6 weeks demonstrate that various toxic metals such as Ba, Mn, Ni, and U can be released from a shale caprock into brine during geologic carbon sequestration. The co-injection of oxygen during geologic carbon sequestration is likely to cause a significant elevation in dissolved Mn and Ni in the brine through interactions with Gothic shale. Under our batch experimental conditions, dissolved Mn and Ni increased up to 3,660 and 10,800 µg/L, respectively. The observed concentrations of Mn and Ni are higher than World Health Organization (WHO) guidelines (Mn: 400 µg/L, Ni: 70 µg/L) for drinking water by a factor of about 9 and about 154. Mn is a known neurotoxin, while Ni may damage the heart and liver.

Relatively high concentrations of Ba up to about 400 µg/L were mobilized in the absence of oxygen. These concentrations are lower than the EPA MCL (2 mg/L) and WHO guidelines (0.7 mg/L) for drinking water. When oxygen is present, oxidation of pyrite releases sulfate, resulting in significantly reduced Ba concentrations as a result of barite precipitation.

Interaction of the CO<sub>2</sub>–brine with Gothic shale also released significant concentrations of uranium. At rock-to-brine ratios of approximately 0.022 to 0.033 g/mL, dissolved U increased up to 14 µg/L in the absence of oxygen, and increased to 8 to 12 µg/L in the presence of oxygen. The quantity of U mobilized was equivalent to less than 0.5 mg/kg U relative to a total of 16 mg/kg U, suggesting that significantly higher concentrations of U could potentially be released from Gothic shale, depending on physical and chemical conditions. It could be expected that the higher rock-to-brine ratios that occur in actual reservoir conditions compared to laboratory experiments could result in higher concentrations of U leaching into the brine. For example, in our experiments, increasing the rock-to-brine ratio by a factor of about 5 resulted in an increase in dissolved U by a factor of approximately 2.

### 3.5 Conclusions

The potential impact of oxygen co-injected with carbon dioxide on mobilization of toxic contaminants from a caprock (Gothic shale from the Aneth Unit in a Utah carbon sequestration site) during geologic carbon storage was investigated. The relative volume percentage of O<sub>2</sub> to CO<sub>2</sub> was adjusted from 0% to 1%, 4%, and 8% in pressure vessels containing 4 or 6 g of crushed Gothic shale (sand-size fraction) and 180 mL of synthetic brine (0.1 M NaCl). Pressure and temperature were maintained at about 1,500 psi and about 75°C throughout the experiment for 4 or 6 weeks to simulate the conditions for deep geologic carbon sequestration. Mineralogical and chemical characterization of Gothic shale using SEM-EDS, XRD, XRF, and chemical extraction indicate that quartz, calcite, dolomite, montmorillonite, and pyrite are major mineral phases, and significant concentrations of Mn, Ni, Ba, Sr, Zn, and U are present in the shale.

ICP-OES analyses of brine leachates equilibrated with CO<sub>2</sub>/O<sub>2</sub> mixtures showed that dissolved S concentrations increased with higher oxygen content. Spectrophotometric analysis confirmed that the dissolved S was primarily in the form of sulfate. Dissolved Fe concentrations were an order of magnitude lower than dissolved S concentrations. This indicates that oxidative dissolution of pyrite occurred in the presence of oxygen and that Fe precipitated as Fe(III) oxides.

Dissolved Mn and Ni concentrations increased up to 3,660 and 10,800 mg/L in the presence of oxygen (4%–8%). These values are far higher than WHO guidelines for drinking water. Dissolved Ba increased up to 427 µg/L in the absence of oxygen, but increased to only 100–150 µg/L in the presence of oxygen. The lower concentrations of dissolved Ba that occurred in the presence of oxygen were attributed to precipitation of barite (BaSO<sub>4</sub>) because of high sulfate released during oxidative dissolution of pyrite.

During contact of Gothic shale with CO<sub>2</sub>-saturated brine over a period of 4–6 weeks, dissolved U increased to 8–14 µg/L; higher concentrations occurred at lower oxygen content. U mobility is likely controlled by sorption onto newly formed Fe(III) oxide precipitates during oxidative dissolution of pyrite in the presence of oxygen. Comparison between ICP-MS and KPA measurements indicated that U was mobilized as both U(IV) and U(VI) in the absence of oxygen, whereas dissolved U was predominantly in the form of U(VI) in the presence of oxygen.

Our data suggest that the co-injected oxygen in supercritical carbon dioxide during geologic carbon sequestration can result in significant oxidation of sulfide minerals in deep geologic formations. During co-injection of oxygen, oxidative dissolution of sulfide minerals and subsequently precipitation of Fe(III) oxides will occur and significantly impact the mobility of toxic contaminants. Elevated pressures resulting from injection of CO<sub>2</sub> into reservoirs for geologic carbon sequestration increase the potential of brine leakage through caprock fractures. In such scenarios, the groundwater quality of overlying drinking water aquifers could potentially be damaged by elevated concentrations of toxic contaminants such as Mn, Ni, Ba, and U released from caprock shale, depending on the redox state and the solubility.



## 4.0 Organic Mobilization and Transport in Geologic Carbon Sequestration

### 4.1 Introduction

Depleted oil reservoirs and deep saline aquifers are often sites selected as sites for CO<sub>2</sub> storage. Organic contents in depleted oil reservoirs are high due to the residual petroleum. Non-oil-bearing saline aquifer could also be the source of toxic organics during scCO<sub>2</sub> injection (Kharaka et al. 2006). The supercritical CO<sub>2</sub> (scCO<sub>2</sub>) is an excellent solvent for organic compounds (Kolak and Burruss 2006). Toxic organic compounds such as benzene, toluene, ethyl-benzene, xylene (BTEX), phenol, and polycyclic aromatic hydrocarbon (PAH) compounds can be effectively solubilized into scCO<sub>2</sub>. As a result, toxic organic compounds can be extracted by injected scCO<sub>2</sub> during carbon storage. If CO<sub>2</sub> leakage were to occur, the organic compounds could be transported into the aquifers overlying the carbon reservoir (Apps et al. 2010).

Groundwater monitoring results from carbon sequestration test fields have shown increased organic concentrations after CO<sub>2</sub> injection (Scherf et al. 2011; Kharaka et al., 2011, 2010, 2009). Concerns of groundwater contamination by toxic organics mobilized and leaked from geological carbon sequestration have been raised. The risk of groundwater contamination by toxic organics mobilized by scCO<sub>2</sub> injection in a geological carbon sequestration site must be addressed in order to gain public acceptance. Knowledge of the mobilization mechanism of organics and their fate and transport in the subsurface is essential in the overall risk assessment for the geological carbon sequestration.

In this study, mobilization of organics by scCO<sub>2</sub> from rock materials obtained from ongoing or planned carbon sequestration sites of EOR reservoirs or coal-bed methane projects across the United States were tested. Compounds that were studied include volatile organic compounds (VOCs), consisting of BTEX, propylbenzene, 1,3,5-trimethylbenzene, and semi-VOC including naphthalene, and alkanes (nC<sub>20</sub>-nC<sub>30</sub>). The kinetics of mobilization by dry and water-vapor-saturated scCO<sub>2</sub> was studied. The organic mobilization by scCO<sub>2</sub> was compared with the extraction by methylchloride (CH<sub>2</sub>Cl<sub>2</sub>). Column experiments were conducted to study the fate of scCO<sub>2</sub> mobilized organics.

### 4.2 Materials and Methods

Six lithological samples were used in the organic mobilization tests. These rock samples were collected from sites being tested or proposed as geological carbon sequestration sites. The locations and the descriptions of the rock samples are summarized in Table 4.1.

The rock samples were extracted by CH<sub>2</sub>Cl<sub>2</sub> (methylchloride) to quantify their initial organic compound content. Prior to extraction, the rock samples were crushed and sieved. Particles sized to less than 1.0 mm were used for the extractions. Five grams of rock particles were placed into 30 mL of CH<sub>2</sub>Cl<sub>2</sub>, and the mixture was sealed in a vial, which was then placed on a rotational mixer. After 7 days of extraction, the mixture was centrifuged to separate small rock particles, and the CH<sub>2</sub>Cl<sub>2</sub> was analyzed for organic compound concentrations.

**Table 4.1.** Lithological Samples Used in Tests

Sample No.	Rock Name	Location; Depth (ft)	Operation Performed	Operation Performed
Rock-1	Desert Creek limestone	Aneth Oil Field, Utah; 5398–5404	Limestone from depleted oil reservoir.	CO <sub>2</sub> enhanced oil recovery (EOR)
Rock-2	Gothic shale	Aneth Oil Field, Utah; 5390–5394	Caprock formation for Desert Creek limestone	NA
Rock-3	Fruitland coal	Pump Canyon Site, New Mexico; 3893	Coal	Enhanced coal-bed methane recovery by CO <sub>2</sub> injection.
Rock-4	Kirtland shale	Pump Canyon Site, New Mexico	Caprock formation for Fruitland coal	NA
Rock-5	Teapot Dome sandstone	Teapot Dome, Wyoming; 5409	Pennsylvanian Tensleep sandstone	CO <sub>2</sub> EOR
Rock-6	Goose Egg shale	Teapot Dome, Wyoming; 5300–5400	Goose Egg shale; caprock for Teapot Dome sandstone	CO <sub>2</sub> EOR

The experimental setup for organic mobilization by scCO<sub>2</sub> and transport is schematically shown in Figure 4.1. Batch mobilization experiments were conducted initially as shown in Figure 4.1 but without the sand column. The batch system consisted of a 100-mL reactor (Parr Instrument Company) with a heat jacket and temperature control system to extract the rock sample with scCO<sub>2</sub>. Rock samples (<1.0-mm particle sizes) was first placed in the reactor. No water was added to the rock sample for the dry scCO<sub>2</sub> mobilization tests. For experiments with water-saturated scCO<sub>2</sub>, a vial with 0.5 mL of deionized water was placed in the reactor prior to pressurizing the vessel with CO<sub>2</sub>. This allowed the scCO<sub>2</sub> to become saturated with water vapor under the test conditions. An ISCO pump was used to pressurize the CO<sub>2</sub>. The pressure and temperature could be adjusted to desired values and were monitored over the course of testing. A needle valve was used to control the flow of CO<sub>2</sub> release from the reactor during sampling. The released CO<sub>2</sub> flowed through two CH<sub>2</sub>Cl<sub>2</sub> baths, and the organic compounds mobilized by scCO<sub>2</sub> were trapped in the CH<sub>2</sub>Cl<sub>2</sub>. A flow meter was used to measure the gas flow rate. The reactor was installed with a system to monitor and record pressure over the course of the experiment and sampling. Stainless steel tubing (1/8-in. outer diameter) was used to connect the reactor with the CH<sub>2</sub>Cl<sub>2</sub> traps. The tubing was heated to 97°C during sampling to minimize condensation of organic compounds. The tubing was extracted with CH<sub>2</sub>Cl<sub>2</sub> to quantify any organic compounds that may have potentially condensed during sampling. The pressures and temperatures before and after sampling were used to calculate the CO<sub>2</sub> mass released from the reactor during sampling.

The columns containing porous media (Figure 4.1) were added to the system to study the transport and fate of the mobilized organic compounds. CO<sub>2</sub> with mobilized organic compounds was released from the reactor and injected through a column (2.54 cm inner diameter by 10 cm long) packed with Accusand. Experiments were performed with both dry sand and wetted (but unsaturated) sand. The wet sand column was established by first saturating the column with deionized water and then draining the column under ambient conditions. After passing through the column, the effluent gas from the column was directed through two CH<sub>2</sub>Cl<sub>2</sub> traps as shown in Figure 4.1. At the end of the experiments, the concentrations of organic compounds both in the column effluent and trapped in the sand column were analyzed. To quantify the organic compounds that condensed in the column, the sands were extracted with CH<sub>2</sub>Cl<sub>2</sub>. Stainless steel tubing (1/8 in.) was used to connect the reactor and the column. This tubing was

also heated and extracted as described above. A total of five column experiments were conducted. Table 4.2 summarizes the tests that were completed.

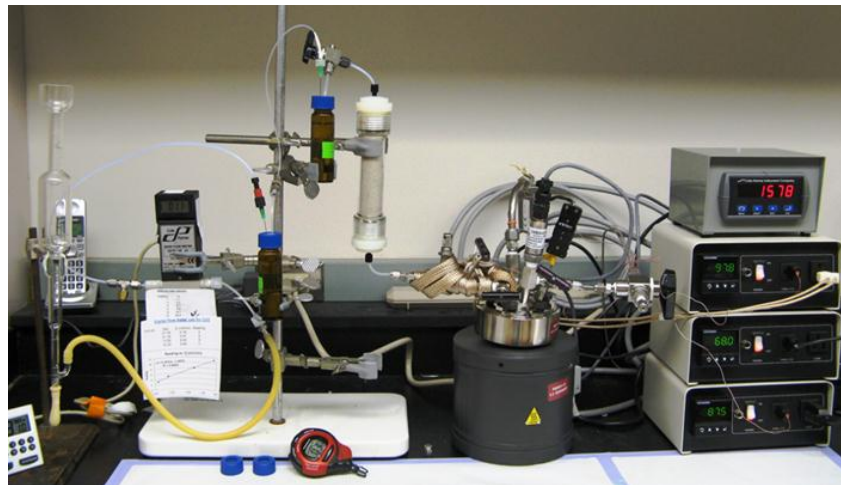
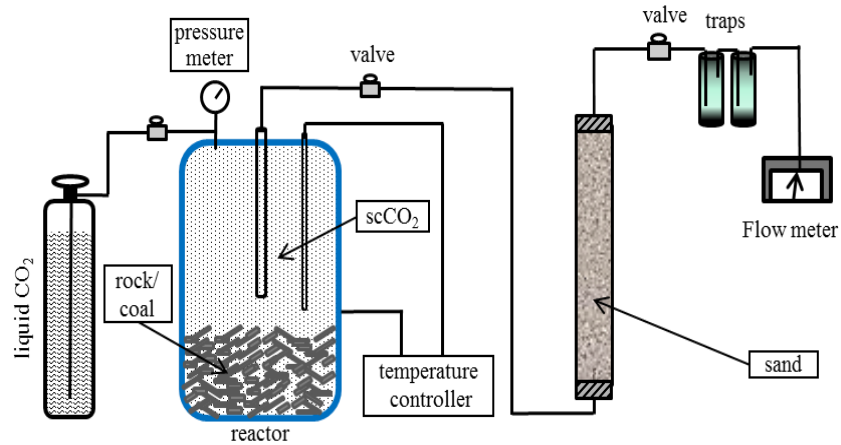


**Figure 4.1.** Schematic of Organic Mobilization and Transport Experimental Setup and Photo of Testing System

**Table 4.2.** Summary of Column Tests Completed

Test Name	Description Packing; Wet/Dry scCO <sub>2</sub> ; Effluent P	Rock for Extraction	P(psi)/T(°C)	Sampling Approach
Col-1	Dry Accusand; Dry CO <sub>2</sub> ; 0 psi	Fruitland coal	1500/65	2 CH <sub>2</sub> Cl <sub>2</sub> traps in effluent; sand extraction with CH <sub>2</sub> Cl <sub>2</sub>
Col-2	Dry Accusand; Wet CO <sub>2</sub> ; 0 psi	Fruitland coal	1500/95	2 CH <sub>2</sub> Cl <sub>2</sub> traps in effluent; sand extraction with CH <sub>2</sub> Cl <sub>2</sub>
Col-3	Wetted Accusand; Wet CO <sub>2</sub> ; 0 psi	Fruitland coal	1500/95	2 CH <sub>2</sub> Cl <sub>2</sub> traps in effluent; sand and water extraction with CH <sub>2</sub> Cl <sub>2</sub>
Col-4	Wetted Accusand; Wet CO <sub>2</sub> ; 0 psi	Gothic shale	1500/95	2 CH <sub>2</sub> Cl <sub>2</sub> traps in effluent; sand and water extraction with CH <sub>2</sub> Cl <sub>2</sub>
Col-5	Wetted Accusand; Wet CO <sub>2</sub> ; 0 psi	Teapot Dome sandstone	1500/95	2 CH <sub>2</sub> Cl <sub>2</sub> traps in effluent; sand and water extraction

An Agilent Technologies 5975C gas chromatograph mass spectrometer (GC-MS) system was used to identify and quantify the organic compounds. An Agilent capillary column (0.25 mm × 30 m × 0.25 μm) was applied to separate the organic compounds. Commercial standards were obtained for GC-MS calibration. The temperature for the GC column was initially set at 32°C and held for 2 min. The temperature was then ramped up at 5°C/minute until 280°C and then held for 5 min. A set of VOCs, semi-VOCs, and alkanes can be identified and quantified using the method. Toxic organic compounds such as BTEX and naphthalene were studied. Additional VOCs including iso-propylbenzene, propylbenzene, 1,3,5-trimethylbenzene and normal alkanes (nC20–nC30) were also included in this study. The compounds and their basic properties are listed in Table 4.3.

**Table 4.3.** Organic Compounds Studied

Chemical Name	Formula	Retention Time (min)	MCL (mg/L)
Benzene	C <sub>6</sub> H <sub>6</sub>	3.228	0.005
Toluene	C <sub>7</sub> H <sub>8</sub>	4.586	1.0
Ethylbenzene	C <sub>8</sub> H <sub>10</sub>	6.694	0.7
m-Xylene and p-Xylene	C <sub>8</sub> H <sub>10</sub>	6.911	10 (total)
o-Xylene	C <sub>8</sub> H <sub>10</sub>	7.550	10 (total)
Iso-Propylbenzene	C <sub>9</sub> H <sub>12</sub>	8.475	
Propylbenzene	C <sub>9</sub> H <sub>12</sub>	9.358	
1,3,5-Trimethylbenzene	C <sub>9</sub> H <sub>12</sub>	9.812	
1,2,4-Trimethylbenzene	C <sub>9</sub> H <sub>12</sub>	10.594	
Tert-butyl-Benzene	C <sub>10</sub> H <sub>14</sub>	10.573	
Sec-Butylbenzene	C <sub>10</sub> H <sub>14</sub>	11.139	
p-Isopropyltoluene	C <sub>10</sub> H <sub>14</sub>	11.583	
Butylbenzene	C <sub>10</sub> H <sub>14</sub>	12.581	NA
Naphthalene	C <sub>10</sub> H <sub>8</sub>	16.555	NA (possible human carcinogen)
<i>n</i> -Decane	C <sub>10</sub> H <sub>22</sub>	10.79	
<i>n</i> -Icosane	C <sub>20</sub> H <sub>42</sub>	36.69	
<i>n</i> -Docosane	C <sub>22</sub> H <sub>46</sub>	40.51	
<i>n</i> -Tetracosane	C <sub>24</sub> H <sub>50</sub>	44.01	
<i>n</i> -Hexacosane	C <sub>26</sub> H <sub>54</sub>	47.24	
<i>n</i> -Octacosane	C <sub>28</sub> H <sub>58</sub>	50.26	
<i>n</i> -Triacotane	C <sub>30</sub> H <sub>62</sub>	53.72	

## 4.3 Results and Discussion

### 4.3.1 Results of Organic Compound Extractions with Methylene Chloride

The CH<sub>2</sub>Cl<sub>2</sub> extractable concentrations of organic compounds were used as an indicator of the organic content in the rock samples and to determine a baseline for comparison with the organic compounds mobilized by scCO<sub>2</sub>. The CH<sub>2</sub>Cl<sub>2</sub> extractable concentrations of organic compounds are listed in Table 4.4. Rock-3 (Fruitland coal) showed the highest VOC and semi-VOC compound concentrations,

followed by Rock-2 and Rock-1. The other rocks showed very low extractable organic compound concentrations. Rock-4 (Kirtland shale) had the highest alkane concentrations, followed by Rock-3, Rock-5, Rock-1, Rock-2, and Rock-6. The focus of this study was the mobilization of VOCs and semi-VOCs; therefore, primarily Rock-3 and Rock-2 were used in subsequent tests because they had relative higher concentrations of these compounds.

**Table 4.4.** Organic Compound Concentrations Extracted by CH<sub>2</sub>Cl<sub>2</sub> from Rock Samples (mg/kg)

	Rock-1	Rock-2	Rock-3	Rock-4	Rock-5	Rock-6
Toluene	1.61	4.62	210.00	0.36	0.36	0.42
Ethylbenzene	0.00	2.28	5.34	0.00	0.00	0.06
Xylene (m&p)	0.00	4.14	98.34	0.00	0.00	0.00
Xylene (o)	0.00	4.92	83.64	0.00	0.00	0.00
Isopropylbenzene	0.00	1.02	1.68	0.00	0.00	0.00
Propylbenzene	0.00	1.56	4.32	0.00	0.00	0.00
1,3,5-Trimethylbenzene	0.00	2.88	24.00	0.00	0.00	0.00
Tert-Butylbenzene	0.00	1.32	8.16	0.00	0.00	0.00
1,2,4-Trimethylbenzene	0.08	10.26	64.32	0.00	0.00	0.00
Sec-Butylbenzene	0.00	1.08	1.86	0.00	0.00	0.00
P-Isopropyltoluene	0.00	0.54	1.02	0.00	0.00	0.00
Butylbenzene	0.00	1.20	2.40	0.00	0.00	0.00
Naphthalene	0.61	2.34	99.30	0.00	0.00	0.00
<i>n</i> -Decane (C <sub>10</sub> H <sub>22</sub> )	1.14	39.48	282.06	0.48	0.30	0.30
<i>n</i> -Icosane (C <sub>20</sub> H <sub>42</sub> )	68.09	69.48	487.32	10.26	193.26	0.48
<i>n</i> -Docosane (C <sub>22</sub> H <sub>46</sub> )	100.06	48.48	629.70	700.74	188.28	2.04
<i>n</i> -Tetracosane (C <sub>24</sub> H <sub>50</sub> )	100.74	27.36	808.98	1436.52	192.36	3.54
<i>n</i> -Hexacosane (C <sub>26</sub> H <sub>54</sub> )	82.95	21.06	782.10	1256.88	164.40	2.46
<i>n</i> -Octacosane (C <sub>28</sub> H <sub>58</sub> )	56.22	14.34	602.58	788.04	141.00	2.34
<i>n</i> -Triacontane (C <sub>30</sub> H <sub>62</sub> )	56.68	13.86	293.94	459.84	105.78	1.20

A comparison of the CH<sub>2</sub>Cl<sub>2</sub> extractable alkane concentrations from the Desert Creek limestone (Rock-1) and its caprock Gothic shale (Rock-2) is shown in Figure 4.2. Very low concentrations of C<sub>10</sub>H<sub>22</sub> alkane were extractable from the depleted oil reservoir limestone relative to the Gothic shale, while much higher C<sub>20</sub>H<sub>42</sub> alkanes and alkanes with higher carbon number could be extracted from the depleted oil reservoir limestone relative to the Gothic shale. These results suggest that the reservoir flushing by scCO<sub>2</sub> during the EOR process might have recovered most of the light alkanes while the recovery of heavier alkanes was more limited.

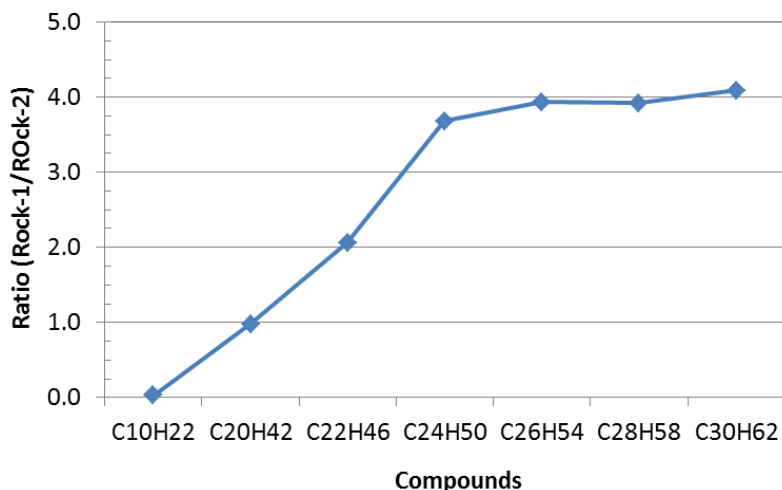


**Figure 4.2.** Ratio of  $\text{CH}_2\text{Cl}_2$  Extractable Alkane Concentrations of Desert Creek Limestone (Rock-1) Relative to its Caprock Gothic Shale (Rock-2) (pressure = 1500 psi and  $65^\circ\text{C}$ ).

### 4.3.2 Organic Compound Mobilization from Gothic Shale (Rock-2)

Organic compounds extracted from Gothic shale (Rock-2) relative to those that were extractable by  $\text{CH}_2\text{Cl}_2$  are shown in Figure 4.3. After 7 days reaction time, the  $\text{scCO}_2$  extracted more VOCs and semi-VOCs from the shale compared to  $\text{CH}_2\text{Cl}_2$  extraction. In contrast,  $\text{scCO}_2$  extractable  $n\text{C}_{10}$  and  $n\text{C}_{20}$  alkane concentrations were much lower than were extractable by  $\text{CH}_2\text{Cl}_2$  for the same reaction times. Alkanes with 22 and higher carbons were virtually non-extractable by  $\text{scCO}_2$ .

The extraction of organic compounds from dry versus water-saturated  $\text{scCO}_2$  is compared in Figure 4.4. There were no significant differences in the extractability of the organic compounds ethylbenzene through butylbenzene between the dry and water-saturated  $\text{scCO}_2$ . In the case of toluene, significantly less was mobilized by the water-saturated  $\text{scCO}_2$  than by the dry  $\text{scCO}_2$ . In contrast, significantly more naphthalene was extracted by the water-saturated  $\text{scCO}_2$  than by the dry  $\text{scCO}_2$ .

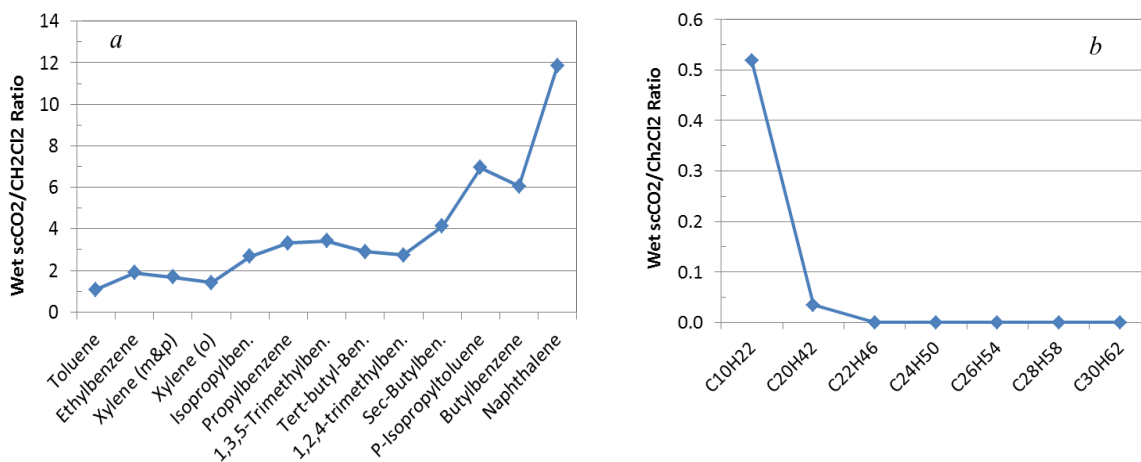


**Figure 4.3.** Extraction of VOCs, semi-VOCs, and Alkanes from Gothic Shale by  $\text{scCO}_2$  (pressure = 1500 psi and  $65^\circ\text{C}$ ) and  $\text{CH}_2\text{Cl}_2$ . a) VOCs and semi-VOCs; b) alkanes).

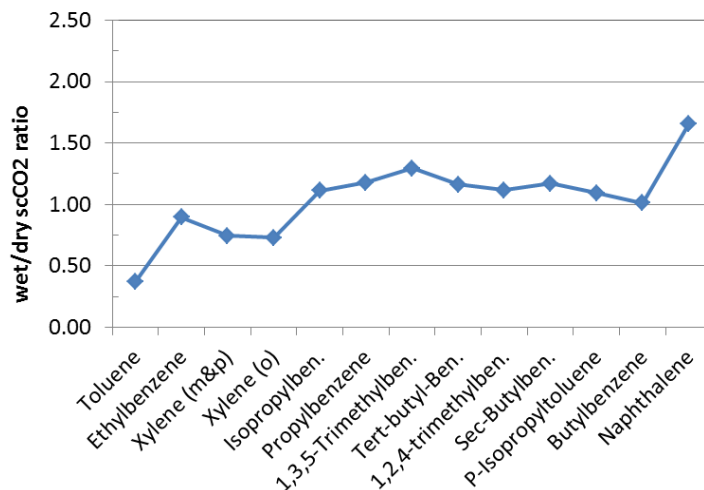


**Figure 4.4.** Comparison between Concentration of Organic Compounds Extracted by Dry scCO<sub>2</sub> and Water-Saturated scCO<sub>2</sub> (pressure = 1500 psi and 65°C).

### 4.3.3 Organic Compound Mobilization from Fruitland Coal (Rock-3)

The results of organic compound extraction using dry and water-saturated scCO<sub>2</sub> from the Fruitland coal (Rock-3) are presented in Table 4.5. The BETX concentrations at different reaction times indicate that the extraction by water-saturated scCO<sub>2</sub> for these compounds reached equilibrium at or before 96 h (Table 4.5; Figure 4.5), whereas the extractable concentrations for these organic compounds continued to increase from 96 to 216 h during extraction with dry scCO<sub>2</sub>.

Figure 4.6 shows the percentage of organic compounds that were extracted from Fruitland coal by scCO<sub>2</sub> relative to that extracted by CH<sub>2</sub>Cl<sub>2</sub>. Under the tested pressure and temperature conditions (1500 psi, 65°C), only fractional amounts, if any, of the CH<sub>2</sub>Cl<sub>2</sub> extractable organic compounds were extracted by scCO<sub>2</sub>. Lighter compounds were more susceptible to mobilization by scCO<sub>2</sub> compared to heavier compounds. Very minor amounts of C<sub>10</sub>H<sub>22</sub> were mobilized by scCO<sub>2</sub> and essentially none for higher-carbon alkanes.

### 4.3.4 Fate and Transport of Organic Compounds Mobilized by scCO<sub>2</sub>

#### 4.3.4.1 Transport of Organic Compounds Through Dry Media

The results of organic compound transport through dry sand columns are presented in Figure 4.7. More than 40% of the lighter compounds (benzene, toluene) entering the column was transported through the sand column with the CO<sub>2</sub> gas (less than 60% was sorbed onto the sand). For most of the heavier organic compounds, over 90% was trapped in the sand column. There was no significant difference between the transport behavior between organic compounds mobilized by dry versus water-saturated scCO<sub>2</sub> (Figure 4.7a versus Figure 4.7b).

**Table 4.5.** Organic Compound Concentrations Extracted from Fruitland Coal with scCO<sub>2</sub> (pressure = 1500 psi and 65°C)

Compounds	Water-Saturated scCO <sub>2</sub> Concentration (mg/kg)			Dry scCO <sub>2</sub> Concentration (mg/kg)		
	24 h	96 h	216 h	24 h	96 h	216 h
	Benzene	37.17	61.02	63.57	36.77	44.88
Toluene	69.46	105.05	111.14	90.10	91.83	133.10
Ethylbenzene	1.77	1.92	0.00	1.87	2.13	2.98
m-Xylene and m-Xylene	24.24	35.43	35.89	26.54	33.62	45.20
o-Xylene	17.56	25.11	15.63	19.25	22.03	30.36
Isopropylbenzene	1.56	0.00	0.00	0.00	0.22	0.00
Propylbenzene	1.86	0.79	0.44	0.00	0.37	0.89
1,3,5-Trimethylbenzene	4.38	6.95	0.65	2.96	5.18	6.29
Tert-Butylbenzene	0.00	2.33	0.00	0.73	0.44	0.40
1,2,4-Trimethylbenzene	3.85	12.47	7.32	8.09	9.81	10.30
Sec-Butylbenzene	0.88	1.88	0.00	0.15	0.00	0.34
p-Isopropyltoluene	1.11	0.00	0.00	0.00	0.19	0.00
Butylbenzene	1.46	0.00	0.00	0.25	0.00	0.00
Naphthalene	9.54	7.77	3.27	4.76	3.18	4.76

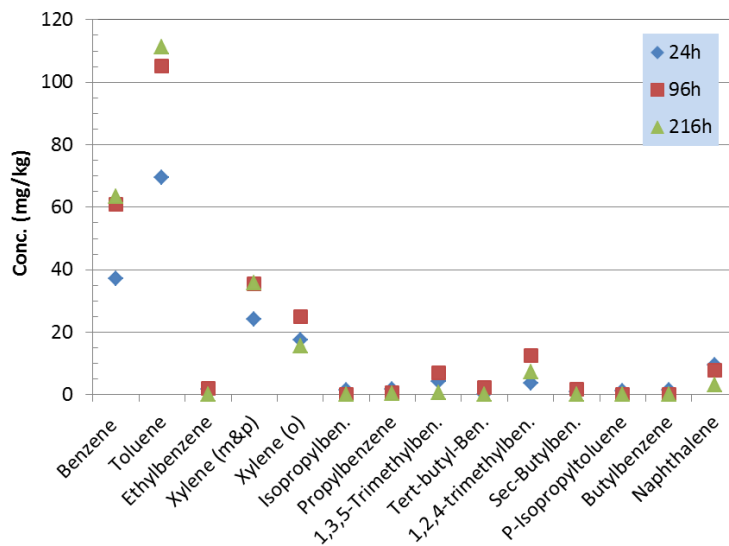


**Figure 4.5.** Extracted Organic Compound Concentration from Fruitland Coal versus Reaction Time for Water-Saturated scCO<sub>2</sub> (pressure = 1500 psi and 65°C)

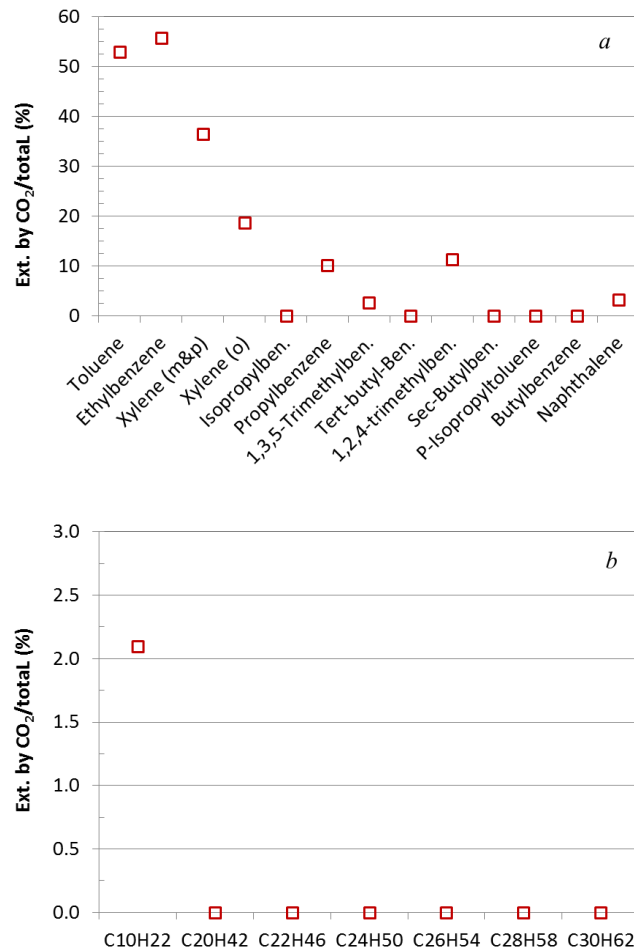


**Figure 4.6.** Comparison Organic Compounds Extractable by scCO<sub>2</sub> versus CH<sub>2</sub>Cl<sub>2</sub>. a) VOCs and Semi-VOCs; b) Alkanes (pressure = 1500 psi and 65°C).

#### 4.3.4.2 Transport of Organic Compounds Through Wet Media

The percentage of organic compounds that were transported through wet sand columns is illustrated in Figure 4.8. Moisture in the column sediment induced remarkable changes in the mobility of the organic compounds through the column. When the sand was damp (with 13.7 wt% of water), the majority (>82%) of all the tested organics were transported through the sand column except naphthalene. Only 16% of naphthalene passed through the sand column in the effluent. The mass percentages of organic compounds that moved through the columns were similar for all three source rock samples. For Col-5 (Figure 4.8c), many compounds moved completely through the column (virtually no adsorption; concentrations were below the detection limit). The differences in the transport behavior of the organic compounds observed between the wet and dry sand appear to be due to a combination of the hydrophobic nature of these organic compounds and their volatility. The presence of a layer of water on the sand is enough to prevent their sorption of the more volatile organics onto the sand grains. In the case of naphthalene, its lower volatility is not sufficient to prevent it from condensing from the gas phase, despite its hydrophobicity.

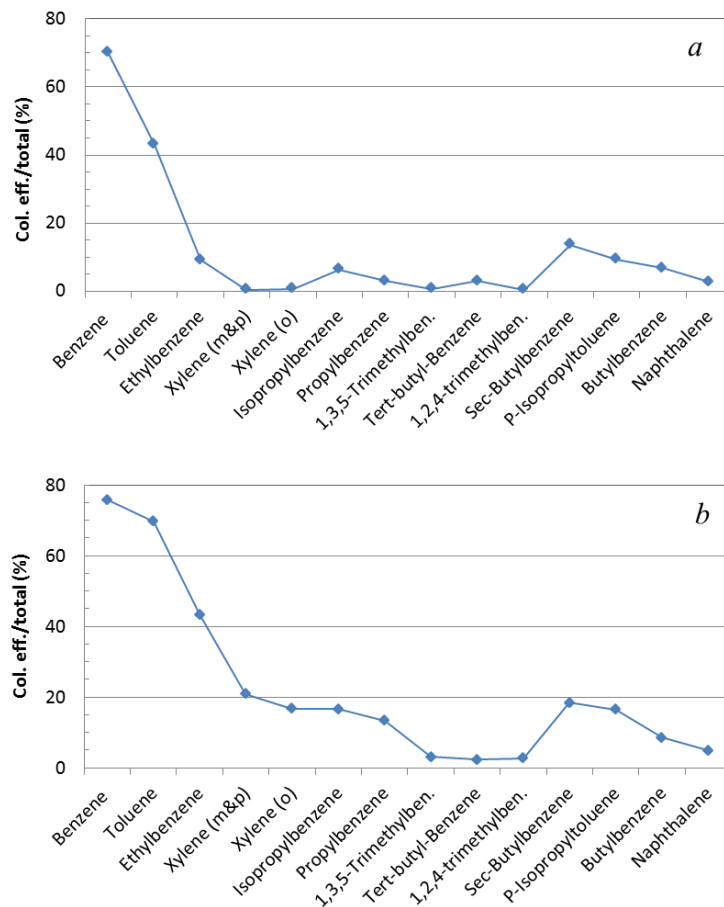


**Figure 4.7.** Percentage of Organic Compounds Transported Through Dry Sand Columns. a) mobilized by dry scCO<sub>2</sub>; b) mobilized by water-saturated scCO<sub>2</sub>.

## 4.4 Summary and Conclusions

Methods to evaluate the mobilization and transport of organic compounds from geologic carbon sequestration reservoir rocks by scCO<sub>2</sub> were developed. A set of rock samples from several potential carbon sequestration sites was tested. The mobilization of VOCs and semi-VOCs, including BTEX, and alkanes, was evaluated.

Extraction by scCO<sub>2</sub> mobilized more VOCs and semi-VOCs from Gothic shale compared to CH<sub>2</sub>Cl<sub>2</sub> extraction, while the extractability of alkanes was much less than that for CH<sub>2</sub>Cl<sub>2</sub> extraction. Dry scCO<sub>2</sub> extracted more toluene but less naphthalene than wet scCO<sub>2</sub>. The differences in the extractability between dry scCO<sub>2</sub> and water-saturated scCO<sub>2</sub> for other organic compounds was insignificant.

For Fruitland coal, no significant differences were observed between the extractability of organic compounds by dry or water-saturated scCO<sub>2</sub>. Reaction equilibrium appears to have been reached by 96 h. Lighter compounds were more susceptible to mobilization by scCO<sub>2</sub> compared to heavier compounds. Alkanes demonstrated very low extractability by scCO<sub>2</sub>.

When the scCO<sub>2</sub> was released from the reactor, less than 60% of the injected lighter compounds (benzene, toluene) were transported through the dry sand column by the CO<sub>2</sub>, while more than 90% of the heavier organics was trapped in the sand column. For wet sand columns, most (80% to 100%) of the organic compounds injected into the sand column except for naphthalene passed through; naphthalene was substantially removed from the CO<sub>2</sub> within the column.

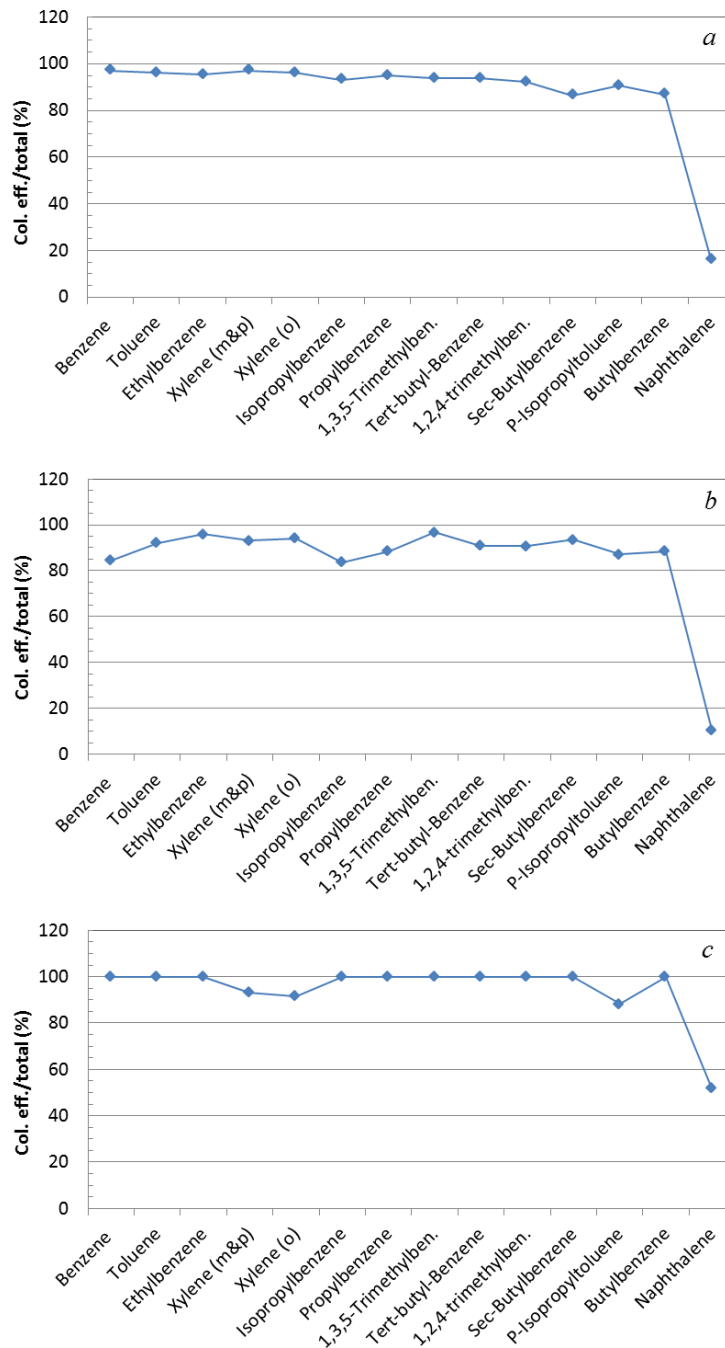


**Figure 4.8.** Percentage of Organic Compounds Transported Through Wet Sand Columns. Source of organic compounds: a) Fruitland coal (Col-3); b) Gothic shale (Col-4); c) Teapot Dome sandstone (Col-5).



## 5.0 In Situ pH Determination Under Geologic CO<sub>2</sub> Sequestration Conditions

### 5.1 Introduction

Injection of CO<sub>2</sub> into geologic formations (often referred to as geologic CO<sub>2</sub> sequestration or GCS) may induce release of toxic metal contaminants from preexisting rocks due to the acidification of brine. If these contaminated brines were to escape the storage reservoir through a fracture, fault, or abandoned well, there is the potential to contaminate overlying aquifers containing valuable freshwater resources. To understand subsurface geochemical reactions that induce toxic metal release, the ability to accurately measure changes in pH associated with GCS is essential. In some previous studies, *ex situ* pH measurements with glass electrodes were made on aqueous samples taken from high-pressure vessels or deep reservoirs in field sites (Daval et al. 2011; Palandri et al. 2005; Suto et al. 2007; Xu et al. 2010), which apparently induced large errors due to the rapid degassing of CO<sub>2</sub> at ambient pressure. A few studies have utilized commercially available high-pressure pH electrodes for pH measurements in rock–CO<sub>2</sub>–brine systems under GCS conditions (Schaefer et al. 2010; Shao et al. 2010; Yang et al. 2011). The accuracy of potentiometric pH determinations, however, may be adversely influenced by potential drift, variation in liquid junction potential, and asymmetric potential variations (Bates 1973; Liu et al. 2006). In addition, the use of glass pH electrodes is problematic under supercritical conditions because a sudden decrease in pressure can cause rapid outgassing of CO<sub>2</sub> from the filling solution and possible damage to the electrode. Consequently, many experimental studies at GCS conditions have relied on thermodynamic modeling to estimate the pH of their reaction systems (Carroll et al. 2011; Luquot and Gouze 2009; Prigiobbe and Mazzotti, 2011; Wigand et al. 2008). Thermodynamic models may also be imperfect and can result in significant errors in pH (Gundogan et al. 2011; Thomas et al. 2012). Biases can result from 1) incomplete or incorrect thermodynamic data for the conditions and components under consideration, 2) uncertainties in the mineral composition, 3) lack of attainment of equilibrium, and 4) limitations of the approaches used to account for ionic strength effects and fugacity at high pressure.

Spectrophotometric techniques using colorimetric pH indicators offer an alternative to potentiometric pH measurement and thermodynamic modeling approaches (Hopkins et al. 2000; Liu et al. 2006; Robert-Baldo et al. 1985; Usha and Atkinson 1992). In buffered solutions, the absorbance spectrum of an indicator is responsive to the solution pH, temperature, pressure, and ionic strength. Thus, at a designated temperature, pressure, and ionic strength, the spectrum of an indicator should be relatable to the pH of the buffer solution. For example, sulfonephthalein dyes, such as bromophenol blue (BPB) and phenol red, exhibit distinct changes in their absorbance characteristics within their useful pH ranges (Bates 1973; Robert-Baldo et al. 1985). Compared to potentiometric techniques, spectrophotometric pH measurements are more stable and sensitive to small changes in pH (Robert-Baldo et al. 1985) and have been used successfully to determine the pH of aqueous solutions at high pressure and low temperature in the deep-sea environment (Hopkins et al. 2000; Robert-Baldo et al. 1985; Usha and Atkinson 1992). To the best of our knowledge, no current study has used spectrophotometry to systematically determine pH under GCS-relevant conditions. Toews et al. (1995) used spectrophotometry to measure pH for the CO<sub>2</sub>–H<sub>2</sub>O system at pressures ranging from 70 to 200 atm and temperatures from 25°C to 70°C (Toews et al. 1995). That study has limited applicability to GCS because the effects of pressure and ionic strength on their calibrations were not considered (see our discussion below).

The objective of this research was to develop an in situ spectrophotometric method for pH determination under GCS conditions using BPB as an indicator. Specifically, we aimed to 1) measure pH in simulated brine (CO<sub>2</sub>-NaCl-H<sub>2</sub>O) systems under variable pressure, temperature, and ionic strength, and compare the results with pH values from other experimental studies and available geochemical models; 2) evaluate the merits of different data analysis methods; and 3) measure pH for a CO<sub>2</sub>-brine system in contact with basalt rock from a GCS field site. This work provides a quantitative basis for the use of spectrophotometry for in situ pH measurement under GCS-relevant conditions.

## 5.2 Materials and Methods

### 5.2.1 Chemical and Rock Samples

Citrate buffer solutions were prepared by combining measured quantities of the stock solutions (0.2 *m*) of citric acid or its sodium salts. The total citrate concentration was 0.01 *m* for all of the buffer solutions, and the ionic strengths were in the range of 0.003–0.02 *m*. High ionic strength (1, 2, and 3 *m*) buffer solutions were made with sodium chloride. The concentration of BPB in the buffer solution was  $1.19 \times 10^{-5}$  *m*. The pH<sub>*m*</sub> of citrate buffer solutions at ambient pressure and variable temperatures was measured with a ROSS Ultra pH electrode and a pH meter in the absolute millivolt mode.

The basalt rock sample used in this study was from the Wallula Basalt Pilot CO<sub>2</sub> Sequestration Project at Wallula, Washington. The rock was taken from the injection zone at 832 m below ground surface. Semi-quantitative XRD analysis indicated that the rock contains 45% (by weight) andesine (Na<sub>0.499</sub>Ca<sub>0.491</sub>Al<sub>1.488</sub>Si<sub>2.506</sub>O<sub>8</sub>), 15% anorthite (Ca<sub>0.63</sub>Na<sub>0.37</sub>Al<sub>1.63</sub>Si<sub>2.37</sub>O<sub>8</sub>), and 40% augite [(Mg<sub>0.81</sub>Fe<sub>0.15</sub>Al<sub>0.03</sub>Ti<sub>0.01</sub>)(Ca<sub>0.76</sub>Na<sub>0.02</sub>Mg<sub>0.04</sub>Fe<sub>0.17</sub>Mn<sub>0.01</sub>)(Si<sub>1.92</sub>Al<sub>0.08</sub>O<sub>6</sub>)]. Preparation of the rock sample included crushing and sieving to collect the 0.05–1.00-mm size fraction, washing and sonicating in water to remove small particles, and drying. Elemental analysis results for wash water suggested the loss of major elements was well below 0.1 mg/g dried sample. The BET surface area of the cleaned sample was  $12.9 \pm 0.1$  m<sup>2</sup>/g (the uncertainty is one standard deviation of triplicate measurements).

### 5.2.2 Instrumentation

Ultraviolet-visible (UV-Vis) spectra over the range 300–1100 nm were measured with an Agilent 8453 diode-array spectrophotometer controlled by a computer with Agilent ChemStation software. Samples containing BPB were placed inside a custom-designed high-pressure vessel (Parr Instrument Company, Moline, Illinois) equipped with integral 1.27-cm-diameter quartz windows on opposite sides to allow the light beam to pass through the vessel. The internal volume of the vessel was 100 mL, and the optical path length was approximately 6.4 cm. The high-pressure vessel used in the research was constructed with HC alloy-276. To avoid potential contamination from dissolution of the vessel's internal surfaces, a glass liner was placed inside the vessel. Temperature was regulated by a controller (Parr Model 4848) that supplied power to an embedded cartridge heater based on the response of a thermocouple suspended inside the vessel. The vessel was also equipped with a magnetic drive and a stir shaft to allow mixing. A syringe pump (Model 500D, Teledyne Isco, Inc., Lincoln, Nebraska) was used to charge the vessel with high-purity gases (nitrogen or CO<sub>2</sub>) from cylinders to the desired pressure.

The spectra of BPB in citrate buffer solutions were measured as follows. Approximately 50 mL of solution were added to the glass liner inside the pressure vessel, and a spectrum was collected after

thermal equilibrium had been reached at the desired temperature. A citrate buffer without BPB served as a blank and was subtracted from the spectra of BPB samples automatically by the software. Baseline shifts in the spectra were reduced by either a single-point offset correction at 700 nm or by subtracting the line fit through the absorbance between 340 and 690 nm (i.e., sloped baseline correction).

The procedures for measuring  $e_1$ ,  $e_2$  and  $e_3$  for BPB as a function of temperature and pressure closely followed those by Hopkins et al. (2000), except that the pH of the acid solutions was adjusted to approximately 1.5 by adding 0.5 *m* HCl solution, and the base solution was 0.01 *m* phosphate buffer solution (pH = 7.0). As reported previously, the first dissociation constant of BPB is approximately 0.95, and the second dissociation constant is approximately 4.20 (Shapovalov 2010), which justified the use of pH 1.5 and 7.0 for  $H^+$  and  $I^{2-}$  molar absorbance measurements, respectively. The pressure effect on  $e_1$ ,  $e_2$ , and  $e_3$  was measured by collecting the spectra of BPB in acid and base solutions under variable nitrogen pressures (1–180 atm).

For experiments in  $CO_2$ –NaCl– $H_2O$  systems, pure water or NaCl solutions were first added to the liner inside the vessel. When the sample reached thermal equilibrium at the desired temperature, a blank spectrum was collected. BPB was then added to the solution (final concentration of  $1.19 \times 10^{-5}$  *m*), the reactor was sealed, and  $CO_2$  was introduced into the reactor. For some experiments, the solution was stirred to accelerate the dissolution process. Spectra were collected every 10 min until equilibrium was reached, which usually required 2–10 h, depending on the pressure, temperature, ionic strength, and stirring rate.

In situ  $pH_m$  for the rock– $CO_2$ –brine system was measured at 75°C and 100 atm. Procedures similar to those described above were used, except 1) the solution was not stirred in order to simulate conditions in areas far from the injection well in  $CO_2$  sequestration reservoirs; 2) rock sample was added to a 1 *m* NaCl solution with a solid-to-solution ratio of 1:45 (by weight); and 3) before  $CO_2$  introduction, the rock–NaCl system was sparged with nitrogen for 20 min to remove any oxygen. To calculate the  $pH_m$  in the rock– $CO_2$ –brine system with geochemical models, we also conducted a rock dissolution experiment in order to monitor the chemical composition change in the aqueous phase. The experiment was conducted in a 300-mL Parr high-pressure vessel. Experimental conditions were the same as in the pH measurement experiment described above. Aqueous samples were collected at desired times for elemental analysis.

### 5.2.3 Data Analysis

Two approaches for the spectrophotometric determination of pH are the absorbance ratio method (ARM) and a model-based regression approach referred to as chemical modeling regression (CMR). Both protocols utilize differences in the spectra of the protonated and deprotonated forms of an indicating dye. The ARM requires absorbance data at only two wavelengths, while CMR is a full-spectrum method that provides useful qualitative and quantitative information about a chemical system. The theory for ARM has been previously discussed (Hopkins et al. 2000; Robert-Baldo et al. 1985; Usha and Atkinson 1992). Briefly, in a buffered solution containing BPB, the pH of the solution on the total hydrogen ion concentration scale can be calculated from the following equation:

$$pH_m = -\log[H^+]_m = pK_a(t, p, \mu) + \log \frac{R - e_1}{e_2 - R e_3} \quad (5.1)$$

where  $[H^+]_m$  is the molal concentration of hydrogen ion;  $K_a(t, p, \mu)$  is the conditional dissociation constant of BPB at temperature  $t$ , pressure  $p$ , and ionic strength  $\mu$ ; and  $R$  is the absorbance ratio ( $R = A_{\lambda_2}/A_{\lambda_1}$ ) at  $\lambda_2$  (591 nm) and  $\lambda_1$  (436 nm), which are the respective wavelengths of absorbance maxima for the deprotonated ( $I^{2-}$ ) and protonated ( $HI$ ) species of BPB (Figure 5.1). The symbols  $e_1$ ,  $e_2$ , and  $e_3$  refer to molar absorbance ratios of  $HI^-$  and  $I^{2-}$  at  $\lambda_1$  and  $\lambda_2$ :

$$e_1 = \epsilon_{HI}^{\lambda_2}/\epsilon_{HI}^{\lambda_1}, \quad e_2 = \epsilon_{I^{2-}}^{\lambda_2}/\epsilon_{HI}^{\lambda_1}, \quad e_3 = \epsilon_{I^{2-}}^{\lambda_1}/\epsilon_{HI}^{\lambda_1}, \quad (5.2)$$

which can be measured experimentally in acid and base solutions where the concentrations of  $HI^-$  and  $I^{2-}$  are equal to the total concentration of BPB, respectively (Hopkins et al. 2000). The dissociation constant of BPB at ambient pressure and high ionic strength ( $\mu \geq 1 \text{ m}$ ) can be determined with Equation (5.1) using citrate buffers of known  $pH_m$  containing BPB and NaCl to adjust the ionic strength. For a system with a low ionic strength that differs from the ionic strength of the calibration solutions, it is necessary to use a zero ionic strength dissociation constant  $K_a^0(t, p)$ , which can be determined using Equation (5.3):

$$pH_m = pK_a^0(t, p) + \log\left(\frac{R-e_1}{e_2-Re_3}\right) - 4A\left(\frac{\sqrt{\mu}}{1+\sqrt{\mu}} - 0.3\mu\right) \quad (5.3)$$

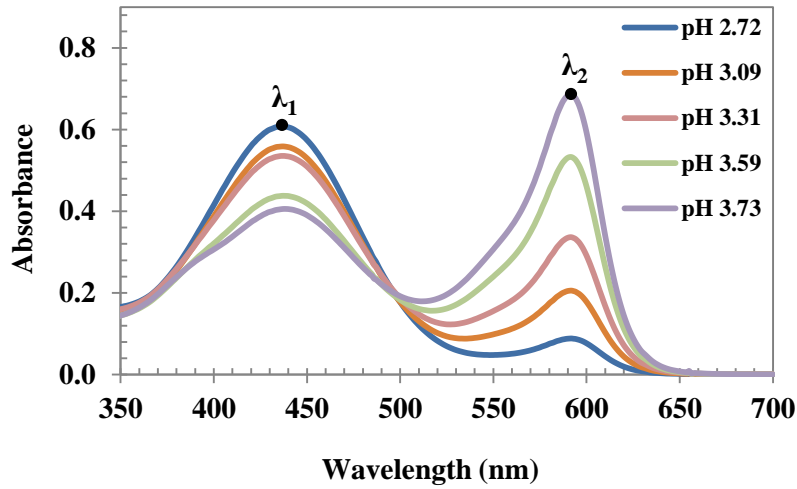


**Figure 5.1.** UV-Vis Spectra of BPB in Citrate Buffer Solutions at Different pH

The last term in Equation (5.3) accounts for the variation of  $I^{2-}$ ,  $HI^-$ , and  $H^+$  activity coefficients with ionic strength using the Davies equation. For pressures above ambient,  $K_a$  can be estimated using Equation (5.4) (Owen and Brinkley 1941):

$$\frac{RT}{(P-1)} \ln \frac{K_a(t, p, \mu)}{K_a(t, 1, \mu)} = -\Delta V + \Delta k \frac{(P-1)}{2} \quad (5.4)$$

where  $K_a(t, 1, \mu)$  is the BPB dissociation constant at ambient pressure. The change of partial molal volume ( $\Delta V$ ) and the compressibility ( $\Delta k$ ) have been reported for BPB (Usha and Atkinson 1992). An alternative version of the ARM was proposed by Toews et al. (1995). In this approach, a calibration

that assumes a linear relationship between hydrogen ion concentration and  $1/R$  is used, where  $R$  is the same as in Equation (5.1). This method is based on a simplified form of Equation (5.1):

$$[H^+] = K_a(t, p, \mu) \left( \frac{e_2}{R} - e_3 \right) \quad (5.5)$$

The simplification is due to the small magnitude of  $e_1$  compared to  $R$ , which is consistent with our experimental results for BPB (Table 5.1) and reported data for other sulfonephthalein dyes (Hopkins et al. 2000; Yao and Byrne 2001). Therefore, at constant temperature, pressure, and ionic strength,  $[H^+]$  varies linearly with  $1/R$ . Hereafter, we refer to this approach as the “simplified absorbance ratio method,” or SARM.

**Table 5.1.** Molar Absorptivity Ratios and  $pK_a$  of BPB at Ambient Pressure Calculated with ARM and CMR<sup>(a)</sup>

T (°C)	25	40	55	75	93
$e_1$	0.0056±0.0002 <sup>(b)</sup>	0.0058±0.0001	0.0056±0.0002	0.0053±0.0002	0.0051±0.0004
$e_2$	3.059±0.002	3.101±0.004	3.012±0.003	3.126±0.006	3.331±0.008
$e_3$	0.0355±0.005	0.0338±0.001	0.0308±0.003	0.0311±0.006	0.0387±0.010
$pK_a^0$	4.215±0.004 <sup>(c)</sup>	4.233±0.004	4.241±0.005	4.275±0.010	4.376±0.010
$pK_a(1)^{(d)}$	3.753±0.004	3.735±0.006	3.714±0.005	3.732±0.007	3.770±0.005
$pK_a(2)$	3.838±0.005	3.818±0.008	3.781±0.009	3.791±0.009	3.798±0.008
$pK_a(3)$	3.972±0.008	3.928±0.005	3.881±0.007	3.865±0.013	3.872±0.009
CMR $pK_a(0)$	4.023	4.025	4.044	4.058	4.188
CMR $pK_a(3)$	3.881	3.801	3.774	3.747	3.663

(a) Unless otherwise indicated,  $pK_a$  values were calculated with ARM.

(b) The uncertainties for  $e_1$ ,  $e_2$ , and  $e_3$  are the standard deviation of three measurements.

(c) Uncertainties for  $pK_a$  are the standard deviation of 12 measurements.

(d) The values in the parentheses refer to NaCl concentrations in BPB solutions.

Another approach for spectrophotometric pH determination is CMR (Shrager 1986; Sylvestre et al. 1974). CMR is a multivariate analysis technique in which a set of orthogonal eigenvectors, computed from absorbance spectra, is iteratively fit to a chemical model by adjusting the model parameters. Thompson and colleagues demonstrated the utility of CMR for estimating the equilibrium constants and species concentrations for the hydrofluoric acid system (Thompson et al. 1997). In the case of pH measurements using an indicating dye, the calibration spectra would consist of constant-concentration dye solutions buffered to span a desired pH range, and the chemical model is derived from the Henderson–Hasselbalch and mass–balance equations for the system:

$$pH_m = pK_a + \log \left( \frac{[I^{2-}]}{[HI^-]} \right), F = [HI^-] + [I^{2-}] \quad (5.6)$$

where  $F$  is the total concentration of the dye in solution. The fitting process yields an optimum estimate of the  $pK_a$ , as well as the concentration profiles and pure-component spectra of the acid and base forms of the indicator. Given the pure-component spectra, concentration estimates of the acid and base forms of

the indicator in an unknown spectrum can be computed using classical least squares (Martens and Næs 1989) (i.e., a full-spectrum expression of Beer's Law), and the pH can be determined from the expressions in Equation (5.6).

## 5.3 Results and Discussion

### 5.3.1 Method Parameters and Dissociation Constants of BPB

The  $pK_a$  and molar absorbance ratio values for BPB at ambient pressure calculated with ARM are given in Table 5.1. Within the pressure range of this work (1–180 atm.),  $e_1$ ,  $e_2$ , and  $e_3$  exhibited very small pressure dependencies, and the dependencies were not sensitive to temperature or ionic strength. The final equations for the influence of pressure on the molar absorptivity ratios, which were calculated from linear least squares fits, are

- $e_1(p) = e_1(1) + 2.03 \times 10^{-6} \times p$
- $e_2(p) = e_2(1) + 7.82 \times 10^{-5} \times p$
- $e_3(p) = e_3(1) + 2.9 \times 10^{-5} \times p$ .

At 25°C, our ARM zero ionic strength  $pK_a^0$  value, 4.215, was slightly higher than the value (4.17) reported by Usha and Atkinson (1992), but the conditional  $pK_a$  at  $\mu = 1$  m was 0.2 unit higher than the value measured by Usha and Atkinson. One possible explanation for this difference is that Usha and Atkinson used  $(CH_3)_4NCl$  as the background electrolyte, whereas NaCl was used in this research.

### 5.3.2 Comparison of Calibration Methods

In this research, three different data-analysis methods (ARM, SARM, and CMR) were used for calibration. Calibration curves for SARM showed a strong linear relationship ( $R^2$  is above 0.999 under all experimental conditions) between  $[H^+]$  and  $1/R$  (see Appendix A, Figure A.1). CMR calculations were performed only for the 0 m and 3 m NaCl data sets. Both matrices of calibration spectra were determined to have a rank of 2, which is consistent with the two forms of BPB present in solution. Fits of the score vectors (unit length eigenvectors of  $\mathbf{R}^T\mathbf{R}$  where  $\mathbf{R}$  is the matrix of calibration spectra in columns) to the equilibrium concentration profiles were good, indicating excellent agreement between the spectra and the equilibrium model (see Appendix A, Figure A.3–Figure A.5, for plots of the score fits, concentration profiles, and pure-component spectra).

At both ionic strength conditions, the CMR  $pK_a$  values were lower than the ARM estimates (Table 5.1). For 0 m NaCl, the CMR values were approximately 0.2 unit lower than the ARM averages, and at 3 m NaCl, the CMR  $pK_a$  were approximately 0.1 unit lower. Part of the discrepancy is likely due to the fact that the CMR calculations require a full set of calibration solutions, and the ionic strength of the citrate buffer in these solutions was not constant. For the ARM, a separate  $pK_a$  was determined for each calibration solution. The variability in ionic strength due to the buffer composition was more significant for the 0 m NaCl solutions, which may explain why the zero-salinity  $pK_a$  values differed more for the two methods.

The equilibrium  $pH_m$  for  $CO_2$ - $NaCl$ - $H_2O$  systems was calculated with three calibration methods (Figure 5.2 and Figure A.2). For high ionic strength systems containing 1, 2, and 3  $m$   $NaCl$ , the three calibration methods generally agreed well (within 0.04  $pH_m$  unit) at all pressures and temperatures (Figure 5.2A is an example). For the  $CO_2$ - $H_2O$  system, however, SARM and CMR produced estimates that were 0.1–0.3  $pH_m$  unit lower than values determined by ARM (Figure 5.2B). Two factors are responsible for these differences. First, the different ionic strengths of the buffer solutions (0.003–0.02  $m$ ) and  $CO_2$ - $H_2O$  system solutions ( $<0.002 m$ ) result in different conditional dissociation constants for BPB in the two systems. ARM makes corrections for this effect of ionic strength based on Equation (5.3) while SARM and CMR do not. Second, because both dissociation constants and molar absorbance ratios are pressure dependent, application of calibration curves determined with SARM or CMR at ambient pressure will cause errors for the  $CO_2$ - $H_2O$  systems at higher pressure. According to Equation (5.3), Equation (5.4), and the pressure dependence of  $e_1$ ,  $e_2$ , and  $e_3$ , neglecting ionic strength differences between the citrate buffer solutions and the  $CO_2$ - $H_2O$  systems results in much larger errors (0.1–0.25  $pH_m$  unit) than neglecting the pressure effect ( $<0.03 pH_m$  unit for pressure less than 200 atm).

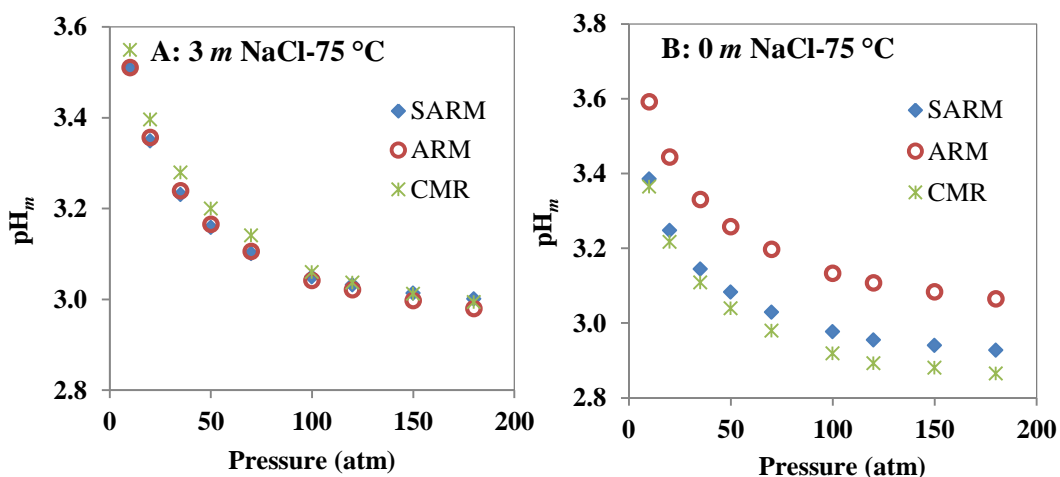


**Figure 5.2.** Comparison of  $pH_m$  Calculated with Different Calibration Methods

At GCS sites where brines generally have high ionic strengths and pressures are typically less than 200 atm, (Kharaka and Hanor 2007; White et al. 2003), all three calibration methods provide good results for spectrophotometric pH determination. CMR is the most complex of the methods, but CMR can yield valuable diagnostic information, including the number of detectable chemical species, discovery of outliers, a measure of agreement with an assumed thermodynamic model, and the pure-component spectra of the indicator's acid and base forms. A limitation of CMR is the need for near-constant ionic strength calibration solutions at low salinities. Compared with ARM, SARM is simpler because experimental measurements of molar absorbance ratios are not necessary; however, ARM has advantages. First, it can be used to determine  $pH_m$  for both high and low ionic strength systems. Second, once the indicator properties, including  $pK_a$  and  $e_1$ ,  $e_2$ , and  $e_3$ , are available, then buffer solutions are not needed for calibration and the  $R$  value is the only parameter required for  $pH_m$  determination. Third, because the absorbance ratio  $R$  is used, changes in indicator concentration do not influence the  $pH_m$  determination in  $CO_2$ -brine systems, which are well buffered. ARM was used for calculating  $pH_m$  values discussed in the following sections.

### 5.3.3 Comparison with Previous Studies and Geochemical Models

Equilibrium  $\text{pH}_m$  measurements for the  $\text{CO}_2$ – $\text{NaCl}$ – $\text{H}_2\text{O}$  systems were carried out at different temperatures, pressures, and ionic strengths (Figure 5.3). In the pressure range of 10 to 70 atm, where  $\text{CO}_2$  is in the gas phase,  $\text{pH}_m$  decreases rapidly as the pressure increases, whereas near or at  $\text{scCO}_2$  pressures (~70–180 atm),  $\text{pH}_m$  changes are small (less than 0.15 unit) for all temperatures and ionic strengths used in the present work. The standard deviations of average  $\text{pH}_m$  from triplicate measurements were in the range of 0.002 to 0.009, which allows evaluation of the small  $\text{pH}_m$  changes in  $\text{CO}_2$ – $\text{NaCl}$ – $\text{H}_2\text{O}$  systems under GCS conditions. Byrne and his colleagues reported a precision of  $\pm 0.0004$  for spectrophotometric pH measurements for seawater at 25°C (Hopkins et al. 2000; Liu et al. 2006; Yao and Byrne 2001). The somewhat lower precision observed in this work may be attributable to slight position changes of the reactor between runs and baseline shifts during measurement, especially at high temperatures.

Our experimental results are compared with those reported by Meysami et al. (1992) and Toews et al. (1995) (Figure 5.3A). To help facilitate the comparison, the pH values (activity scale) measured potentiometrically by Meysami et al. (1992) were converted to  $\text{pH}_m$ . Meysami's data are consistent with our experimental data if we consider the slightly higher temperature they used (42°C compared to ours, 40°C) (Meysami et al. 1992). In contrast, the results of Toews et al. (1995) at 40°C are more than 0.2 unit lower than our results. This large difference is due to the fact that Toews et al. (1995) did not account for the effects of ionic strength and pressure on their calibration (SARM), as discussed in the preceding section.

We used four different geochemical models to calculate  $\text{pH}_m$  for the  $\text{CO}_2$ – $\text{NaCl}$ – $\text{H}_2\text{O}$  system for comparison with our experimental measurements, including the OLI Analyzer version 3.1 (OLI; OLI Systems Incorporated, Morris Plains, New Jersey), Duan's model (Li and Duan 2007), PHREEQC (Parkhurst and Appelo 1999), and the Geochemist's Workbench (GWB; Bethke and Yeakel 2009). The OLI and Duan models are capable of calculating  $\text{CO}_2$  fugacities from  $\text{CO}_2$  pressures. PHREEQC and GWB do not account for non-ideal effects on gases at high pressure (Parkhurst and Appelo 1999). For the comparison, we performed two calculations with PHREEQC. In one case, the  $\text{CO}_2$  pressure was input directly to the model (the results are shown in Figure 5.3 as PHREEQC-P). In the second case, the  $\text{CO}_2$  solubility was calculated using Duan's model (Li and Duan 2007) and was input to PHREEQC. These results are shown as PHREEQC-Duan (Figure 5.3). For the GWB calculation, we used the thermo.phqpitz database and the  $\text{CO}_2$  solubility calculated using Duan's model (Li and Duan 2007), which is shown as GWB-Duan in Figure 5.3. As expected, the PHREEQC results without fugacity correction are significantly lower than our experimental results as well as the values predicted by other models. This demonstrates that ignoring the non-ideal behavior of  $\text{CO}_2$  at high pressure can result in overestimates of hydrogen ion concentrations.

The agreement of calculated  $\text{pH}_m$  by models other than PHREEQC-P and our experimental data is generally good, especially at lower pressure, but the agreement depends upon the pressure, temperature, and ionic strength of the aqueous system being investigated. For  $\text{CO}_2$ – $\text{H}_2\text{O}$  systems without NaCl, all four models are reasonably consistent, but the results from Duan's model are slightly higher than those of the other models (Figure 5.3A and B). At high ionic strength (e.g., 3 m NaCl), the OLI model provided  $\text{pH}_m$  values that deviated the most from our experimental data, whereas the Duan, PHREEQC-Duan, and GWB-Duan are generally in good agreement (Figure 5.3C and D). For all of our experimental conditions, the GWB-Duan model was the most consistent with our experimental results.

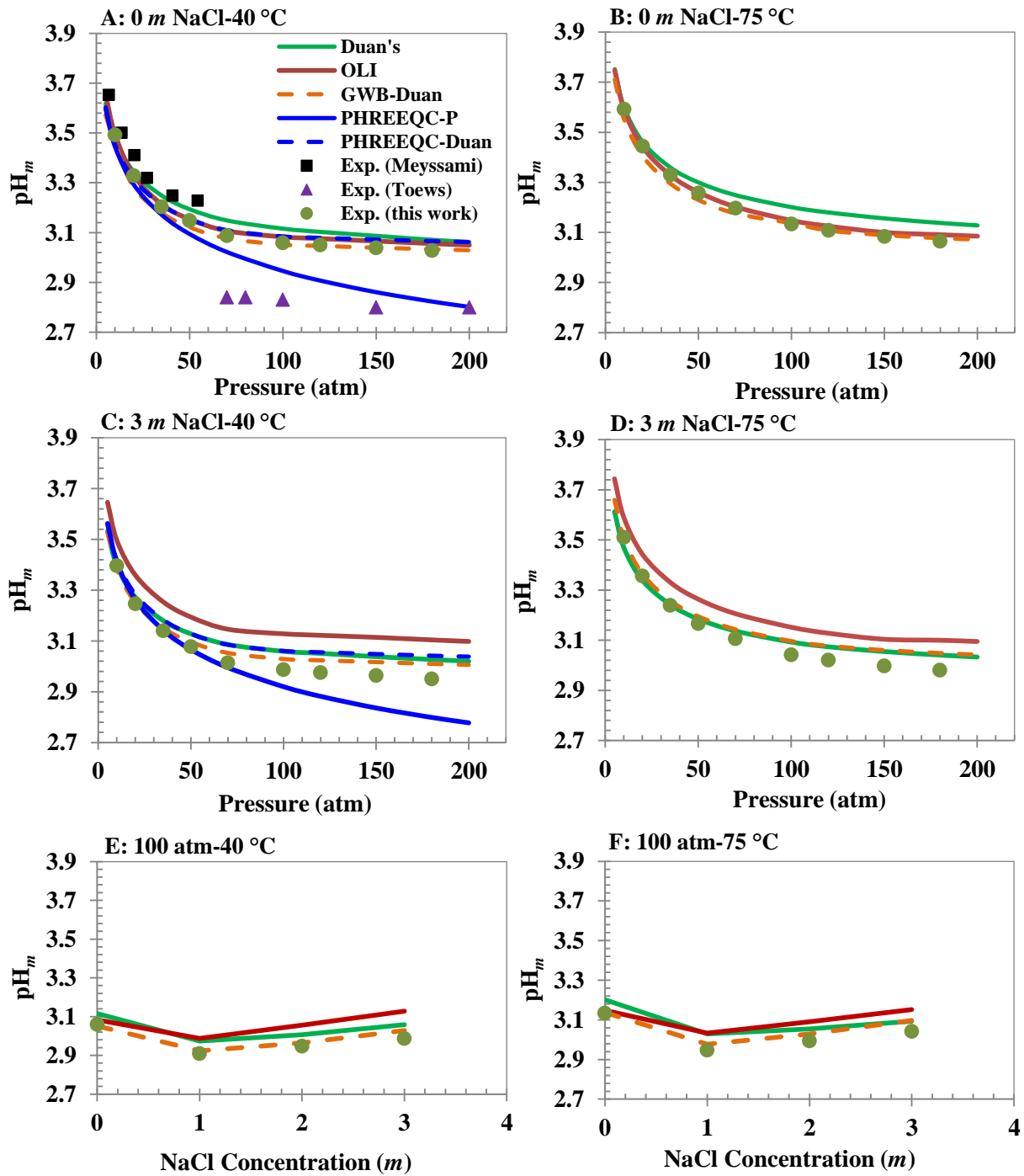


**Figure 5.3.** Comparison of Experimentally Measured  $pH_m$  and Predicted Values with Models. The uncertainties for the experimental data in this work are in the range of 0.002 to 0.009 and are not shown in the graphs.

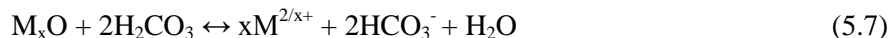
Differences between the Duan, PHREEQC-Duan and GWB-Duan models are likely due to variations in their respective thermodynamic databases for dissociation constants of carbonic acid and their different strategies for calculating activity coefficients for aqueous species. Thomas et al. (2012) found that geochemical predictions including pH calculation under GCS conditions are not sensitive to the choice of the sub-model used to calculate aqueous CO<sub>2</sub> activity coefficient (Thomas et al. 2012), but others have shown that the choice of sub-model for activity coefficient of ionic species and thermodynamic database can have a significant effect on the results of geochemical simulations (Gundogan et al. 2011). Gundogan et al. (2011) calculated pH for sandstone reservoirs with PHREEQC-Duan (inputting CO<sub>2</sub> fugacity calculated from Duan's model), GEM, and TOUGHREACT and found the differences in predicted pH values between the models could be as large as 0.27 pH unit (Gundogan et al. 2011). Detailed comparison of the effects of these sub-models on the accuracy of model prediction is beyond the scope of this paper; however, key points are as follows: 1) there are some discrepancies in pH<sub>m</sub> values predicted with the different models, and 2) our experimental results agree very well with model predictions at low pressure (less than 50 atm) in the CO<sub>2</sub>-H<sub>2</sub>O system where low ionic strength (<0.001 *m*) and low pressures reduce the discrepancies between model predictions.

### 5.3.4 In Situ pH Measurement for Rock-CO<sub>2</sub>-Brine

To illustrate the use of the spectrophotometric pH determination method under GCS conditions, in situ pH<sub>m</sub> was measured in a brine (1 *m* NaCl) in contact with a basalt rock from the Wallula Pilot Basalt CO<sub>2</sub> Sequestration site and scCO<sub>2</sub> at 100 atm and 75°C (Figure 5.4A). All the concentrations of cations and anions were well below 5 mM (Figure 5.4B) and did not contribute significantly to ionic strength of the aqueous phase. Therefore, the conditional dissociation constant for BPB in 1 *m* NaCl at 75°C and 100 atm was used to calculate pH<sub>m</sub> using ARM.

Initially, the pH<sub>m</sub> dropped rapidly due to rapid dissolution of CO<sub>2</sub> into the aqueous phase (Figure 5.4A). However, the pH<sub>m</sub> did not drop as low as it did in the analogous experiment that did not include a rock sample (insert in Figure 5.4A) because the rock dissolution consumes hydrogen ions. Within 2 h, the pH<sub>m</sub> dropped to 3.25 and then started to increase slowly as more cations leached from the rock. The rate of pH<sub>m</sub> increase declined with time: in about 10 days, the pH<sub>m</sub> increased 0.27 unit (from 3.25 to 3.52), while in the last 5 days, an increase of only 0.02 was observed. This lowering of the rate of pH<sub>m</sub> increase is consistent with the decreasing rock dissolution rate (Figure 5.4B).

A model calculation was performed using the measured chemical composition in the rock-CO<sub>2</sub>-brine system for comparison with the measured pH<sub>m</sub>. The calculation was conducted by assuming that alkalinity was generated in the system according to the following reaction for monovalent and divalent metal oxides:



The model used for the calculation was GWB-Duan (using the thermophqptz.dat database, CO<sub>2</sub> fugacity calculated with Duan's model (Li and Duan 2007) and assuming all dissolved iron occurs as Fe<sup>2+</sup>). The model results are compared in Figure 5.4A. The calculated pH<sub>m</sub> values are 0.22–0.25 unit higher than the measured values. Two reasons might be responsible for this discrepancy: 1) the dissolved species might interact—for example, complex with BPB—and interfere with pH determination, and 2) reactions that consume less acidity (or produce less alkalinity) have not been taken into account.

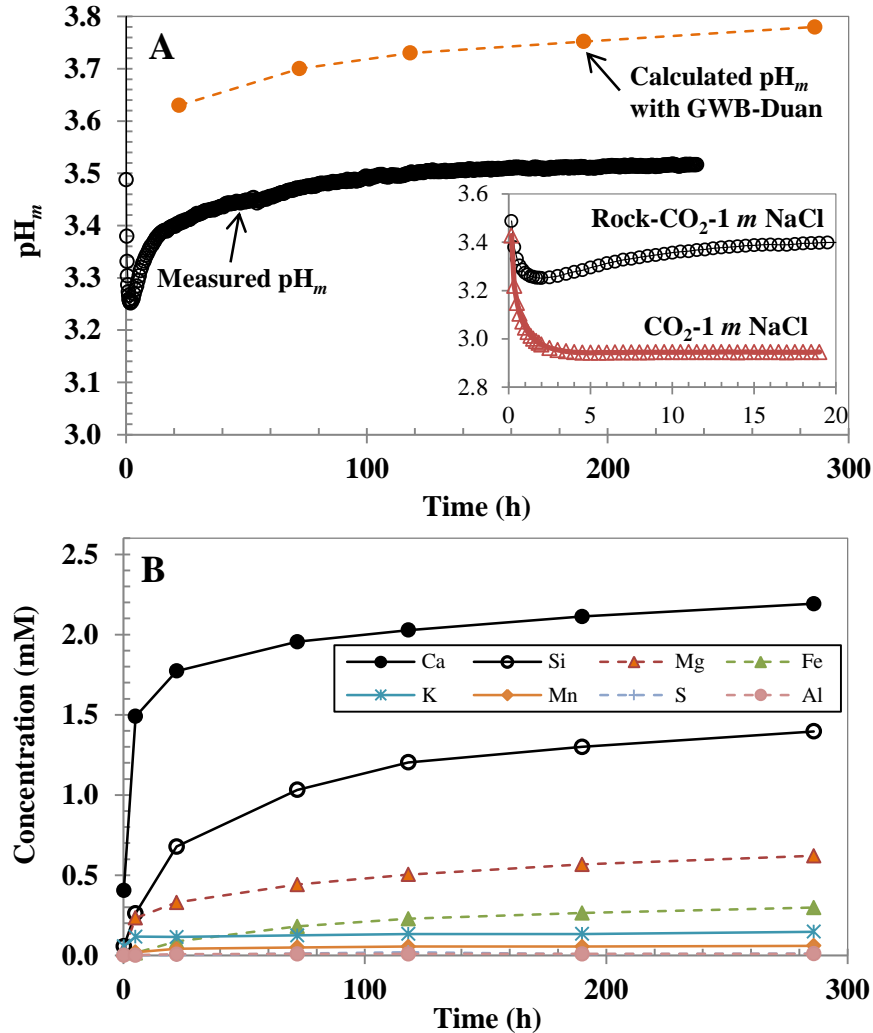


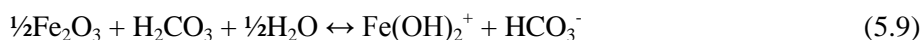
**Figure 5.4.** Changes in pH<sub>m</sub> (A) and Major Element Concentrations (B) with Time in Rock–CO<sub>2</sub>–1 m NaCl System at 75°C and 100 atm. The calculated pH<sub>m</sub> with GWB-Duan was based on the chemical composition result in the aqueous phase (see text). The insert in A shows the pH<sub>m</sub> changes with time in both rock–CO<sub>2</sub>–1 m NaCl and CO<sub>2</sub>–1 m NaCl systems during the first 20 h.

We conducted an experiment to test the first possibility. CaCl<sub>2</sub>, MgCl<sub>2</sub>, and FeCl<sub>2</sub> were added to citrate buffer solutions containing 1 m NaCl and  $1.19 \times 10^{-5}$  m BPB. The pH<sub>m</sub> of the buffer solution was 3.574, and the concentrations of Ca, Mg, and Fe in the buffer solutions were 10 mM, 10 mM, and 1 mM, respectively, which were approximately 5, 15, and 3 times higher than their concentrations measured for the rock–CO<sub>2</sub>–brine system, respectively. In this experiment, care was taken to prevent oxidation of Fe(II) by 1) dissolving FeCl<sub>2</sub>·4H<sub>2</sub>O in 0.1 M HCl solution to prepare a FeCl<sub>2</sub> stock solution, and 2) BPB spectra were collected within 30 s after FeCl<sub>2</sub> was added to citrate buffer solutions. Results showed that addition of Mg<sup>2+</sup>, Ca<sup>2+</sup>, and Fe<sup>2+</sup> at the noted concentrations did not significantly impact *R* values. Therefore, we ruled out the first possibility for the inconsistency between measured and model-calculated pH<sub>m</sub> for the rock–CO<sub>2</sub>–brine system.

The most likely source of the discrepancy is the assumption that all the dissolved iron was ferrous iron. In addition to ferrous iron, basalts may contain significant fractions of ferric iron. The average  $\text{Fe}_2\text{O}_3/\text{FeO}$  weight ratio determined for basalt samples from the same formation as the samples used in our experiments was 0.25 (Hooper et al. 1994). This is equivalent to a  $\text{Fe}^{3+}/\text{Fe}^{2+}$  ratio of 0.23 or 18% of the total iron as  $\text{Fe}^{3+}$ . If a major portion of the ferric iron in solution exists as  $\text{Fe}(\text{OH})_2^+$  at  $\text{pH}_m$  3.52 (see Appendix B), then significantly fewer protons would be consumed as the basalt is dissolved. For example, the dissolution equation for ferrous iron is



For ferric iron, the corresponding equation is



From these equations, dissolution of basalt to produce  $\text{Fe}^{2+}$  in solution requires twice as much acidity as for production of  $\text{Fe}(\text{OH})_2^+$ . The reaction for ferric iron was not accounted for in the model calculation because Pitzer parameters for the  $\text{Fe}^{3+}$  ion and its various solution complexes are not available in thermophqpitiz.com. This exercise illustrates that model calculations based solely on chemical composition in the aqueous phase may neglect processes that affect hydrogen ion concentrations, resulting in inaccurate estimates of solution pH. The absence of reliable thermodynamic constants for high-pressure and high-temperature conditions can make the situation even worse. As a result, direct pH measurement is preferable to modeling for accurate thermodynamic or reactive modeling of rock,  $\text{CO}_2$ , and brine interactions.

Spectrophotometric pH determination has advantages over potentiometric techniques or thermodynamic modeling, but spectrophotometry has some limitations. First, it is more influenced by medium effects (Bates 1973) compared to potentiometric methods. The presence of suspended fine particles will scatter light and cause measurement errors. Spectral interferences caused by dissolved mineral components are also possible. Chemical reactions between solutes such as heavy metal ions and indicators are additional potential sources of error (Bates 1973). However, as demonstrated here, by choosing suitable experimental conditions, spectrophotometric methods can provide accurate and precise in situ pH values for rock- $\text{CO}_2$ -brine systems under GCS conditions for laboratory studies.

In this work, a relatively simple system was studied where minimal weathering of basalt did not greatly increase the pH of the  $\text{CO}_2$ -brine system; however, GCS reservoir materials containing highly soluble minerals such as calcite, dolomite, or feldspars may result in significantly higher pH values. For example, Schaefer et al. (2010) measured pH for a basalt- $\text{CO}_2$ - $\text{H}_2\text{O}$  system under GCS conditions and found the pH could increase to 7.43, which is outside the range appropriate for BPB. In this case, other indicators such as bromocresol green and bromocresol purple would be required.

## 6.0 References

- Alemu BL, P Aagaard, IA Munz, and E Skurtveit. 2011. "Caprock Interaction with CO<sub>2</sub>: A Laboratory Study of Reactivity of Shale with Supercritical CO<sub>2</sub> and Brine." *Applied Geochemistry* 26:1975–1989.
- Apps JA, L Zheng, Y Zhang, Y Xu, and JT Birkholzer. 2010. "Evaluation of Potential Changes in Groundwater Quality in Response to CO<sub>2</sub> Leakage from Deep Geologic Storage." *Transport in Porous Media* 82:215–246.
- ASTM E1915-01. *Standard Test Methods for Analysis of Metal Bearing Ores and Related Materials by Combustion Infrared Absorption Spectrometry*. ASTM International, West Conshohocken, Pennsylvania.
- Bates RG. 1973. *Determination of pH: Theory and Practice*. John S. Wiley & Sons, Inc., New York.
- Bethke CM and S Yeakel. 2009. *GWB Essentials Guide*. RockWare, Inc., Golden, Colorado.
- Birkholzer JT, J Apps, L Zheng, Y Zhang, T Xu, and CF Tsang. 2008. *Research Project on CO<sub>2</sub> Geological Storage and Groundwater Resources, Water Quality Effects Caused by CO<sub>2</sub> Intrusion into Shallow Groundwater*. Technical Report, Earth Sciences Division, Lawrence Berkeley National Laboratory, Berkeley, California.
- Carroll SA, WW McNab, and SC Torres. 2011. "Experimental Study of Cement-Sandstone/Shale-Brine-CO<sub>2</sub> Interactions." *Geochemical Transactions* [Online] 12:9. Available at <http://www.geochemicaltransactions.com/content/12/1/9> (accessed September 2012).
- Chou L, RM Garrels, and R Wollast. 1989. "Comparative-Study of the Kinetics and Mechanisms of Dissolution of Carbonate Minerals." *Chemical Geology* 78:269–282.
- Credoz A, O Bildstein, M Jullien, J Raynal, JC Petronin, M Lillo, C Pozo, and G Geniaut. 2009. "Experimental and Modeling Study of Geochemical Reactivity between Clayey Caprocks and CO(2) in Geological Storage Conditions." In *Greenhouse Gas Control Technologies 9*, J Gale, H Herzog, and J Braitsch (eds.), Elsevier Science B.V., Amsterdam, pp. 3445–3452.
- Dalai TK, SK Singh, JR Trivedi, and S Krishnaswami. 2002. "Dissolved Rhenium in the Yamuna River System and the Ganga in the Himalaya: Role of Black Shale Weathering on the Budgets of Re, Os, and U in Rivers and CO<sub>2</sub> in the Atmosphere." *Geochimica et Cosmochimica Acta* 66:29–43.
- Daval D, O Sissmann, N Menguy, GD Saldi, F Guyot, I Martinez, J Corvisier, B Garcia, I Machouk, KG Knauss, and R Hellmann. 2011. "Influence of Amorphous Silica Layer Formation on the Dissolution Rate of Olivine at 90°C and Elevated pCO<sub>2</sub>." *Chemical Geology* 284:193–209.
- DOE – U.S. Department of Energy. 2007. *Carbon Sequestration Technology Roadmap and Program Plan*. U.S. Department of Energy and Office of Fossil Energy, National Energy Technology Laboratory, Washington, D.C.

EPA – U.S. Environmental Protection Agency. 2003. *National Primary Drinking Water Regulations*. EPA816-F-03-016, Washington, D.C. [Online] Available at <http://www.epa.gov/safewater/contaminants/index.html#primary> (accessed December 2008).

EPA – U.S. Environmental Protection Agency. 2009. “Code of Federal Regulations.” In EPA816-F-09-0004 (ed.), 40 CFR Part 141 and 143, Washington, D.C.

Evangelou VP and YL Zhang. 1005. “A Review: Pyrite Oxidation Mechanisms and Acid-Mine Drainage Prevention.” *Critical Reviews in Environmental Science and Technology* 25:141–199.

Fisher QJ and PB Wignall. 2001. “Palaeoenvironmental Controls on the Uranium Distribution in an Upper Carboniferous Black Shale (*Gastrioceras listeri* Marine Band) and Associated Strata; England.” *Chemical Geology* 175:605–621.

Flaathen TK, SR Gislason, EH Oelkers, and AE Sveinbjornsdottir. 2009. “Chemical Evolution of the Mt. Hekla, Iceland, Groundwaters: A Natural Analogue for CO<sub>2</sub> Sequestration in Basaltic Rocks.” *Applied Geochemistry* 24:463–474.

Griffith CA, DA Dzombak, and GV Lowry. 2011. “Physical and Chemical Characteristics of Potential Seal Strata in Regions Considered for Demonstrating Geological Saline CO<sub>2</sub> Sequestration.” *Environmental Earth Sciences* 64:925–948.

Gundogan O, E Mackay, and A Todd. 2011. “Comparison of Numerical Codes for Geochemical Modelling of CO<sub>2</sub> Storage in Target Sandstone Reservoirs.” *Chemical Engineering Research and Design* 8:1805–1816.

Hite RJ and SW Lohman. 1973. *Geological Appraisal of Paradox Basin Salt Deposits for Waste Emplacement*. Open File Report 73-114, U.S. Geological Survey, Denver, Colorado.

Hooper PR, SP Reidel, DM Johnson, and CM Knaack. 1994. “Umatilla Columbia River Basalt UMAT-1.” *Geostandards Newsletter* 18:203–210.

Hopkins AE, KS Sell, AL Soli, and RH Byrne. 2000. “In-Situ Spectrophotometric pH Measurements: The Effect of Pressure on Thymol Blue Protonation and Absorbance Characteristics.” *Marine Chemistry* 71:103–109.

Huertadiaz MA and JW Morse. 1990. “A Quantitative Method for Determination of Trace-Metal Concentrations in Sedimentary Pyrite.” *Marine Chemistry* 29:119–144.

IEAGHG – IEA Greenhouse Gas R&D Programme. 2004. *Impact of Impurities on CO<sub>2</sub> Capture, Transport and Storage*. Report No. PH4/32, Cheltenham, Gloucestershire, United Kingdom.

Inoue A and H Minato. 1979. “CA-K Exchange-Reaction and Interstratification in Montmorillonite.” *Clays and Clay Minerals* 27:393–401.

Jaffe LA, B Peucker-Ehrenbrink, and ST Petsch. 2002. “Mobility of Rhenium, Platinum Group Elements and Organic Carbon During Black Shale Weathering.” *Earth and Planetary Science Letters* 198:339–353.

Jia L, Y Tan, C Wang, and EJ Anthony. 2007. "Experimental Study of Oxy-Fuel Combustion and Sulfur Capture in a Mini-CFBC." *Energy & Fuels* 21:3160–3164.

Keating EH, J Fessenden, N Kanjorski, DJ Koning, and R Pawar. 2010. "The Impact of CO<sub>2</sub> on Shallow Groundwater Chemistry: Observations at a Natural Analog Site and Implications for Carbon Sequestration." *Environmental Earth Sciences* 60:521–536.

Keating EH, DL Newell, H Viswanathan, JW Carey, G Zvoloski, and R Pawar. 2012. "CO<sub>2</sub>/Brine Transport into Shallow Aquifers Along Fault Zones." *Environmental Science & Technology* DOI:10.1021/es301495x.

Kharaka YK and JS Hanor. 2007. "Deep Fluids in the Continents: 1. Sedimentary Basins." In *Surface and Ground Water, Weathering, and Soils: Treatise on Geochemistry*, Vol 5; JI Drever (ed.), Elsevier B.V., Amsterdam, Chapter 5.16.

Kharaka YK, P Campbell, and RB Thomas. 2011. "Environmental Impacts of Geologic Sequestration of CO<sub>2</sub>: Mobilized Toxic Organic Compounds." In *International Symposium on Isotopes in Hydrology, Marine Ecosystems, and Climate Change Studies*, International Atomic Energy Agency, Monaco, March 29, 2011.

Kharaka YK, DR Cole, SD Hovorka, WD Gunter, KG Knauss, and BM Freifeld. 2006. "Gas-Water-Rock Interactions in Frio Formation Following CO<sub>2</sub> Injection: Implications for the Storage of Greenhouse Gases in Sedimentary Basins." *Geology* 34:577–580.

Kharaka YK, JJ Thordsen, SD Hovorka, HS Nance, DR Cole, TJ Phelps, and KG Knauss. 2009. "Potential Environmental Issues of CO<sub>2</sub> Storage in Deep Saline Aquifers: Geochemical Results from the Frio-I Brine Pilot Test, Texas, USA." *Applied Geochemistry* 24:1106–1112.

Kharaka YK, JJ Thordsen, E Kakouros, G Ambats, WN Herkelrath, SR Beers, JT Birkholzer, JA Apps, NF Spycher, L Zheng, RC Trautz, HW Rauch, and KS Gullickson. 2010. "Changes in the Chemistry of Shallow Groundwater Related to the 2008 Injection of CO<sub>2</sub> at the ZERT Field Site, Bozeman, Montana." *Environmental Earth Sciences* 60:273–284.

Knauss KG and TJ Wolery. 1988. "The Dissolution Kinetics of Quartz as a Function of pH and Time at 70°C." *Geochimica et Cosmochimica Acta* 52:43–53.

Kolak JJ and RC Burrus. 2006. "Geochemical Investigation of the Potential for Mobilizing Non-Methane Hydrocarbons during Carbon Dioxide Storage in Deep Coal Beds." *Energy Fuels* 20:566–574.

Larsen F and D Postma. 1997. "Nickel Mobilization in a Groundwater Well Field: Release by Pyrite Oxidation and Desorption from Manganese Oxides." *Environmental Science & Technology* 31:2589–2595.

Lemieux J-M. 2011. "The Potential Impact of Underground Geological Storage of Carbon Dioxide in Deep Saline Aquifers on Shallow Groundwater Resources." *Hydrogeology Journal* 19:757–778.

- Lewicki JL, J Birkholzer, and C-F Tsang. 2007. "Natural and Industrial Analogues for Leakage of CO<sub>2</sub> from Storage Reservoirs: Identification of Features, Events, and Processes and Lessons Learned." *Environmental Geology* 52:457–467.
- Li D and Z Duan. 2007. "The Speciation Equilibrium Coupling with Phase Equilibrium in the H<sub>2</sub>O–CO<sub>2</sub>–NaCl System from 0 to 250 °C, from 0 to 1000 Bar, and from 0 to 5 Molality of NaCl." *Chemical Geology* 244:730–751.
- Liang Q, H Jing, and DC Gregoire. 2000. "Determination of Trace Elements in Granites by Inductively Coupled Plasma Mass Spectrometry." *Talanta* 51:507–513.
- Little MG and RB Jackson. 2010. "Potential Impacts of Leakage from Deep CO<sub>2</sub> Geosequestration on Overlying Freshwater Aquifers." *Environmental Science & Technology* 44:9225–9232.
- Liu F, P Lu, C Griffith, SW Hedges, Y Soong, H Hellevang, and C Zhu. 2012. "CO<sub>2</sub>–Brine–Caprock Interaction: Reactivity Experiments on Eau Claire Shale and a Review of Relevant Literature." *International Journal of Greenhouse Gas Control* 7:153–167.
- Liu X, ZA Wang, RH Byrne, EA Kaltenbacher, and RE Bernstein. 2006. "Spectrophotometric Measurements of pH In-Situ: Laboratory and Field Evaluations of Instrumental Performance." *Environmental Science & Technology* 40:5036–5044.
- Lowson RT. 1982. "Aqueous Oxidation of Pyrite by Molecular Oxygen." *Chemical Reviews* 82:461–497.
- Luquot L and P Gouze. 2009. "Experimental Determination of Porosity and Permeability Changes Induced by Injection of CO<sub>2</sub> into Carbonate Rocks." *Chemical Geology* 265:148–159.
- Marini L. 2007. *Geological Sequestration of Carbon Dioxide – Thermodynamics, Kinetics, and Reaction Path Modeling*. Elsevier B.V., Amsterdam.
- Martens H and T Næs. 1989. *Multivariate Calibration*. John Wiley & Sons, Ltd., New York.
- Meysami B, MO Balaban, and AA Teixeira. 1992. "Prediction of pH in Model Systems Pressurized with Carbon Dioxide." *Biotechnology Progress* 8:149–154.
- Miller CA, B Peucker-Ehrenbrink, BD Walker, and F Marcantonio. 2011. "Re-Assessing the Surface Cycling of Molybdenum and Rhenium." *Geochimica et Cosmochimica Acta* 75:7146–7179.
- Moses CO, DK Nordstrom, JS Herman, and AL Mills. 1987. "Aqueous Pyrite Oxidation by Dissolved Oxygen and by Ferric Iron." *Geochimica et Cosmochimica Acta* 51:1561–1571.
- Nelson CR, JM Evans, JA Sorensen, and EN Steadman. 2005. *Factors Affecting the Potential for CO<sub>2</sub> Leakage from Geologic Sinks*. Plain CO<sub>2</sub> Reduction (PCOR) Partnership, Energy & Environment Research Center, University of North Dakota. [Online] Available at <http://www.undeerc.org/PCOR/newsandpubs/pdf/FactorsAffectingPotential.pdf> (accessed September 2012).

Owen BB and SR Brinkley Jr. 1994. "Calculation of the Effect of Pressure upon Ionic Equilibria in Pure Water and in Salt Solutions." *Chemical Reviews* 29:461–474.

Palandri JL, RJ Rosenbauer, and YK Kharaka. 2005. "Ferric Iron in Sediments as a Novel CO<sub>2</sub> Mineral Trap: CO<sub>2</sub>–SO<sub>2</sub> Reaction with Hematite." *Applied Geochemistry* 20:2038–2048.

Parkhurst DL and CAJ Appelo. 1999. *User's Guide to PHREEQC (Version 2) – A Computer Program for Speciation, Batch-Reaction, One-Dimensional Transport, and Inverse Geochemical Calculations*. Water-Resources Investigations Report 99-4259, U.S. Geological Survey, Denver, Colorado.

Peucker-Ehrenbrink B and RE Hannigan. 2000. "Effects of Black Shale Weathering on the Mobility of Rhenium and Platinum Group Elements." *Geology* 28:475–478.

Pingitore NE, FW Lytle, BM Davies, MP Eastman, PG Eller, and EM Larson. 1992. "Mode of Incorporation of Sr<sup>2+</sup> in Calcite: Determination by X-Ray Absorption Spectroscopy." *Geochimica et Cosmochimica Acta* 56:1531–1538.

Pokrovsky OS, SV Golubev, and J Schott. 2005. "Dissolution Kinetics of Calcite, Dolomite and Magnesite at 25 Degrees C and 0 to 50 atm pCO(2)." *Chemical Geology* 217:239–255.

Prigobbe V and M Mazzotti. 2011. "Dissolution of Olivine in the Presence of Oxalate, Citrate, and CO<sub>2</sub> at 90 Degrees C and 120 Degrees C." *Chemical Engineering Science* 66:6544–6554.

Robert-Baldo G, MJ Morris, and RH Byrne. 1985. "Spectrophotometric Determination of Seawater pH Using Phenol Red." *Analytical Chemistry* 57:2564–2567.

Rutledge J. 2010. *Southwest Regional Partnership on Carbon Sequestration Phase II – Geologic Demonstration at the Aneth Oil Field, Paradox Basin, Utah*. Topical Report for the period 09/01/07 through 09/30/2010, New Mexico Institute of Mining and Technology, Socorro, New Mexico. [Online] Available at <http://www.osti.gov/bridge/servlets/purl/1029292/1029292.pdf> (accessed September 2012).

Schaefer H, BP McGrail, and AT Owen. 2010. "Carbonate Mineralization of Volcanic Province Basalts." *International Journal of Greenhouse Gas Control* 4:249–261.

Scherf A-K, C Zetzl, I Smirnova, M Zettlitzer, A Vieth-Hillebrand, and CO<sub>2</sub>SINK-Group. 2011. "Mobilisation of Organic Compounds from Reservoir Rocks Through the Injection of CO<sub>2</sub>—Comparison of Baseline Characterization and Laboratory Experiments." *Energy Procedia* 4:4524–4531.

Shao H, JR Ray, and Y-S Jun. 2010. "Dissolution and Precipitation of Clay Minerals under Geologic CO<sub>2</sub> Sequestration Conditions: CO<sub>2</sub>-Brine-Phlogopite Interactions." *Environmental Science & Technology* 44:5999–6005.

Shapovalov SA. 2010. "Interaction of Sulfophthaleine Anions with Cationic Dyes in Aqueous Solution." *Russian Journal of General Chemistry* 80:953–963.

Shrager RI. 1986. "Chemical Transitions Measured by Spectra and Resolved Using Singular Value Decomposition." *Chemometrics and Intelligent Laboratory Systems* 1:59–70.

Sohlenius G and I Oborn. 2004. "Geochemistry and Partitioning of Trace Metals in Acid Sulphate Soils in Sweden and Finland Before and After Sulphide Oxidation." *Geoderma* 122:167–175.

Spangler LH, LM Dobeck, KS Repasky, AR Nehrir, SD Humphries, JL Barr, CJ Keith, JA Shaw, JH Rouse, AB Cunningham, SM Benson, CM Oldenburg, JL Lewicki, AW Wells, JR Diehl, BR Strazisar, JE Fessenden, TA Rahn, JE Amonette, JL Barr, WL Pickles, JD Jacobson, EA Silver, EJ Male, HW Rauch, KS Gullickson, R Trautz, Y Kharaka, J Birkholzer, and LA Wielopolski. 2009. "A Shallow Subsurface Controlled Release Facility in Bozeman, Montana, USA, for Testing Vear Surface CO<sub>2</sub> Detection Techniques and Transport Models." *Environmental Earth Sciences* 60:227–239.

Stumm W. 1992. *Chemistry of the Solid-Water Interface – Processes at the Mineral-Water and Particle-Water Interface in Natural Systems*. Wiley-Interscience, New York.

Suto Y, L Liu, N Yamasaki, and T Hashida. 2007. "Initial Behavior of Granite in Response to Injection of CO<sub>2</sub>-Saturated Fluid." *Applied Geochemistry* 22:202–218.

Swanson VE. 1061. *Geology and Geochemistry of Uranium in Marine Black Shales, a Review*. Geological Survey Professional Paper 356-C, United States Government Printing Office, Washington, D.C.

Sylvestre EA, WH Lawton, and MS Maggio. 1974. "Curve Resolution Using a Postulated Chemical Reaction." *Technometrics* 16:353–368.

Thomas MW, M Stewart, M Trotz, and JA Cunningham. 2012. "Geochemical Modeling of CO<sub>2</sub> Sequestration in Deep, Saline, Dolomitic-Limestone Aquifers: Critical Evaluation of Thermodynamic Sub-Models." *Chemical Geology* 306–307:29–39.

Thompson CJ, JDS Danielson, and JB Callis. 1997. "Quantification of Hydrofluoric Acid Species by Chemical-Modeling Regression of Near-Infrared Spectra." *Analytical Chemistry* 69:25–35.

Toews KL, RM Shroll, and CM Wai. 1995. "pH-Defining Equilibrium between Water and Supercritical CO<sub>2</sub>. Influence on SFE of Organics and Metal Chelates." *Analytical Chemistry* 67:4040–4043.

Tromp DE. 1995. *Clays as Indicators of Depositional and Diagenetic Conditions in Pennsylvanian Black Shales, Paradox Basin, Utah and Colorado*. M.S. Thesis, Colorado School of Mines, Golden, Colorado.

Tuttle ML and TR Klett. 1996. "Geochemistry of Two Interbeds in the Pennsylvanian Paradox Formation, Utah and Colorado: A Record of Deposition and Diagenesis of Repetitive Cycles in a Marine Basin." In *Evolution of Sedimentary Basins – Paradox Basin*, AC Huffman (ed.), U.S. Geological Survey Bulletin 2000-N, United States Government Printing Office, Washington, D.C., pp. N1–N86.

Usha AV and G Atkinson. 1992. "The Effect of Pressure on the dissociation Constant of Hydrofluoric Acid and the Association Constant of the NaF Ion Pair at 25 °C." *Journal of Solution Chemistry* 21:477–488.

- Wang S and PR Jaffe. 2004. "Dissolution of a Mineral Phase in Potable Aquifers due to CO<sub>2</sub> Releases from Deep Formations; Effect of Dissolution Kinetics." *Energy Conversion and Management* 45:2833–2848.
- White CM, BR Strazisar, EJ Granite, JS Hoffman, and HW Pennline. 2003. "Separation and Capture of CO<sub>2</sub> from Large Stationary Sources and Sequestration in Geological Formations--Coalbeds and Deep Saline Aquifers." *Journal of the Air & Waste Management Association* 53:645–715.
- Wigand M, JW Carey, H Schütt, E Spangenberg, and J Erzinger. 2008. "Geochemical Effects of CO<sub>2</sub> Sequestration in Sandstones under Simulated In Situ Conditions of Deep Saline Aquifers." *Applied Geochemistry* 23:2735–2745.
- Wilke FDH, M Vasquez, T Wiersberg, R Naumann, and J Erzinger. 2012. "On the Interaction of Pure and Impure Supercritical CO<sub>2</sub> with Rock Forming Minerals in Saline Aquifers: An Experimental Geochemical Approach." *Applied Geochemistry* 27:1615–1622.
- Xu T, YK Kharaka, C Doughty, BM Freifeld, and TM Daley. 2010. "Reactive Transport Modeling to Study Changes in Water Chemistry Induced by CO<sub>2</sub> Injection at the Frio-I Brine Pilot." *Chemical Geology* 271:153–164.
- Yang Y, C Ronzio, and Y-S Jun. 2011. "The Effects of Initial Acetate Concentration on CO<sub>2</sub>-Brine-Anorthite Interactions under Geologic CO<sub>2</sub> Sequestration Conditions." *Energy & Environmental Science* 4:4596–4606.
- Yao W and RH Byrne. 2001. "Spectrophotometric Determination of Freshwater pH Using Bromocresol Purple and Phenol Red." *Environmental Science & Technology* 35:1197–1201.
- Zheng L, JA Apps, X Zhang, T Xu, and JT Birkholzer. 2009. "On Mobilization of Lead and Arsenic in Groundwater in Response to CO<sub>2</sub> Leakage from Deep Geological Storage." *Chemical Geology* 268:281–297.



## **Appendix A**

### **Additional Figures for In Site pH Measurement Method Development**



# Appendix A

## Additional Figures for In Situ pH Measurement Method Development

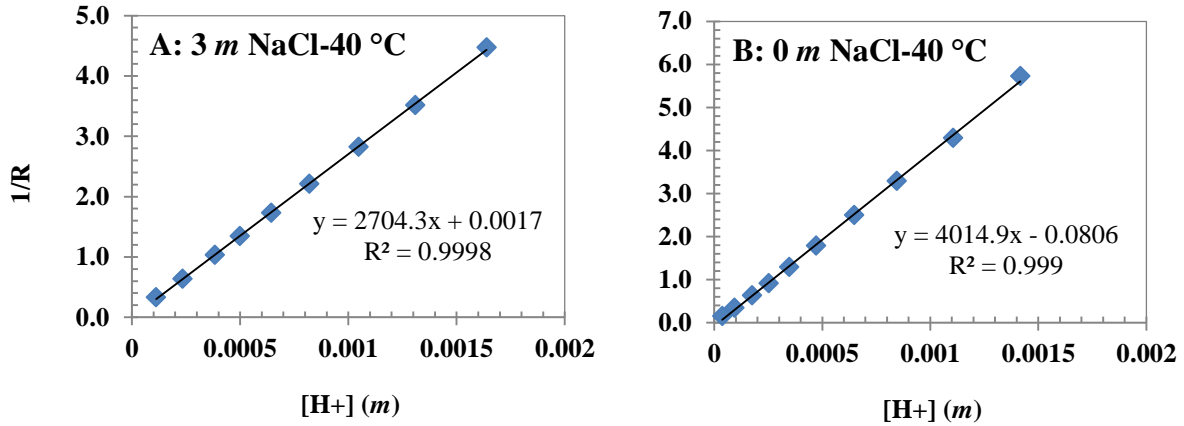


**Figure A.1.** Calibration Curves for SARM Obtained from 1/R versus Hydrogen Ion Concentration for Citrate Buffers Having  $pH_m$  between 2.8 and 4.6 Containing BPB at Ambient Pressure and 40°C.

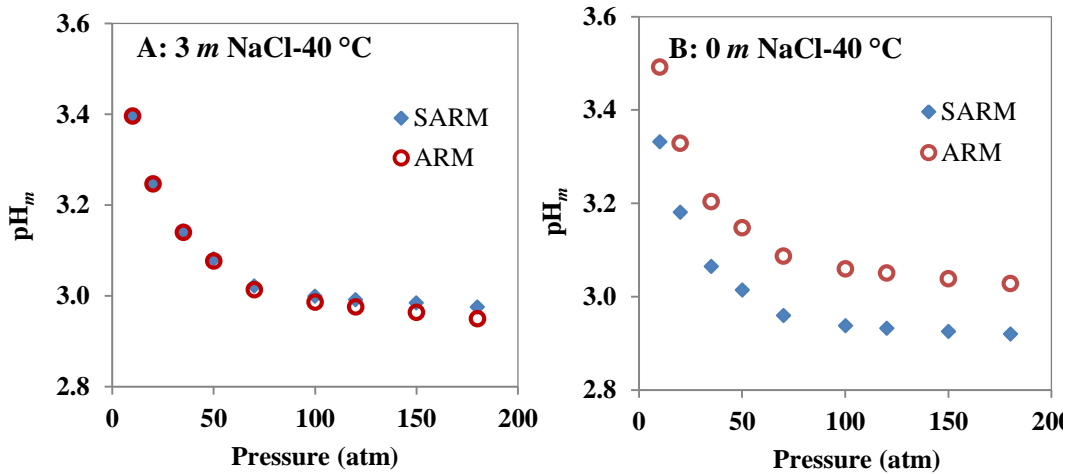


**Figure A.2.** Comparison of  $pH_m$  Calculated with Different Calibration Methods.

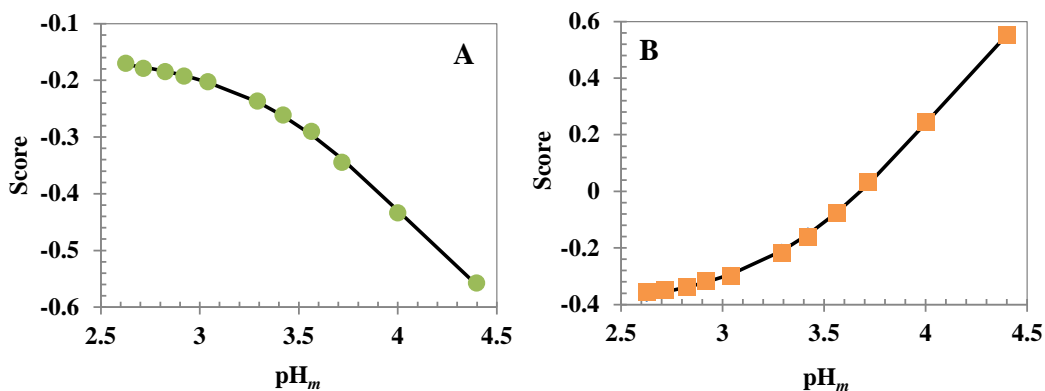


**Figure A.3.** Optimized Score Vectors' Fits for CMR for the 75°C, 0 *m* NaCl Data Set. Data markers represent the actual score values, and the estimated values are represented by solid lines: A) first eigenvector and B) second eigenvector.

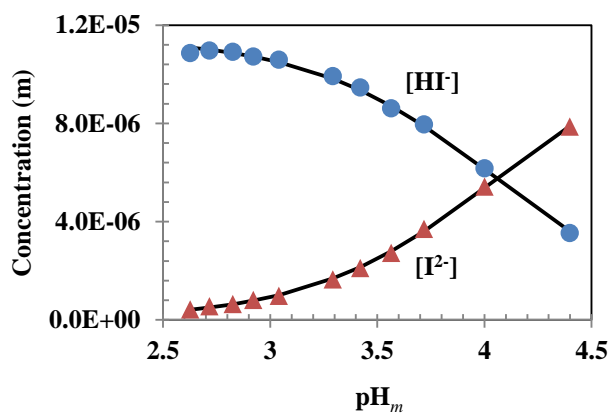


**Figure A.4.** Estimated Concentrations of the Acid and Base Forms of BPB from CMR of the 75°C, 0 *m* NaCl Data Set. Data markers denote the rotated scores, and the solid lines represent the model values.

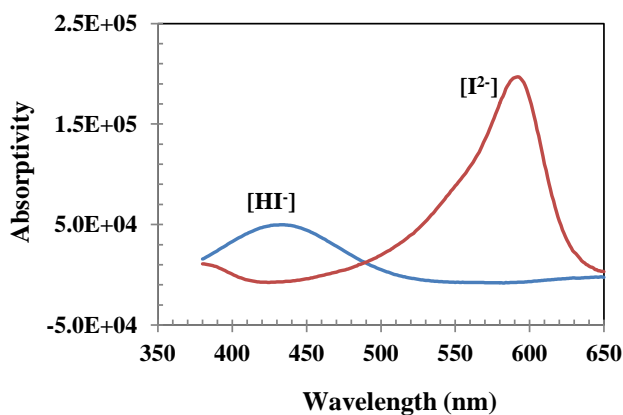


**Figure A.5.** Pure-Component Spectra of the Acid and Base Forms of BPB from CMR of the 75°C, 0 *m* NaCl Data Set. Similar spectra were obtained for the 75°C, 3 *m* NaCl data set.

## **Appendix B**

### **Geochemist's Workbench Calculation to Determine Dominant Fe(III) Species in the CO<sub>2</sub>-Brine System**



## Appendix B

### Geochemist's Workbench Calculation to Determine Dominant Fe(III) Species in the CO<sub>2</sub>–Brine System

To evaluate the hypothesis that  $\text{Fe}(\text{OH})_2^+$  was the dominant ferric species in solution for the rock-CO<sub>2</sub>-brine experiment, the speciation of ferric iron was calculated as a function of pH with the Geochemist's Workbench (GWB; Aqueous Solutions LLC, Champaign, Illinois) using the thermo.com.v8.r6+.dat thermodynamic database and the following input parameters: 1.0 m NaCl,  $6 \times 10^{-5}$  m total ferric iron, CO<sub>2</sub>(g) fugacity of 65, and 25°C (Figure B.1). The calculation was conducted at 25°C because data for ferric iron hydrolysis at higher temperatures are not available in this database. These results indicate that at pH 3.5,  $\text{FeOH}^{2+}$  is the dominant ferric iron species in solution and that  $\text{Fe}(\text{OH})_2^+$  does not become the dominant species until pH is well above 4.

For our hypothesis to be true, ferric iron hydrolysis must be greater at 75°C. Liu and Millero (1999) present equations for conditional iron(III) hydrolysis constants as a function of temperature and ionic strength for sodium chloride solutions (Liu and Millero 1999). Using these equations, the hydrolysis constants for  $\text{Fe}(\text{OH})_2^+$  at 25°C and 75°C were calculated ( $\log \beta_2^*(25^\circ\text{C}) = -6.57$  and  $\log \beta_2^*(75^\circ\text{C}) = -5.61$ ). Thus, the hydrolysis of ferric iron increases significantly when the temperature increases from 25°C to 75°C. This evidence supports our assertion that the majority of the discrepancy between our measured  $\text{pH}_m$  values and the model-calculated  $\text{pH}_m$  values for basalt dissolution is likely due to the fact that a significant fraction of the iron in solution occurs as  $\text{Fe}(\text{OH})_2^+$ .

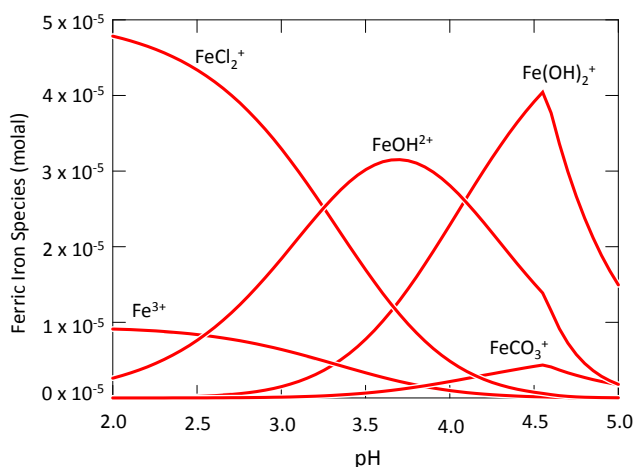


**Figure B.1.** Ferric Iron Speciation in 1.0 m NaCl,  $6 \times 10^{-5}$  m Total Ferric Iron and CO<sub>2</sub>(g) Fugacity of 65 (25°C)

### Reference

Liu X and FJ Millero. 1999. "The Solubility of Iron Hydroxide in Sodium Chloride Solutions." *Geochimica et Cosmochimica Acta* 63:3487–3497.



## **Appendix C**

### **Characterization of Rock Samples**



## Appendix C

### Characterization of Rock Samples

**Table C.1.** Summary of XRF Results for Rock Samples for Major Elements (unit: wt% of dried sample)

	Wallula Reservoir Rock	Wallula Caprock	Michigan Reservoir Rock	Utah Reservoir Rock
SiO <sub>2</sub>	50.97	52.84	0.39	1.34
TiO <sub>2</sub>	1.78	2.04	0.00	0.005
Al <sub>2</sub> O <sub>3</sub>	14.86	13.85	0.06	0.08
Fe as Fe <sub>2</sub> O <sub>3</sub>	13.06	14.15	0.23	0.03
MnO	0.22	0.24	0.00	0.005
MgO	5.11	4.58	20.44	1.37
CaO	9.63	8.36	31.65	53.33
Na <sub>2</sub> O	2.81	2.89	<0.1	0.04
K <sub>2</sub> O	0.97	1.07	0.04	0.01
P <sub>2</sub> O <sub>5</sub>	0.36	0.35	0.01	0.017
Loss on ignition	0.67	0.21	46.90	43.15
<b>Total</b>	<b>100.44</b>	<b>100.59</b>	<b>99.51</b>	<b>99.39</b>

**Table C.2.** Summary of XRF Results for Rock Samples for Trace Elements (unit: mg/kg dried sample)

	Wallula Reservoir Rock	Wallula Caprock	Michigan Reservoir Rock	Utah Reservoir Rock
As	<2	<2	<2	<2
Ba	152	522.9	0	370
Ce	31	40.8	4	0
Co	39	33.2	0	0
Cr	94	33.6	0	11
Cu	42	47	8	7
Ga	23	21.4	0	2
La	9	23.7	3	5
Mo	1	2.4	1	0
Nb	10	10.4	1	0.6
Nd	24	24.4	3	0
Ni	29	27.6	2	4
Pb	5	7.9	5	7
Rb	20	32.8	1	1
Sr	400	379.5	60	403
V	150	330.5	5	7
Zn	98	111.7	4	3
Zr	142	171	3	2
sum	1268	1820.8	99	822

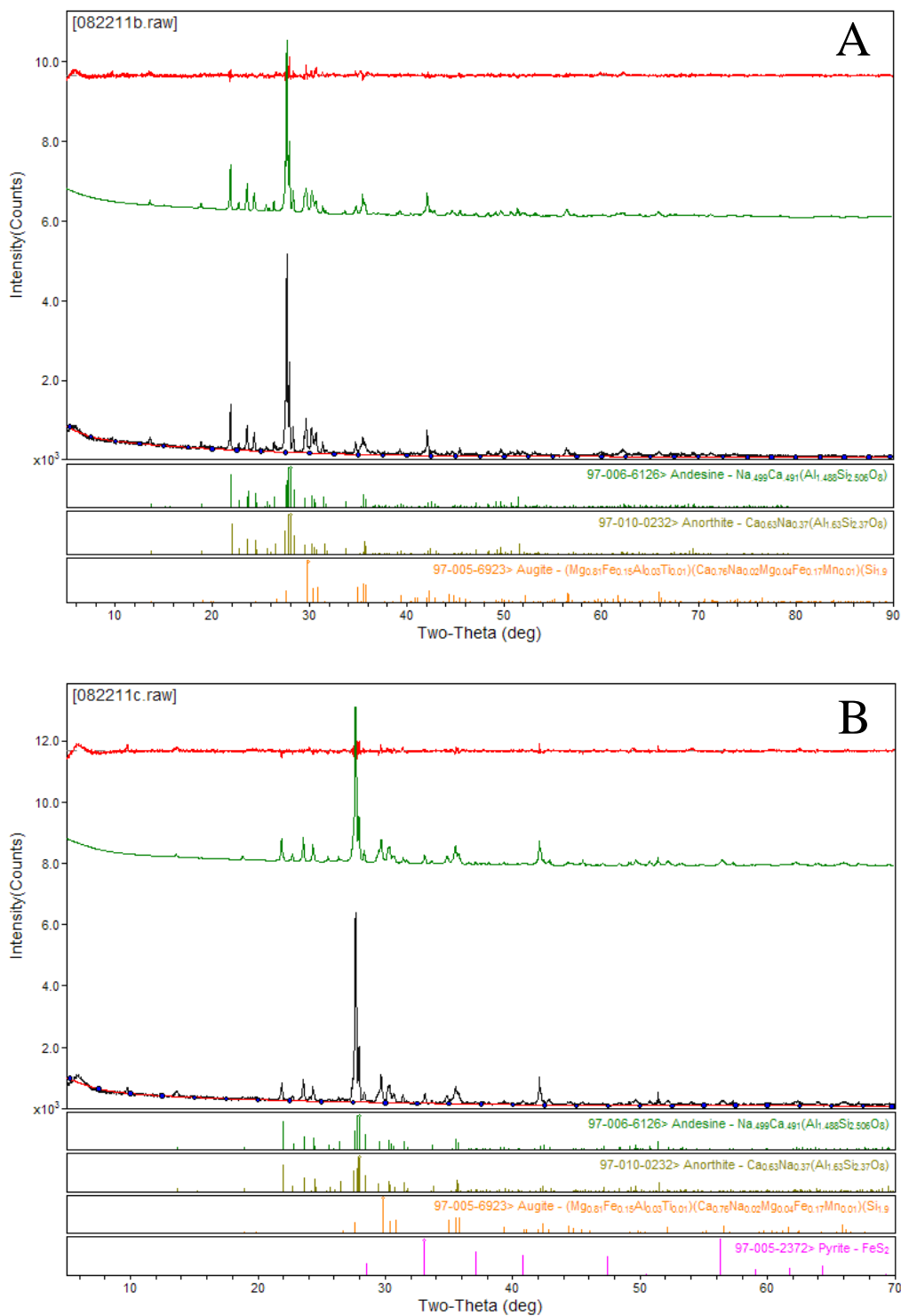


**Figure C.1.** X-Ray Diffraction Data for Wallula Caprock (A) and Wallula Reservoir Rock (B) Along with the Reference Data for the Crystalline Phases Identified. The black curve is the observed X-ray powder pattern, the red curve underneath it is the background, the green curve is the simulated powder pattern based on the identified crystalline phases, and the red curve on the top is the difference between the calculated and the observed powder patterns.

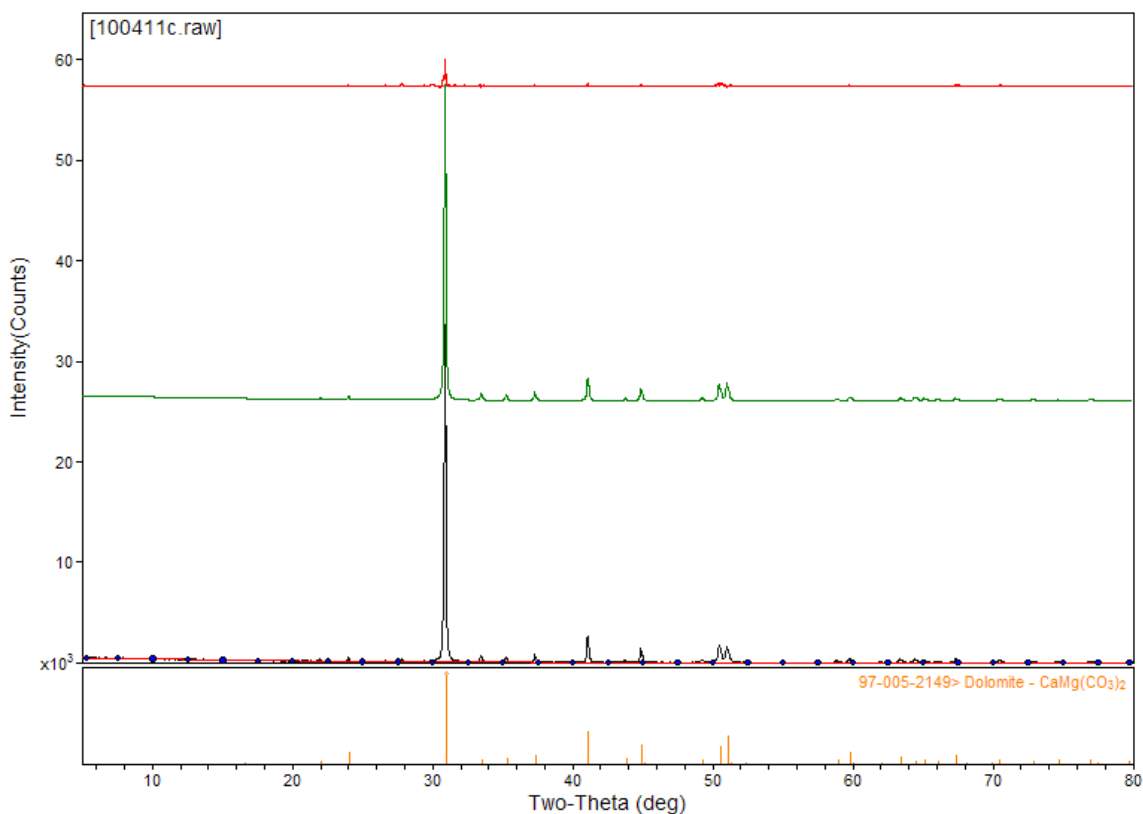


**Figure C.2** X-Ray Diffraction Data for Shao C (100411c) Along with the Reference Data for the Crystalline Phases Identified. The black curve is the observed X-ray powder pattern, the red curve underneath it is the background, the green curve is the simulated powder pattern based on the identified crystalline phases, and the red curve on the top is the difference between the calculated and the observed powder patterns.

**Table C.3.** Sample Compositions Based on the Whole Powder Pattern Refinement Data from XRD Spectra for Rock Samples Used in This Work

Sample	Phase Name	Phase Formula	wt%
Wallula caprock	Andesine	$\text{Na}_{0.499}\text{Ca}_{0.491}\text{Al}_{1.488}\text{Si}_{2.506}\text{O}_8$	19.2 (3.8) <sup>(a)</sup>
	Anorthite	$\text{Ca}_{0.63}\text{Na}_{0.37}\text{Al}_{1.63}\text{Si}_{2.37}\text{O}_8$	45.2 (6.5)
	Augite	$(\text{Mg}_{0.81}\text{Fe}_{0.15}\text{Al}_{0.03}\text{Ti}_{0.01})(\text{Ca}_{0.76}\text{Na}_{0.02}\text{Mg}_{0.04}\text{Fe}_{0.17}\text{Mn}_{0.01})(\text{Si}_{1.92}\text{Al}_{0.08}\text{O}_6)$	35.6 (5.6)
Wallula reservoir rock	Andesine	$\text{Na}_{0.499}\text{Ca}_{0.491}\text{Al}_{1.488}\text{Si}_{2.506}\text{O}_8$	45.6 (7.3)
	Anorthite	$\text{Ca}_{0.63}\text{Na}_{0.37}\text{Al}_{1.63}\text{Si}_{2.37}\text{O}_8$	15.6 (3.8)
	Augite	$(\text{Mg}_{0.81}\text{Fe}_{0.15}\text{Al}_{0.03}\text{Ti}_{0.01})(\text{Ca}_{0.76}\text{Na}_{0.02}\text{Mg}_{0.04}\text{Fe}_{0.17}\text{Mn}_{0.01})(\text{Si}_{1.92}\text{Al}_{0.08}\text{O}_6)$	3.9 (6.6)
Michigan reservoir rock	Calcite	$\text{CaCO}_3$	0
	Dolomite	$\text{CaMg}(\text{CO}_3)_2$	100
	Quartz	$\text{SiO}_2$	0

(a) The numbers in the parentheses are uncertainties.







**Pacific Northwest**  
NATIONAL LABORATORY

*Proudly Operated by **Battelle** Since 1965*

902 Battelle Boulevard  
P.O. Box 999  
Richland, WA 99352  
1-888-375-PNNL (7665)  
[www.pnnl.gov](http://www.pnnl.gov)



U.S. DEPARTMENT OF  
**ENERGY**